Track Performance in Tunnels and Rail Transition Areas with Under Tie Pads and Under Ballast Mats

UF-22-1

June 2022

Dr. Kyle A. Riding, Civil & Coastal Engineering, UF

Dr. Jennifer A. Bridge, Civil & Coastal Engineering, UF

Dr. Justin R. Davis, Engineering, ECU

Dr. Shanyue Guan, Civil and Coastal Engineering, UF

Stephen Gonzalez, UF

Abstract

Railroads have begun to use under tie pads (UTP) and under ballast mats (UBM) in rail track construction to reduce maintenance costs by better distributing loads, reducing the track modulus, and increasing ballast contact areas with ties. Locations such as tunnels, bridges, and bridge approaches are especially strong candidates for UTP and UBM use due to the high support stiffness they provide to the ballast. In this study, the University of Florida (UF) instrumented the Virginia Avenue Tunnel in Washington D.C., which uses UTP and UBM, during construction to monitor track pressure distribution, tie movement, and tunnel floor vibration during the first 20 months of use (July 2018 – February 2020). Track pressure distributions across ties were measured for hundreds of trains at the tunnel floor transition area and inside the tunnel. Measurements showed that the track settlement occurred over the first 6 months of measurement after track was opened, after which it stabilized to less than 0.157 in. (4 mm).

Corresponding Author: Dr. Kyle A. Riding (kyle.riding@essie.ufl.edu)

U.S. Department of Transportation
Federal Railroad Administration

METRIC/ENGLISH CONVERSION FACTORS

ENGLISH TO METRIC

LENGTH (APPROXIMATE)

1 inch (in)	=	2.5 centimeters (cm)
1 foot (ft)	=	30 centimeters (cm)
1 yard (yd)	=	0.9 meter (m)
1 mile (mi)	=	1.6 kilometers (km)

AREA (APPROXIMATE)

1 square inch (sq in, in^2)	=	6.5 square centimeters (cm^2)
1 square foot (sq ft, ft^2)	=	0.09 square meter (m^2)
1 square yard (sq yd, yd^2)	=	0.8 square meter (m^2)
1 square mile (sq mi, mi^2)	=	2.6 square kilometers (km^2)
1 acre = 0.4 hectare (he)	=	4,000 square meters (m^2)

MASS - WEIGHT (APPROXIMATE)

1 ounce (oz)	=	28 grams (gm)
1 pound (lb)	=	0.45 kilogram (kg)
1 short ton = 2,000 pounds (lb)	=	0.9 tonne (t)

VOLUME (APPROXIMATE)

1 teaspoon (tsp)	=	5 milliliters (ml)
1 tablespoon (tbsp)	=	15 milliliters (ml)
1 fluid ounce (fl oz)	=	30 milliliters (ml)
1 cup (c)	=	0.24 liter (l)
1 pint (pt)	=	0.47 liter (l)
1 quart (qt)	=	0.96 liter (l)
1 gallon (gal)	=	3.8 liters (l)
1 cubic foot (cu ft, ft^3)	=	0.03 cubic meter (m^3)
1 cubic yard (cu yd, yd^3)	=	0.76 cubic meter (m^3)

TEMPERATURE (EXACT)

$[(x-32)(5/9)]$ °F = y °C

METRIC TO ENGLISH

LENGTH (APPROXIMATE)

1 millimeter (mm)	=	0.04 inch (in)
1 centimeter (cm)	=	0.4 inch (in)
1 meter (m)	=	3.3 feet (ft)
1 meter (m)	=	1.1 yards (yd)
1 kilometer (km)	=	0.6 mile (mi)

AREA (APPROXIMATE)

1 square centimeter (cm^2)	=	0.16 square inch (sq in, in^2)
1 square meter (m^2)	=	1.2 square yards (sq yd, yd^2)
1 square kilometer (km^2)	=	0.4 square mile (sq mi, mi^2)
10,000 square meters (m^2)	=	1 hectare (ha) = 2.5 acres

MASS - WEIGHT (APPROXIMATE)

1 gram (gm)	=	0.036 ounce (oz)
1 kilogram (kg)	=	2.2 pounds (lb)
1 tonne (t)	=	1,000 kilograms (kg)
	=	1.1 short tons

VOLUME (APPROXIMATE)

1 milliliter (ml)	=	0.03 fluid ounce (fl oz)
1 liter (l)	=	2.1 pints (pt)
1 liter (l)	=	1.06 quarts (qt)
1 liter (l)	=	0.26 gallon (gal)
1 cubic meter (m^3)	=	36 cubic feet (cu ft, ft^3)
1 cubic meter (m^3)	=	1.3 cubic yards (cu yd, yd^3)

TEMPERATURE (EXACT)

$[(9/5) y + 32]$ °C = x °F

QUICK INCH - CENTIMETER LENGTH CONVERSION

Inches: 0 1 2 3 4 5

Centimeters: 0 1 2 3 4 5 6 7 8 9 10 11 12 13
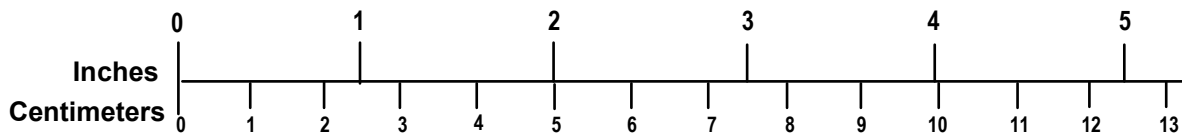
QUICK FAHRENHEIT - CELSIUS TEMPERATURE CONVERSION

°F	-40°	-22°	-4°	14°	32°	50°	68°	86°	104°	122°	140°	158°	176°	194°	212°
°C	-40°	-30°	-20°	-10°	0°	10°	20°	30°	40°	50°	60°	70°	80°	90°	100°
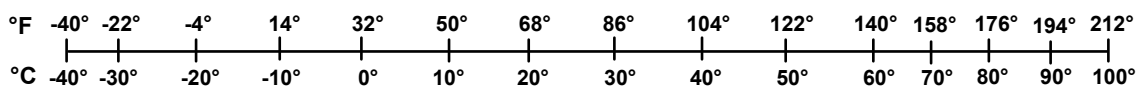
For more exact and or other conversion factors, see NIST Miscellaneous Publication 286, Units of Weights and Measures. Price $2.50 SD Catalog No. C13 10286

Acknowledgements

Contents

Illustrations

Tables

Executive Summary

Under tie pads (UTP) and under ballast mats (UBM) have been increasingly used in rail track construction to reduce maintenance costs by better distributing loads, reducing the track modulus, and increasing ballast contact areas with ties. Locations such as tunnels, bridges, and bridge approaches are especially strong candidates for UTP and UBM use due to the high support stiffness they provide to the ballast.

In this study, the Virginia Avenue Tunnel in Washington D.C., which uses UTP and UBM, was instrumented by the University of Florida during construction to monitor track pressure distribution, tie movement, and tunnel floor vibration during the first 20 months of use (July 2018 – February 2020). The pressure during loading was examined to determine the tie axle loading. To quantify the distribution of axle loads between ties, the pressure distribution for the third axle on the first locomotive was examined for each train recorded during this study. Settlement measurements showed that the track settlement occurred over the first six months of measurement, after which it stabilized to less than 0.157 in. (4 mm) of total settlement. Changes in track distance from the tunnel wall with time corresponded to ambient temperature changes over time.

The research team obtained track data collected by the FRA Automated Track Inspection Program (ATIP) system. Changes in track profile, gage, crosslevel, and curvature between successive ATIP measurements were calculated. Little difference in profile, gage, and curvature was seen, however an increase in crosslevel of 0.029 in. (0.7 mm) on average was measured. These measurements are indicative of the track quickly reaching a steady state with little deterioration in conditions after that with time.

1. Introduction

The track structure for the Virginia Avenue Tunnel (VAT) was instrumented to monitor the track performance with time. This report describes the track instrumentation plan, installation, data collected, and analysis performed.

1.1 Background

Trains are a vital part of the infrastructure of the United States, and while the technology and materials used by the railroad industry have advanced, the general design principles have remained the same, as described in the following paragraphs.

1.1.1 Typical Track Systems

Track systems are typically composed of rails, ties, ballast, subballast, and subgrade (Figure 1.1) [1]. The steel rail provides the smooth riding surface and spreads the wheel loads onto multiple ties, which in turn distribute the load onto the ballast over a wide area. Historically, ties were mostly made of timber; more recently, prestressed concrete ties have also been used in North America [2]. Under the ties, ballast, composed of granular stone (see Figure 1.2) of various types, is used to distribute load over an even larger area as the forces propagate downward, allow water to drain, and limit movement of the ties. 12 in. of ballast bellow the tie is typically provided by CSX in mainline track. The subballast provides a transition between the ballast and the subgrade so that particles do not migrate between the two layers over time. Finally, the subgrade provides a stiff foundation to transfer loads to the ground.
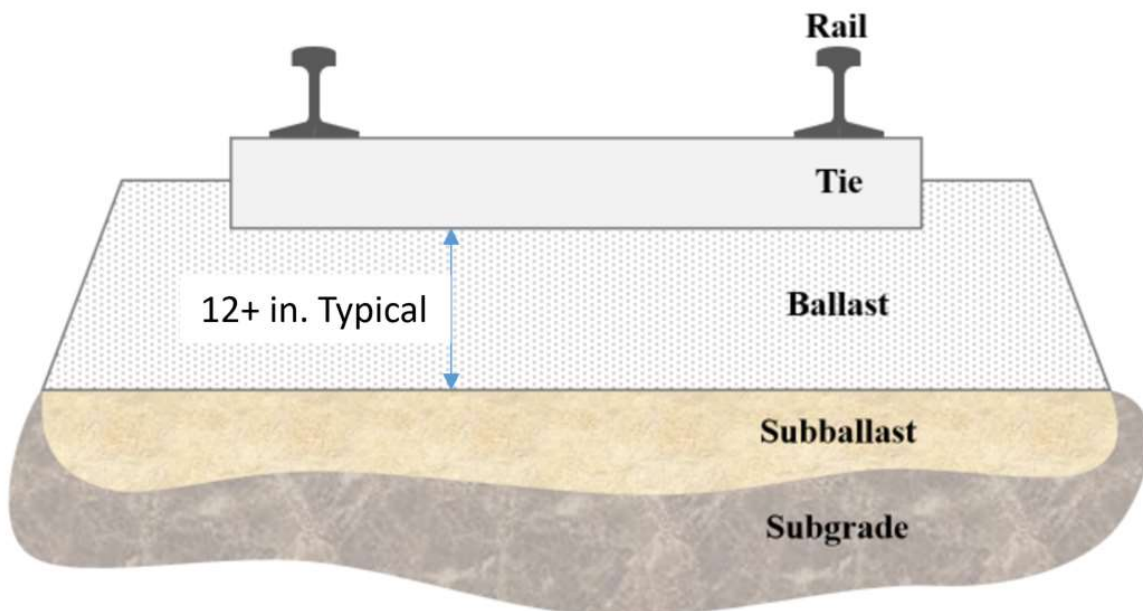
Figure 1.1. Cross-section of a standard railway

Figure 1.2. Rail at the west entrance to the tunnel showing the rail, prestressed concrete ties, fastener system, and ballast

1.1.2 Railway System Maintenance

As railway systems age, ballast can breakdown and foul the track due to the large strains induced in the ballast particles by the train loads. The rate of breakdown increases with increased moisture. As ballast deteriorates, voids in the ballast can form under ties, causing increased displacements and loads at those locations. These increased loads can cause cracking and accelerated tie deterioration. To lengthen the life of the rail structure, ballast is tamped frequently. The practice of tamping typically involves using a rail-mounted tamping unit, which lifts and realigns the rail and ties and pushes ballast under the ties, as illustrated in Figure 1.3. In doing this, any voids that have formed due to ballast breakdown are filled, greatly extending the longevity of ties while not having to replace the ballast.
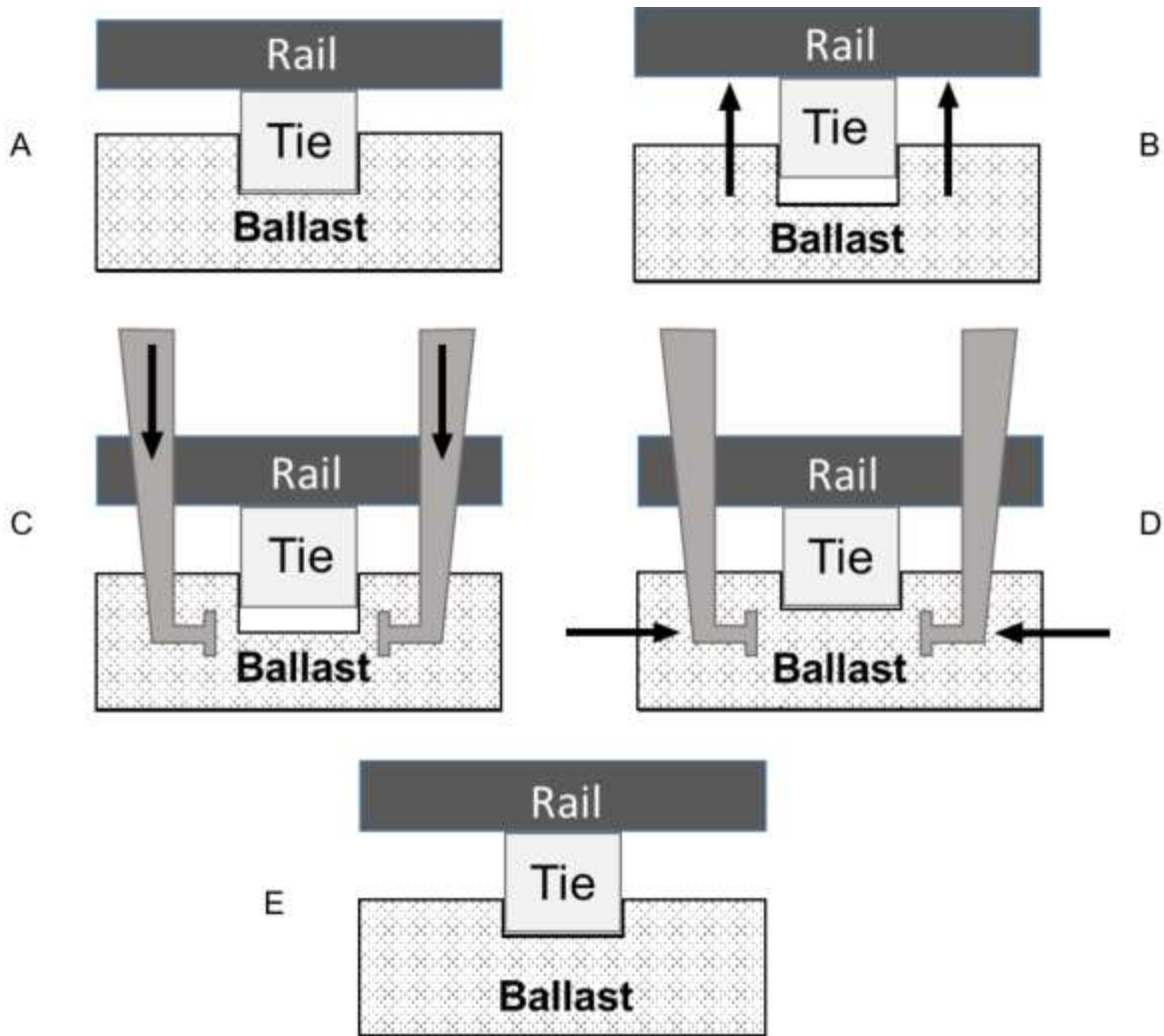
Figure 1.3. The process of tamping, a) track sitting low in the track, b) track is lifted to restore profile, c) tamping tines downfeed, d) tamping tines squeeze in ballasat, and e) tie profile restored with ballast support, after [3]

Even when proper maintenance is performed on the railway system, ties will eventually deteriorate and require replacement. Railroad companies often replace every second or third tie every few years rather than replacing them all at once to minimize the likelihood of neighboring ties decaying at the same time, and to minimize downtime of the railway.

1.1.3 Railway Structures

Railroad structures, such as tunnels and bridges, tend to have stiffer support conditions than standard track systems. Stiff track sections can cause accelerated ballast breakdown, excessive vibration, differential settlement, and higher track maintenance needs. These effects are even more pronounced at the approaches to railway structures, where subgrade changes from less stiff off the structure, to stiffer on the structure. To prevent breakdown in these areas, the subgrade in the approaches is typically transitioned gradually from the subgrade used off the structure, to the

subgrade used on the structure, which may be the concrete floor of a tunnel or the concrete slab of a bridge. These structure subgrades are stiffer than typical subgrade, and these differences in stiffness contribute to the change in behavior of the track system. To combat the increased rate of ballast and tie deterioration caused by stiff track conditions, engineers often utilize under ballast mats (UBMs) and under tie pads (UTPs) made of elastomeric material in their designs.

1.1.4 The Virginia Avenue Tunnel

CSX Corporation built the Virginia Avenue Tunnel in Washington, DC. It runs parallel to Virginia Avenue and a portion of I-695 as shown in Figure 1.4. Construction began in May of 2015 and was substantially complete in June of 2018, with the first trains running through the tunnel in mid-July. At the west entrance to the tunnel (Figure 1.5), there are two parallel tracks. After a few hundred feet the tunnel separates into two side-by-side tunnels (Figure 1.6). The tunnel is 22.5 feet tall and 17 feet wide in the regions where a single railway runs through the tunnel and was built in 48-foot segments of reinforced concrete. The tunnel walls are 30 inches thick and the floor, which acts as the subgrade of the rail system, is 36 inches thick. Granite ballast and prestressed concrete ties at a spacing of 20 inches on center were utilized in the tunnel. Figure 1.7 shows a schematic of the track section inside the tunnel. This tunnel is a classic example of a railroad structure with stiff track section and transition areas and was designed with UBM and UTP throughout the tunnel, however there is no UBM in the transition areas just outside of the tunnel. The UBM is composed of resin-bonded rubber with a polypropylene non-woven geotextile bonded to the surface. The UBM, is 0.39 inches thick, and has a puncture resistance of 978 pounds [4]. The UTP is 0.28 inches thick and has a tensile strength of 138 psi [5]. UTP and UBM were used in the tunnel to reduce the track modulus, reduce pressure on ballast particles to reduce ballast breakdown and maintenance, and reduce track vibration and noise. Figure 1.8 shows a picture of the instrumented ties before installation with the tie bottoms facing up, showing the UTP. Figure 1.9 shows the UBM during installation in the tunnel.
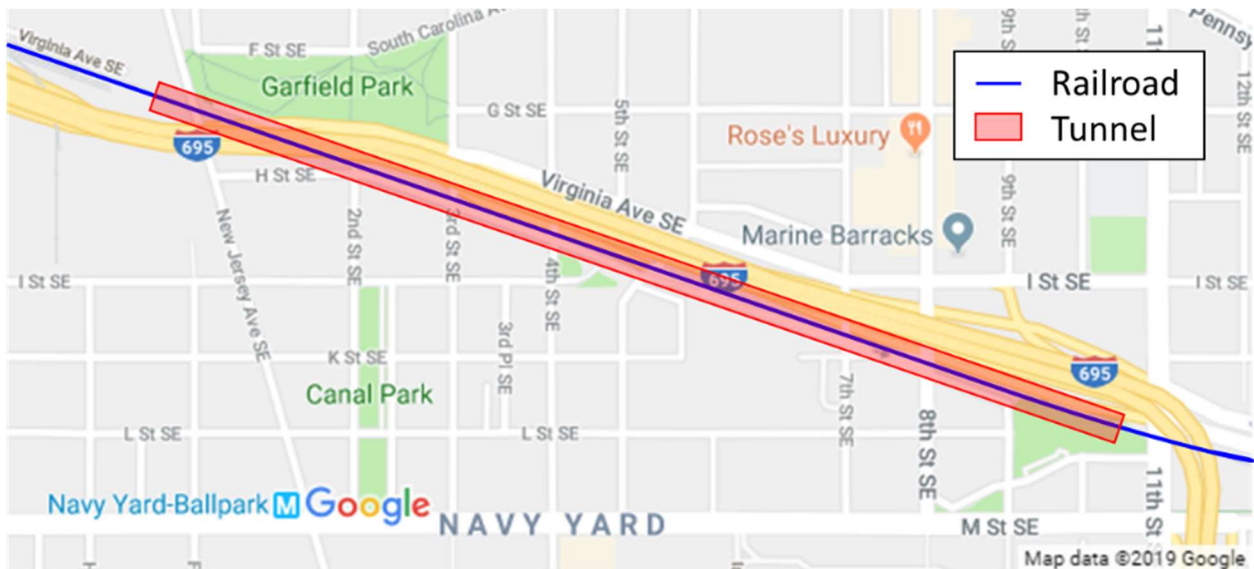
Figure 1.4. Map view showing the location of the railway and the tunnel [6]
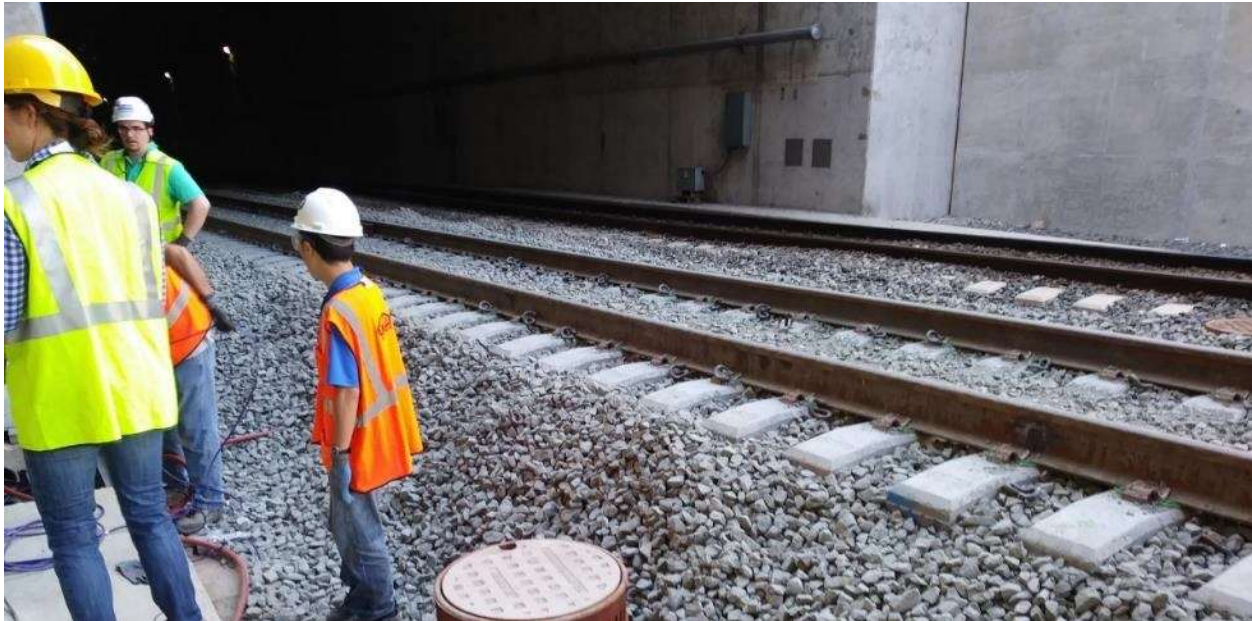
Figure 1.5. Rails running parallel through the tunnel at the west entrance

Wall that splits tunnel into two tunnels
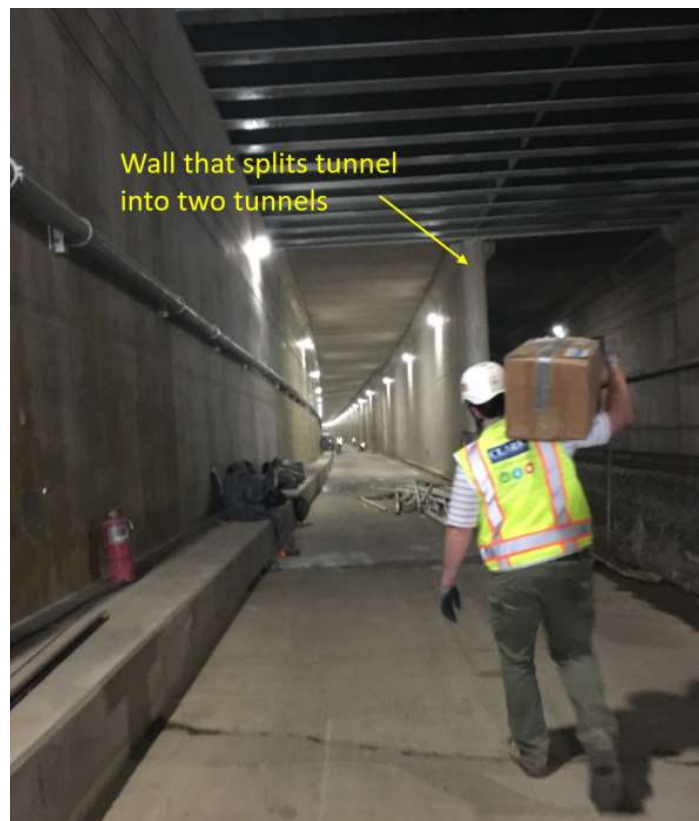
Figure 1.6. Partially obstructed view of the beginning of the wall where the tunnel splits into two tunnels
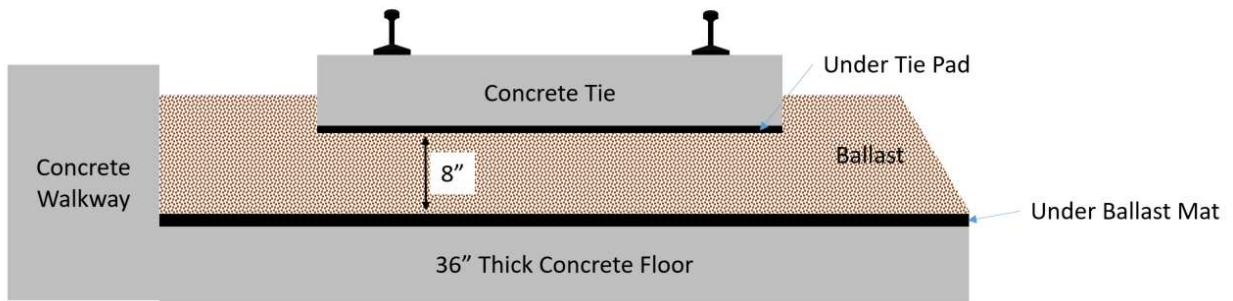
Figure 1.7. Schematic for track section inside tunnel

Figure 1.8. Instrumented prestressed concrete ties with the tie bottom side up showing the UTP at the tunnel storage yard before installation, with sensor wires protruding from the ties and stored in a crate on top of the ties

Figure 1.9.UBM during installation in the tunnel

Three locations along the tunnel were selected for instrumentation, hereafter referred to as the Portal, Station 16, and Station 23. These three locations were selected to provide a representative view of the tunnel.

The Portal is located at the west tunnel entrance where the subgrade transitions from asphalt outside of the tunnel to concrete inside the tunnel as illustrated in Figure 1.10. There are two parallel tracks entering the tunnel at this location, as shown in Figure 1.5. There is no UBM in this area and the depth of the ballast changes from 14 to 8 in. Sensors were deployed at this location to enable assessment of the transition area behavior.
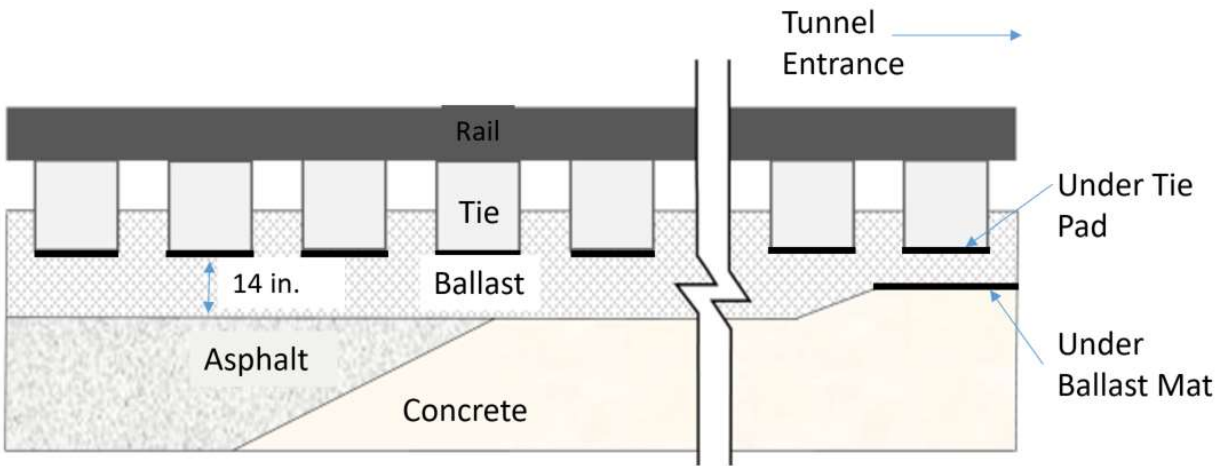
Figure 1.10. Illustration of transition from asphalt to concrete at the Portal location

Station 16 is located at the lowest elevation in the tunnel and is 768 ft from the Portal. In this section of tunnel, the two parallel tracks are separated by a concrete wall. As this is the lowest point in the tunnel, there is a drainage system with a sump pump to prevent a buildup of water. Since the presence of water expedites the breakdown of ballast, the ballast in the vicinity of this location may be particularly susceptible to breakdown. Monitoring this location is intended to provide insight into the effect of moisture on the breakdown of ballast over time.

Station 23 is a more typical area of the tunnel and it is located 336 ft from Station 16 or 1,104 ft from the Portal. Only one rail system runs through this section of tunnel.

1.2   Objectives

The objective of this project is to quantify long-term settlements and changes in force distributions on track systems with stiff support conditions and in railroad structure transition areas, as well as to assess the benefits of UBM and UTP to decrease the rate of deterioration of the ballast and ties. These system changes and benefits are quantified over an extended period by means of a comprehensive monitoring system that was developed and deployed in the tunnel during its construction. Data processing methods were developed to quantify pressure distributions, vibration levels, and displacements in the track structure and to monitor the change in the system over time.

1.3   Overall Approach

This study three sections of newly constructed railroad track. Two sections were inside of the tunnel, while a third was in the transition area just outside of the tunnel for comparison. Measurements included track pressure, tie acceleration, track moisture content, and rail strain.

1.4 Scope

This work covers instrumentation of track at the Virginia Avenue Tunnel and analysis of the collected data. It does not include any modeling performed to extrapolate the benefits of UTP and UBM to other track conditions.

1.5 Organization of the Report

This report is organized as follows: Chapter 2 summarizes the sensor selection and installation configuration. Chapter 3 explains the data acquisition and management system that was developed for this project. Chapter 4 describes the sensor and data acquisition system installation process done during the tunnel and track construction. Chapter 5 provides a description filtering and processing methods used. Chapter 6 contains results of the measured track performance. Finally, conclusions based on the data analysis are given in Chapter 7.

2. Instrumentation

The Virginia Avenue Tunnel, built by CSX Corporation, uses both UBM and UTP, making it a good case study to quantify the impact of their use on track load distributions and geometry. UBM and UTP are thought to improve track performance and reduce maintenance requirements at track transition areas and in areas of stiff track conditions, which are commonly found in tunnels and bridges [7] [8]. A monitoring and data acquisition system was designed for installation at two locations inside the tunnel and at the west entrance to the tunnel. Each location was unique and therefore the systems deployed at each location varied slightly to reflect that. The details of the sensors that were selected, as well as where they were deployed, are discussed in this chapter.

2.1 Sensor Selection

Sensors were selected to measure the distribution of pressures in the ballast, tie and tunnel floor vibration, moisture content in the ballast, horizontal and vertical tie displacement, and vertical rail strain in the web. Since the sensors were to be installed in and around the ballast, all sensors selected are waterproof and resilient to extreme conditions and excessive shock. These characteristics were required to ensure accurate and reliable measurements throughout the course of data collection.

2.1.1 Pressure Cell

The purpose of deploying pressure cells in the tunnel was to measure the distribution of the forces imposed by each train as they propagate through the ballast. Using multiple pressure cells at different depths and locations within the ballast, and at each of the different locations along the tunnel provides data that allows for a better understanding of force distribution throughout the ballast, as well as how force distributions change as the ballast settles and breaks down. Geokon 3515 earth pressure cells [9] were selected for this purpose. These pressure cells were designed specifically for railroad track applications; therefore, they have sufficient ruggedness to provide reliable data over the monitoring period. These pressure cells consist of two stainless steel plates welded together with a fluid-filled cavity in-between (Figure 2.1). The incompressible fluid transfers the force applied to the plates to a pressure transducer, following the basic principles of hydraulics, via a small stainless-steel tube. This sensor has a measurement range of vacuum to 870 psi.
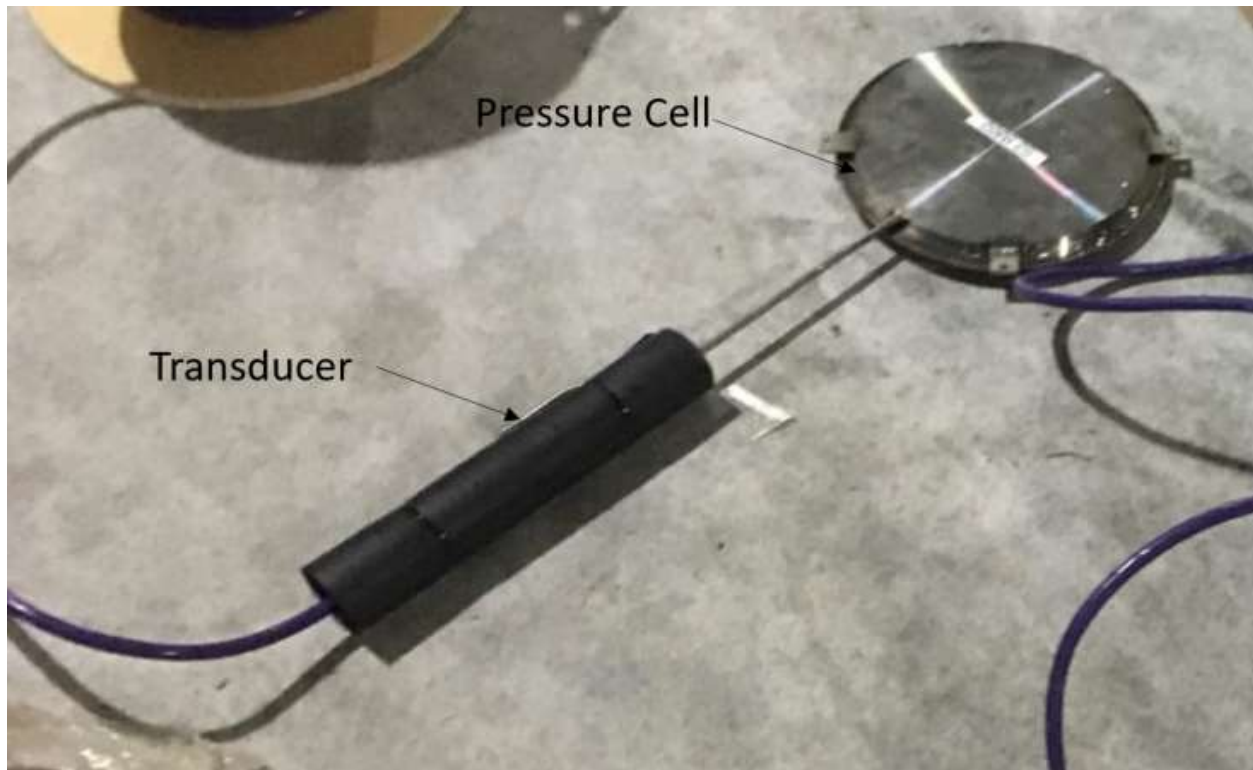
Figure 2.1. Geokon 3515 pressure cell

The purpose of using accelerometers was to gain an understanding of how vibrations propagate from the rail to the tunnel floor, and how this propagation changes over time. Furthermore, accelerometers have low levels of noise and may be used to reliably identify the approach of a train to the monitoring locations. Identification of a train is key to developing an automated data collection triggering system (see Chapter 4). PCB W356B11 triaxial accelerometers were selected to measure vertical, horizontal, and longitudinal accelerations at ties, as shown in Figure 2.2. These accelerometers have a sensitivity of 10 mV/(m/s²), a measurement range of ±4,905 m/s², and can sample at frequencies from 2 to 7,000 Hz.

Figure 2.2. A PCB 356A01 triaxial accelerometer installed at the Portal

Dytran 3217A uniaxial accelerometers were selected to measure the accelerations in the track floor. These accelerometers have a sensitivity of 10 mV/(m/s²), a measurement range of ±490 m/s², and can sample at frequencies from 1 to 10,000 Hz. Uniaxial accelerometers were chosen for these locations because the acceleration in the vertical axis should be most significant and because uniaxial accelerometers are more affordable than the triaxial accelerometers.

2.1.2 Strain Gage

Vishay 350 Ω quarter-bridge foil strain gages as shown mounted on the rail web in Figure 2.3 were selected to obtain a relative measure of the force imposed on the track. These sensors are inexpensive and the data from these gages can be used to determine exactly when the train is passing over that point in the track because, unlike the accelerometers or pressure cells, the strain gage will see very little to no strain until the train is directly overhead. This makes the strain gages also very useful to determine when a train passes, see Chapter 4 for more information.

Figure 2.3. Photo of Vishay 350 Ω quarter-bridge foil strain gage on the web of the rail before protective coating was applied

2.1.3 Moisture Sensor

Breakdown of ballast is expedited by increased moisture, therefore, to analyze and compare the breakdown of the ballast at different locations, it is important to quantify the moisture in the ballast. The Decagon GS1 Rugged VWC moisture sensor was selected for this purpose. This sensor has a measurement range of 0 to 100% volumetric water content (VWC) and a frequency of 100 Hz.

2.1.4 Displacement Sensors

As ballast settles and breaks down over time, it is expected that the ties will undergo vertical settlement. In addition, the ties will experience short-term displacements caused during the passage of each train. BOD 63M laser displacement sensors were selected to measure these displacements at the ties (Figure 2.4). These sensors have a measurement range of 200 to 2000 mm with an accuracy of ±5%. By utilizing two sensors at each location, with each one pointed at targets with different known angles of inclination as shown in Figure 2.4, vertical and horizontal displacements can be determined. Black and yellow visibility tape was used to minimize the risk of anyone tripping on the equipment.

Figure 2.4. a) Laser displacement sensors attached to the wall and b) the laser targets mounted on the top of the tie end

2.2 Sensor Configuration

The research team deployed a total of 35 sensors at the Portal and Stations 16 and 23 to collect data to provide insight into the behavior of the track and the effects of the UTP and UBM. Table 2.1 shows the number and types of sensors deployed at each location. The research team mounted three strain gauges vertically on consecutive ties at Station 16 to determine if the train was above the tie, or on one next to it to help determine load distribution. The research team did not end up needing to use the strain gauge data in the analysis because the pressure data collected had sufficient resolution to determine when a train was passing and at what speed.

Table 2.1. Number of sensors at each location.

Sensor type	Portal	Station 16	Station 23
Pressure Cell	5	6	6
Triaxial Accelerometer	1	1	1
Uniaxial Accelerometer	1	1	1
Strain Gage	1	3	1
Moisture Sensor	1	1	1
Laser Displacement Sensor	0	2	2

2.2.1 Pressure Cells

At the different locations, pressure cells were deployed in various configurations. In total, 17 pressures cells were installed. Eight pressure cells were embedded in the bottom of the ties, and the remaining nine were placed on or in the tunnel floor. Some sensors were aligned directly beneath the rail and others beneath the center of the ties. UBM and UTP were removed at some locations so that the pressure cells are in direct contact with the ballast. Details on the configuration of each of the pressure cell are given in Table 2.2 and in Figure 2.5. The individual pressure cells were labeled using the abbreviation for the location of the sensor within the tunnel and the sensor numbers at that location found on Table 2.2.

Table 2.2. Location and configuration of the pressure cells

Pressure cell number at location	Portal (PP)	Station 16 (16P)	Station 23 (23P)
1	On concrete tunnel floor, aligned with rail (no UBM)	Embedded in tunnel floor, aligned with center of tie (beneath UBM)	Embedded in tunnel floor, aligned with center of tie (beneath UBM)
2	On transition floor, aligned with rail (no UBM)	On top of UBM, aligned with center of tie	On tunnel floor, aligned with rail (no UBM)
3	On asphalt base, aligned with rail (no UBM)	On top of UBM, aligned with rail	On top of UBM, aligned with rail
4	Embedded in tie over asphalt base, aligned with rail (over UTP)	Embedded in tie, aligned with rail (no UTP)	Embedded in tie, aligned with rail (no UTP)
5	Embedded in tie over concrete base, aligned with rail (over UTP)	Embedded in tie, aligned with center of tie (over UTP)	Embedded in tie, aligned with center of tie (over UTP)
6	-	Embedded in tie, aligned with rail (over UTP)	Embedded in tie, aligned with rail (over UTP)

a)

A A
B B
C C

Concrete

Transition

Asphalt

b)

Rail

Under Tie Pad

PP5

Concrete Tie

Pressure Sensors

14"

Granite Ballast

PP1

Concrete Floor

A-A
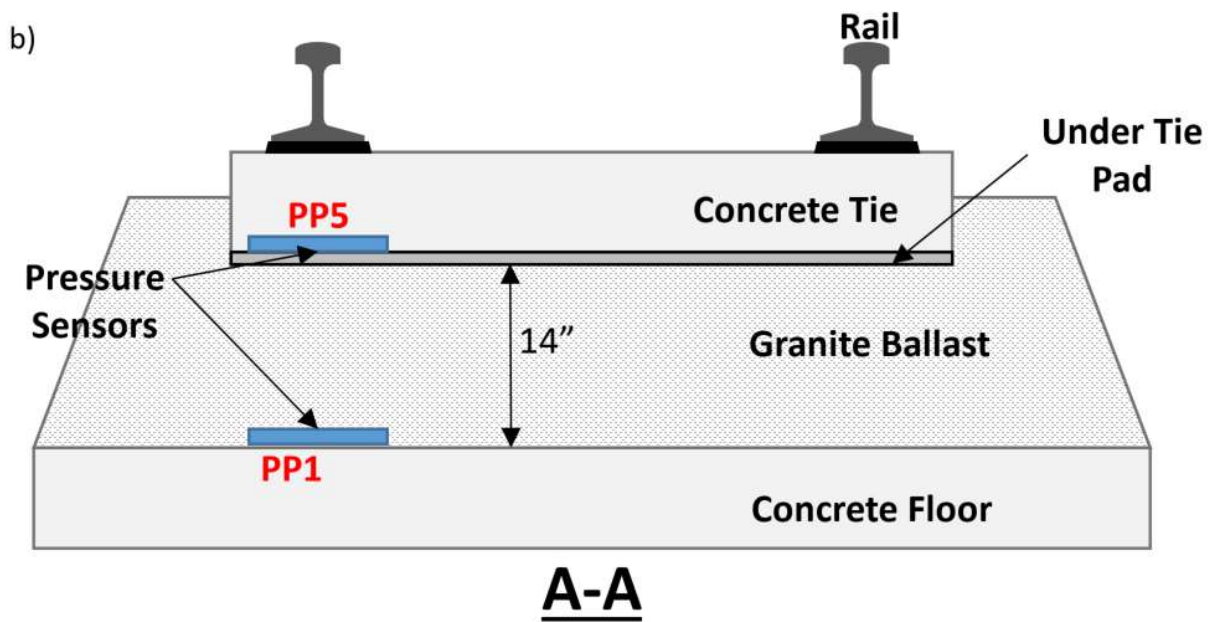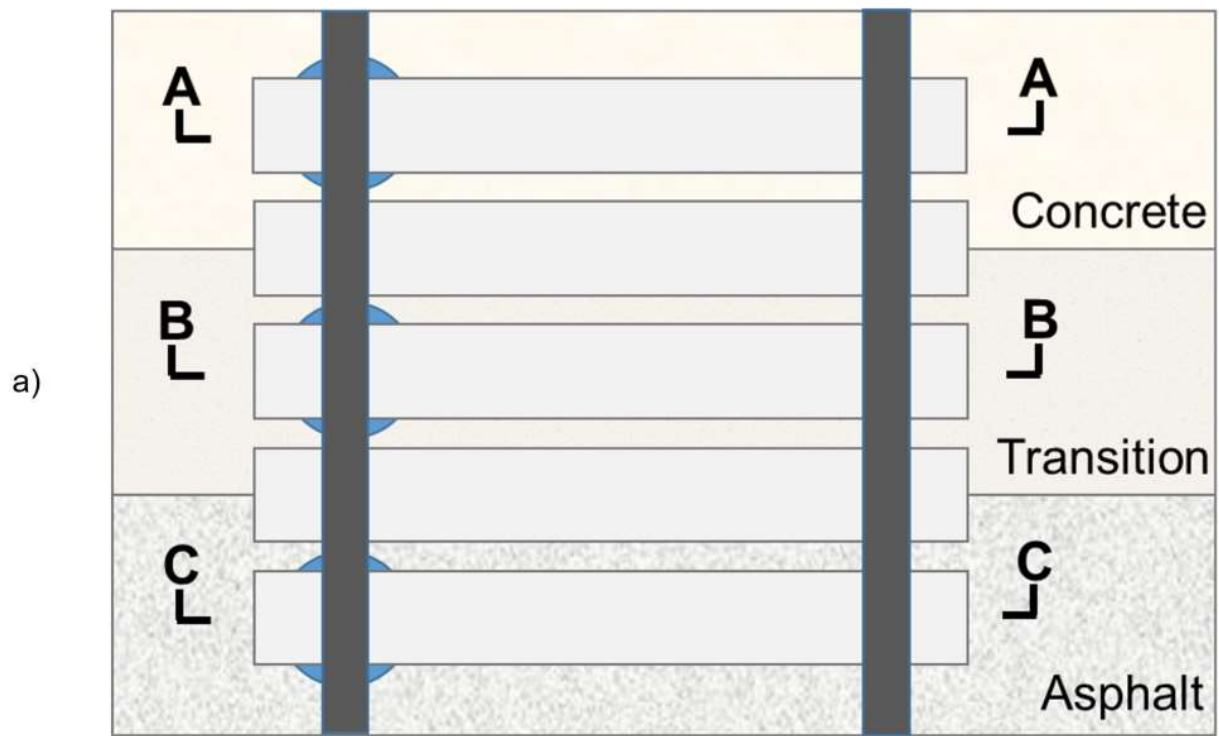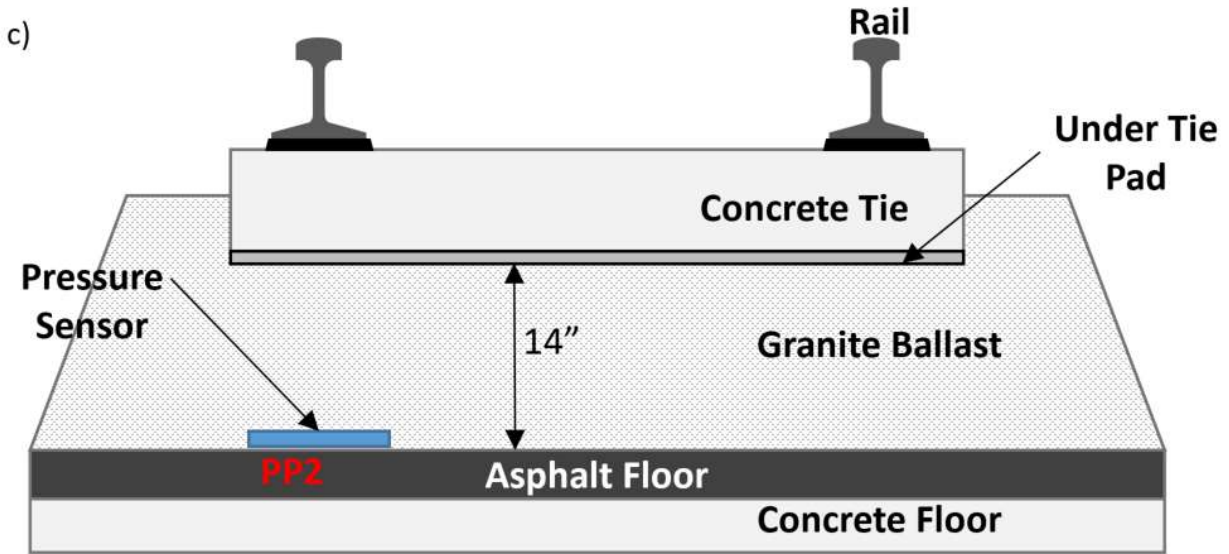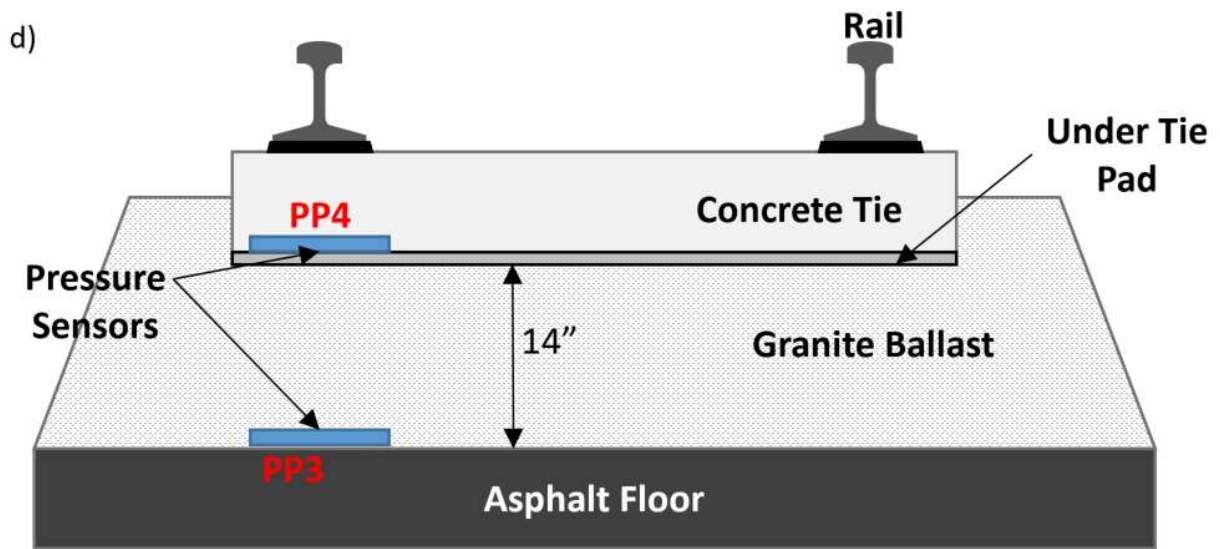
Figure 2.5. Diagrams depicting the pressure sensor deployment at Portal a) top view, b) side cross-sectional view of concrete zone in area A-A shown in top view, c) side cross-section view of transition zone in area B-B of top view, and d) side cross-section view of asphalt zone in area C-C of top view

2.2.2 Accelerometers

The triaxial accelerometers were all attached to thin and flat steel plates or rectangle boxes using Loctite Liquid Adhesive. The steel plates were mounted to the ties with multiple screws. The uniaxial accelerometer at the Portal was adhered to the concrete tunnel floor using steel plates, while those at Station 16 and Station 23 were embedded and grouted in the concrete floor along with the pressure cells. The accelerometer configurations can be found in Figure 2.6 and Figure 2.7. The accelerometers mounted on the concrete floor at the Portal was placed under the rail seat area as that was deemed the likely location of the highest vibrations and concrete floor acceleration. Because of limitations from construction, the accelerometers placed on the tunnel floor could only be placed under the center of the tie.
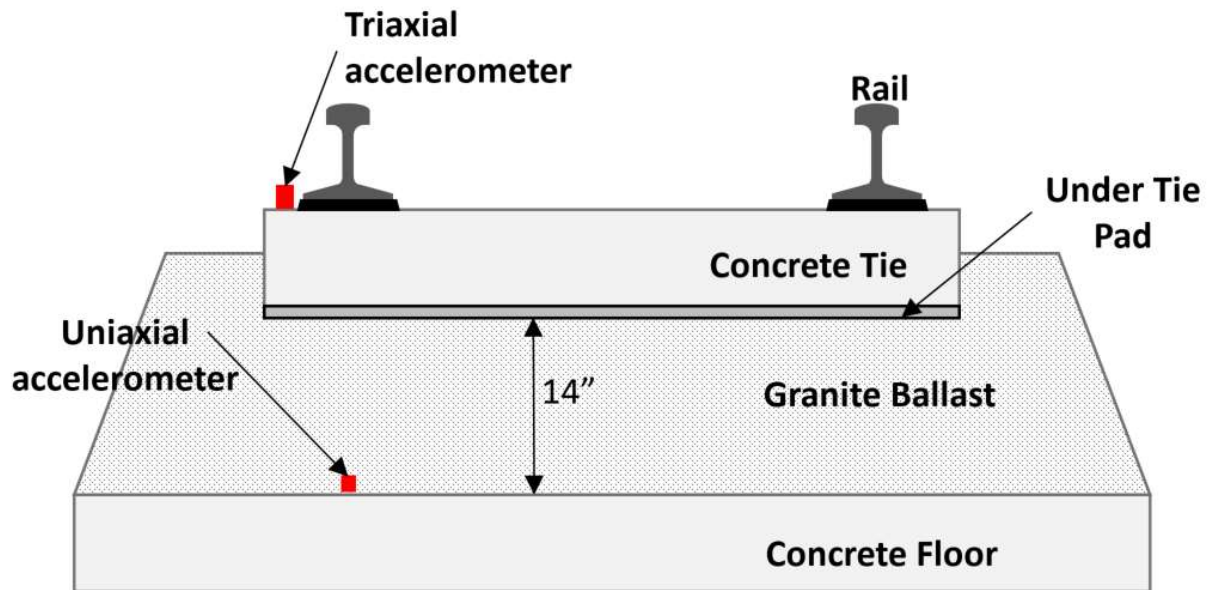
Figure 2.6. Accelerometer configuration at Portal Location
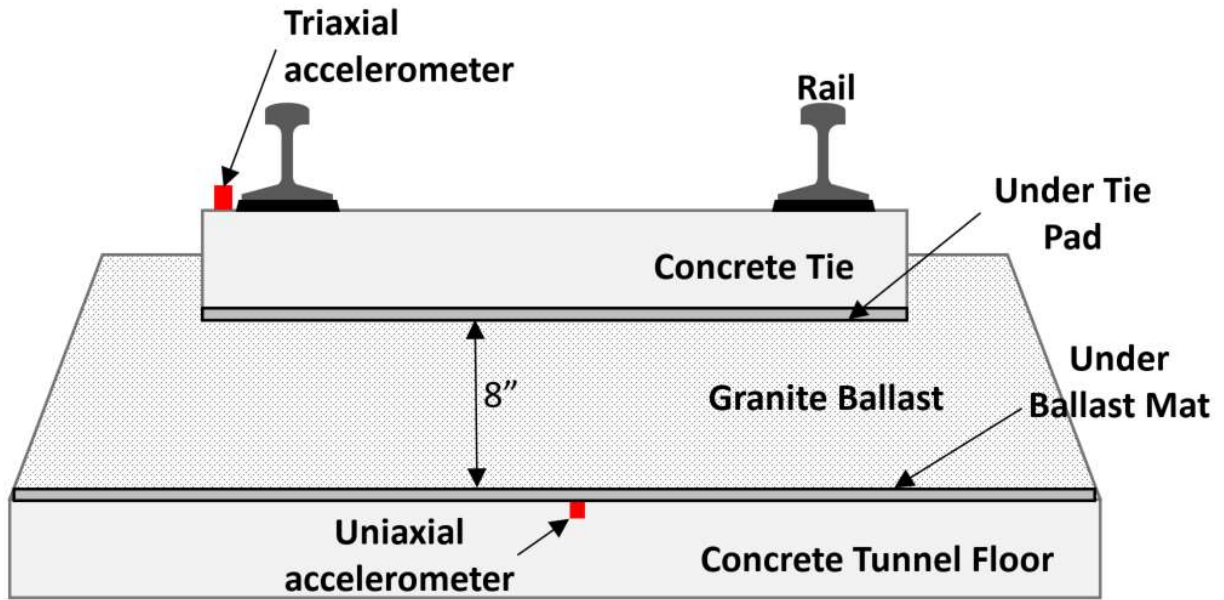
Figure 2.7. Accelerometer configuration at Stations 16 and 23

2.2.3 Strain Gage

The strain gages were adhered to the web of the rail closest to the walkway using standard liquid strain gauge adhesive (Figure 2.8). The rail surfaces were cleaned and degreased prior to installation to ensure a secure bond.
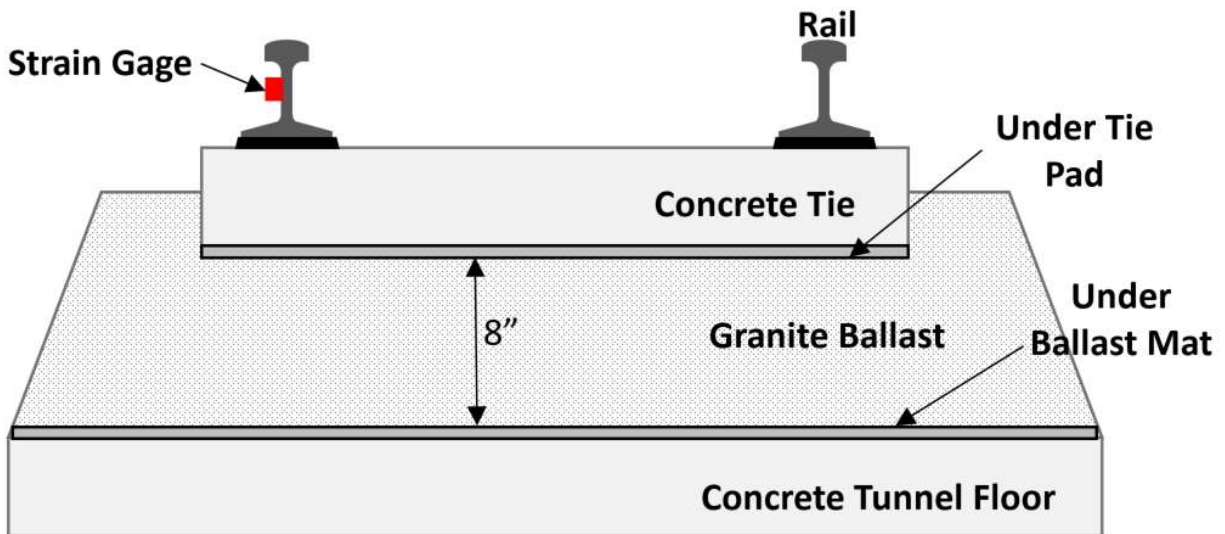
Figure 2.8. Strain gage configuration at the Portal and Stations 16 and 23

2.2.4 Moisture Sensor

The moisture sensors were fastened to the UBM and embedded within the ballast, as shown in Figure 2.9. The moisture sensor was embedded in the track section nearest the walkway to simplify wiring.
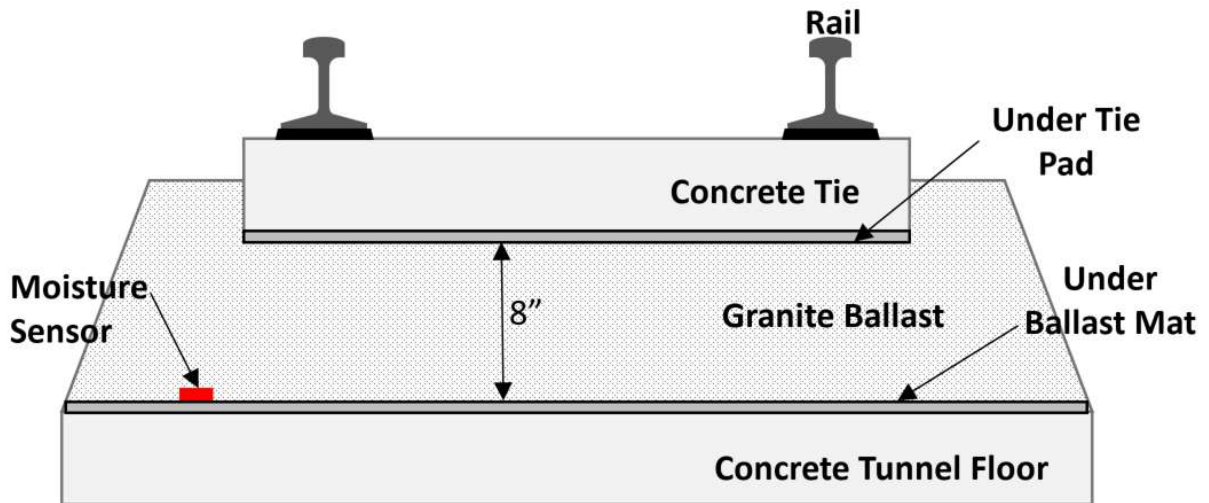
Figure 2.9. Moisture sensor configuration at the Portal and Stations 16 and 23

2.2.5 Laser Displacement Sensor

As described previously, two laser sensors were deployed at Station 16 and at Station 23. The sensors were placed in protective enclosures and attached to the walkway that runs along the length of the tunnel. The lasers were pointed to steel targets which were attached to a tie and located 55 to 58 inches away from the sensor, as seen in Figure 2.4 and Figure 2.10.
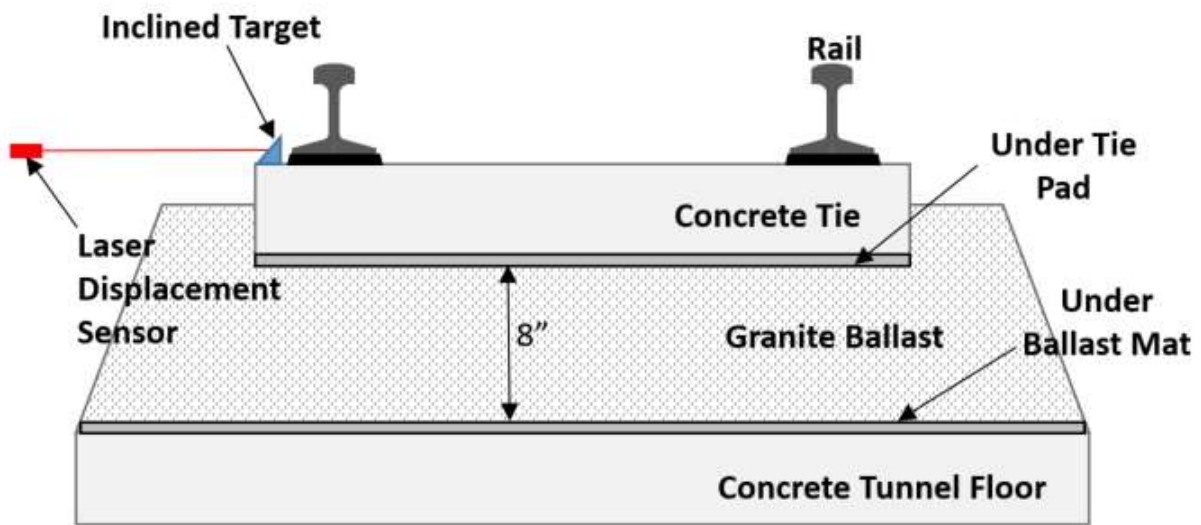
Figure 2.10. Configuration of a laser displacement sensor

3. Data Acquisition and Management

The sensors discussed in Chapter 2 output analog signals as a voltage and/or current. These signals are converted into a digital form so that they can be collected and transferred to a server for storage and analysis. The process of converting the raw output of the sensors into data that can be analyzed was performed by the data acquisition and management system. An overview of this system can be seen in Figure 3.1 and is described in more detail in the following sections.
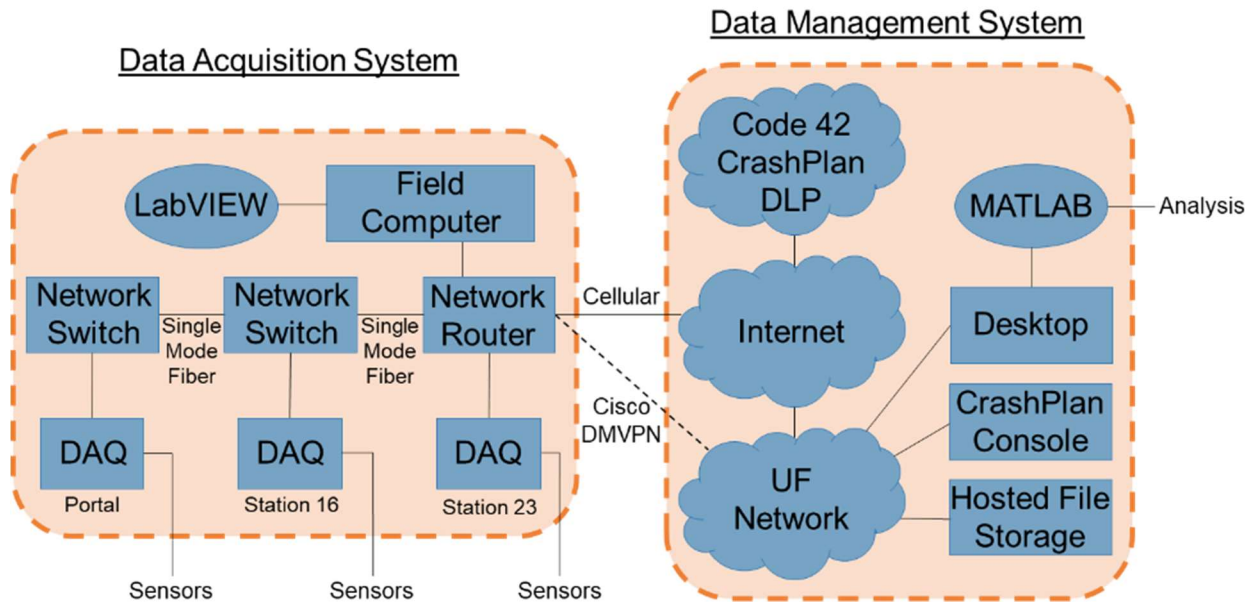
Figure 3.1. Overview of the data acquisition and management system

3.1　Data Acquisition System

The data acquisition system collected output from the sensors, converted it into a digital data stream, and then transferred that data to the data management system, which will be discussed in section 3.2. The different components of the data acquisition system were stored in secured data acquisition cabinets at each of the three locations. At Stations 16 and 23, recesses in the wall were left during construction for the data acquisition cabinets, as shown in Figure 3.2. The cables belonging to each sensor were protected from the ballast by a protective flexible conduit and they passed through the conduit into an accessible recess below the walkway, as shown in Figure 3.3. Conduit running vertically from the recess brought the cables into the cabinet. Conduit installed along the length of the tunnel in the walkway housed the fiber optic cables used for networking which ran between the cabinets at the three locations, seen in Figure 3.4. The cabinets were powered by standard 120 VAC outlets which were located close to the cabinets. The different components which made up the data acquisition system housed in the data acquisition cabinets are shown in Figure 3.5. Figure 3.6 shows a schematic overview of these different components used for data acquisition and networking.

Figure 3.2. View of a recess used for the data acquisition cabinet at Station 23

Figure 3.3. View of cables passing through recess under the walkway to the conduit leading to the data acquisition cabinet
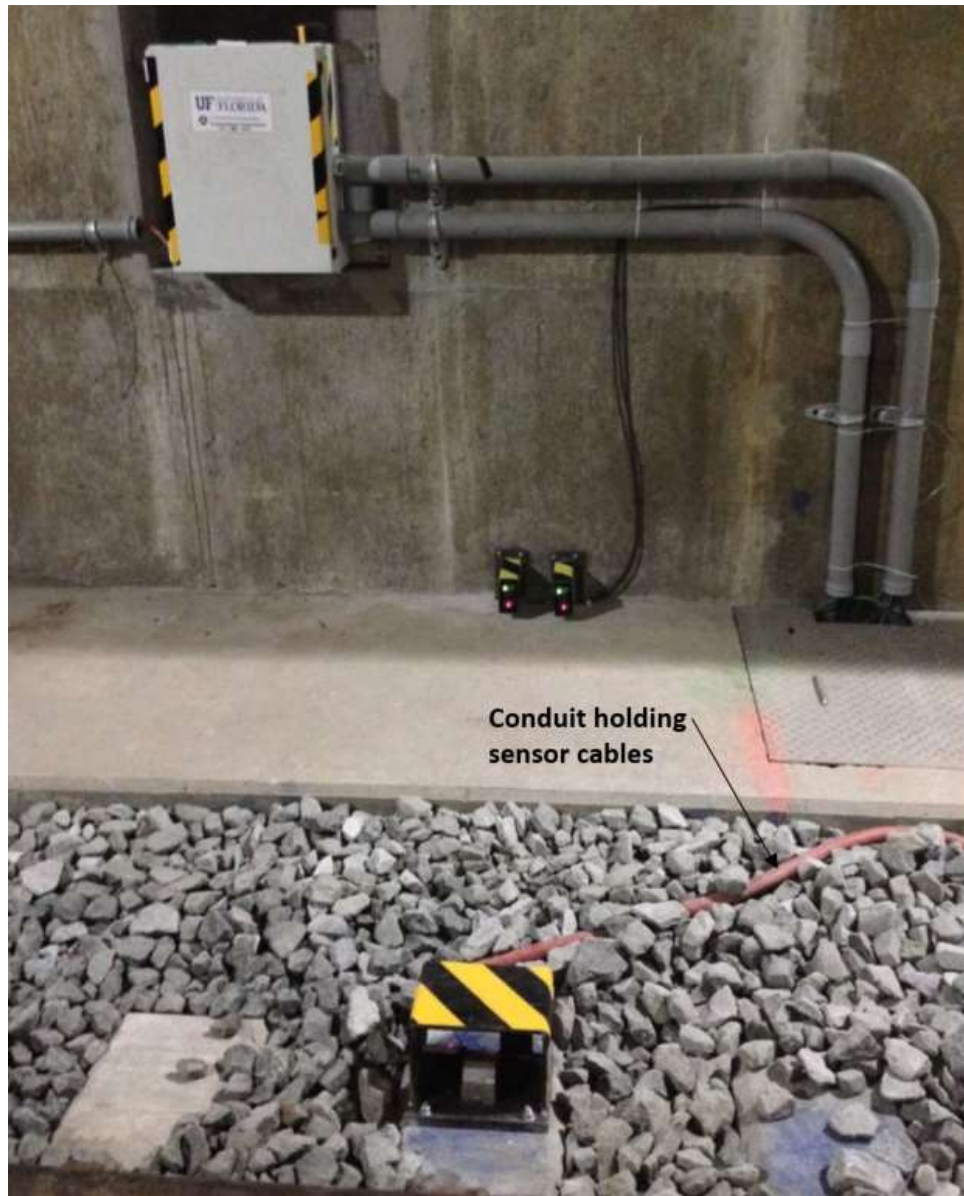
Figure 3.4. View of the data acquisition cabinet at Station 23 showing the conduit through which the sensor cables and fiber optic cables pass
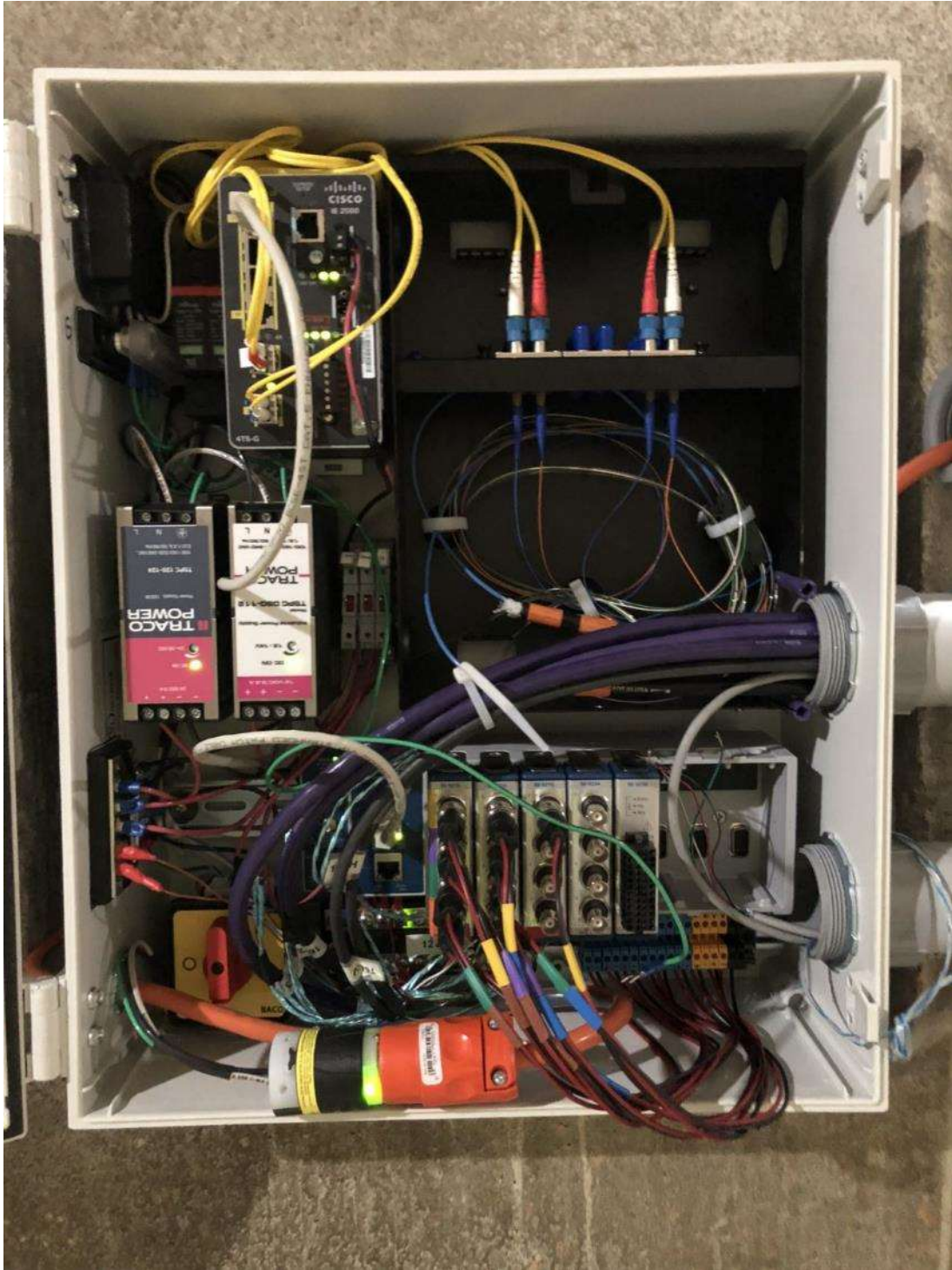
Figure 3.5. Interior of the data acquisition cabinet at Station 16
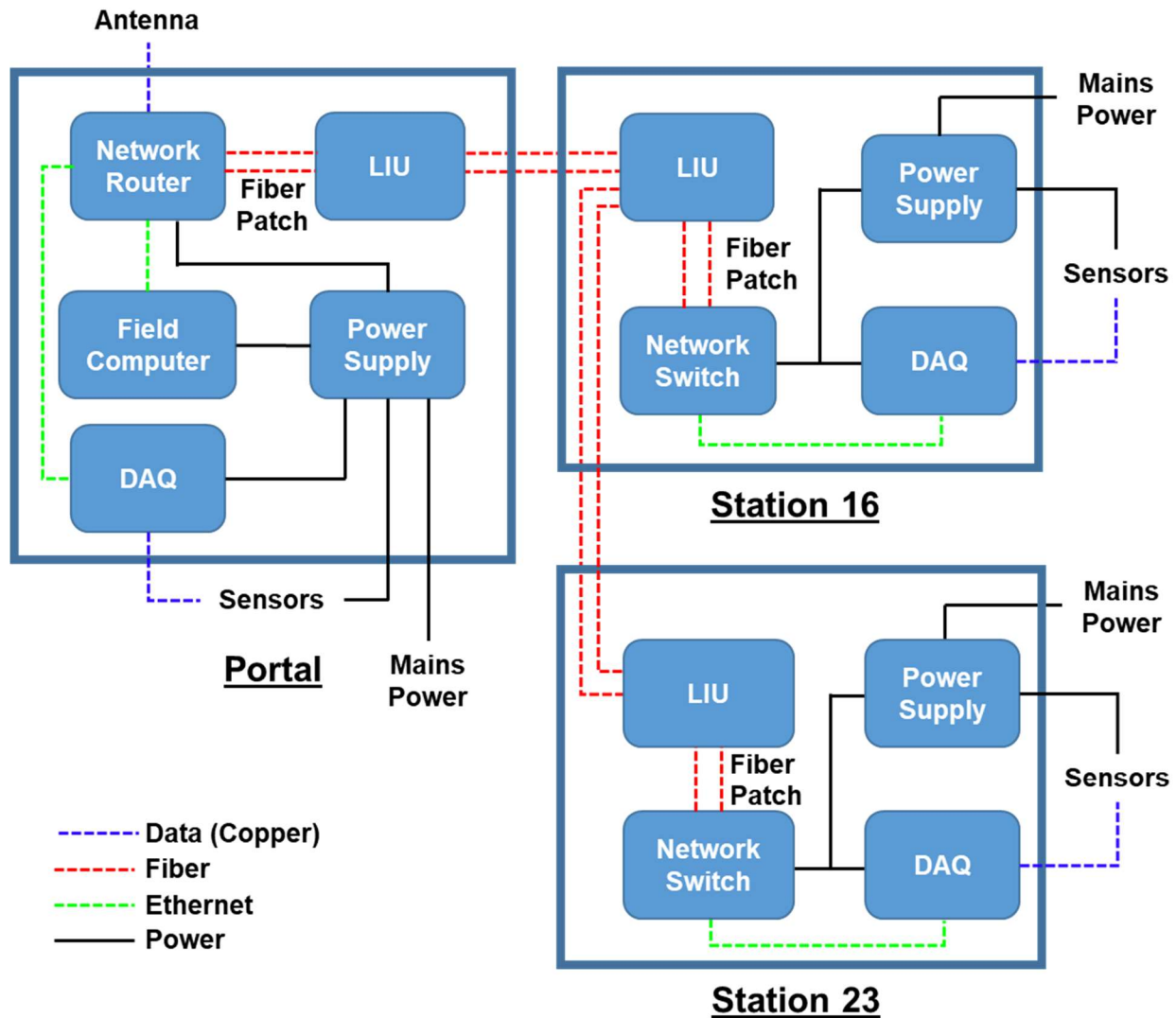
Figure 3.6. Diagram showing the components inside of the data acquisition cabinets at the three locations within the tunnel, with the light interface unit (LIU) used to facilitate communication between locations

3.1.1 CompactDAQ system

To obtain data from the sensors, the analog output (voltage or current) collected by the sensors needed to be digitized before they could be recorded and processed. The research team elected to use a National Instruments CompactDAQ System, from here on referred to as the DAQ, for data sampling and analog-to-digital conversion.

The data acquisition (DAQ) was comprised of the CompactDAQ chassis and the CompactDAQ modules that connected to it. A four-slot cDAQ-9185 CompactDAQ networked chassis was used at the Portal, and eight-slot cDAQ-9188 CompactDAQ networked chassis were used at Station 16 and Station 23. The specific module paired with each sensor depended on the output of the

sensor and whether it was powered by an external power supply or by the CompactDAQ directly. Table 3.1 shows the data acquisition module type used with each sensor type used.

Table 3.1. CompactDAQ Module used for each type of sensor.

Sensor	CompactDAQ Module	Number of Channels	Description
Pressure Cell	NI-9215	4	C Series Voltage Input Module
Laser Displacement Sensor	NI-9215	4	C Series Voltage Input Module
Moisture Sensor	NI-9215	4	C Series Voltage Input Module
Strain Gage	NI-9236	8	C Series Strain/Bridge Input Module
Triaxial Accelerometer	NI-9234	4	C Series Sound and Vibration Input Module
Uniaxial Accelerometer	NI-9234	4	C Series Sound and Vibration Input Module

The pressure, laser, and moisture sensors all required an external power source and output voltage signals, and were connected to an NI-9215 module (4 channels). The piezoelectric accelerometers were connected to NI-9234 modules (4 channels), as they required a current source for power. The strain gages connected to the NI-9236 module (8 channels), which were made specifically for strain gages and other bridge-based sensors.

The digitized signals from each DAQ were transmitted via fiber optic cable to the field computer at the Portal location, which ran National Instruments LabVIEW software. A LabVIEW VI wrote the data to a file and stored it on the field computer's local storage until it was sent to the Data Management System via Internet.

3.1.2 Network switch

At Stations 16 and 23, Cisco Industrial Ethernet 2000 Series Switches were used to take the data that is being output from the DAQ via 100 Base-TX Ethernet cable, and transfer it via single mode fiber optic cable installed between each monitoring location to the field computer.

3.1.3 Network router

At the Portal location, a Cisco 829 Industrial Integrated Services Router was used. This router had the same capabilities as the network switch; however, it also used the Verizon LTE Network to connect the network to the University of Florida computer network over the Internet, by means of a Dynamic Multipoint Virtual Private Network (DMVPN). An unlimited data plan with Verizon was used; however, traffic shaping (aka data throttling) was possible when data transfers exceeded 25-GB during a month of service.

Once the field computer was connected to the Internet, the files that were stored locally were transferred to the UF hosted file storage and the Code 42 CrashPlan data loss prevention (DLP) data backup system, which were both part of the Data Management System. Automated scripts were written to transfer files from the local storage on the field computer to the UF hosted file storage via the Cisco DMVPN, however transferring the files directly to both Code 42 CrashPlan DLP and the hosted storage would use up twice as much cellular service and cause usage to surpass the data limit of the cellular plan more quickly.

3.1.4 Fiber patch panel

A fiber patch panel, also referred to as a light interface unit (LIU) was used to manage and rout the fiber optic cables that transfer data between the data acquisition cabinets. Each device was connected using two cables, one for transmitting, and one for receiving.

3.1.5 Power supply

Each cabinet had two direct current (DC) power supplies, 12 V and 24 V. The power supplies took the AC power and converted it to the set DC voltages required to power the sensors and DAQ components.

3.2 Data Management System

3.2.1 Code 42 CrashPlan DLP and CrashPlan Console

The Network Router transferred the data that was stored locally on the field computer to Code 42 CrashPlan DLP over the Internet. Code 42 CrashPlan DLP is a cloud-based data backup service that allows users to upload data for safe storage and, if necessary, allows them to restore their data using the application CrashPlan Console and manage the data stored on the CrashPlan servers. CrashPlan Console also verified that the data stored on their servers matched exactly with the data stored on the field computer.

3.2.2 Hosted File Storage

One terabyte of hosted file storage was purchased from UF for safe, redundant storage of the raw and processed data. To transfer the sensor data into the hosted file storage, a member of the UF research team periodically used CrashPlan Console to restore the data stored on the CrashPlan servers into the hosted file storage. By transferring data into hosted storage, the ease and speed of access was significantly increased, and redundant storage was ensured.

3.2.3 Data Processing and Analysis

Once the data files were made available on the UF hosted file storage, the data was easily accessed via desktop and data analysis was performed. The research team has developed data processing algorithms in MATLAB that separated data files into individual trains to perform analysis. These algorithms are discussed in Chapter 4.

3.2.4 Remote Management

With the computer connected to the UF Network via cellular connection to the Internet and a VPN, remote management was easily conducted through the Microsoft Remote Desktop tools. Maintenance activities included periodic monitoring of data signals and updating of the LabVIEW VIs. The field computer used the Windows 10 operating system which, by default, ran windows updates and reboots the computer periodically to apply the updates. These abilities were disabled to ensure that the automated updating process did not interfere with data collection. As such, maintenance activities also include periodically running the windows updates tools by hand and rebooting when necessary to minimize the potential of these activities occurring while a train was passing.

4. Installation

The installation of the sensors and data acquisition equipment described in Chapters 2 and 3 was carried out in stages between February and August 2018 that were dictated by the tunnel construction schedule. Prior to installation, each sensor and data acquisition component was tested in the laboratory at UF to ensure they were operating correctly. In addition, the data acquisition, power, and communications systems were connected end-to-end in the laboratory to test the full system operation.

4.1 Installation at Concrete Tie Plant

In February, members of the research team went to the Rocla Concrete Tie Plant in Sciotoville, Ohio to install eight Geokon model 3515 earth pressure cells into the ties that were to be placed at the Portal, and Tunnel Stations 16 and 23. The sensors were embedded in the still-fluid concrete, set flush with the tie bottom surface, and had the cables exit the ends of the ties, as shown in Figure 4.1. The sensor cables were labelled and protected for shipping and installation. Following curing, UTP was attached using construction adhesive to the underside of all ties, with portions of UTP cut away in two of the ties as shown in Figure 1.8.

Figure 4.1. Pressure sensor installed in a tie at Rocla Concrete Tie Plant

4.2 Sensor Installation in Tunnel and Ballast

In April, pressure sensors and uniaxial accelerometers were installed in the tunnel floor at Stations 16 and 23. Block outs were made in the tunnel floor to allow the tops of the pressure sensors to be flush with the floor. Accelerometers were sealed in small steel boxes that were also placed in the block outs. Sensor cables were run along the tunnel floor to access holes in the walkway hand hole. After placement of the sensors, grout was used to fill the remainder of the voids as shown in Figure 4.2.

Figure 4.2. Pressure sensor grouted into block out in the tunnel floor with sensor cables protected and run to the walkway hand hole

In early May, the research tem installed pressure sensors at the floor level but not embedded in the concrete at Stations 16 and 23. These were installed either over the UBM or directly on the floor with the UBM around cut out, as shown in Figure 4.3. In June, pressure sensors were also installed at the Portal under the ballast: one fully on concrete, one fully on the asphalt at the entrance of the tunnel, and one over the transition between asphalt and concrete. In addition, the uniaxial accelerometer was installed at the Portal over the transition. All cables were run through flexible conduit to the walkway hand holes.
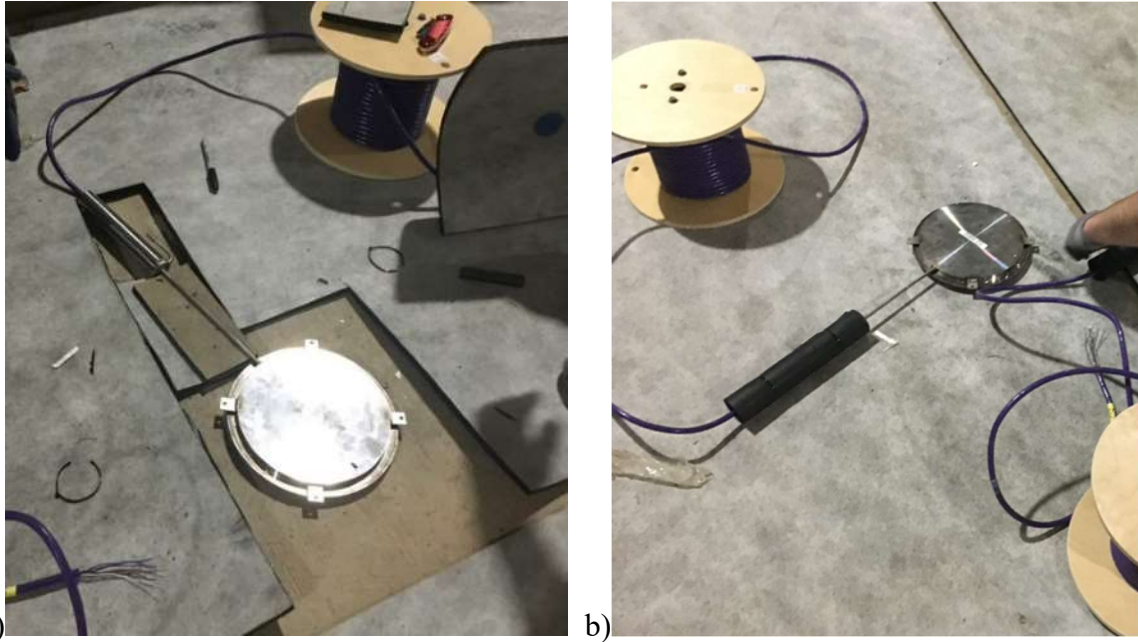
Figure 4.3. Pressures sensors installed a) directly on tunnel floor, and b) over the UBM

After the ballast, ties, and rails were laid in the tunnel, the research team returned in mid-July and early August to install the remaining sensors. At the Portal, the triaxial accelerometers were enclosed in a steel enclosure that was epoxied to a tie top surface on the field side of the rail. The base of the box was fabricated with an angle to compensate for the slope of the tie, ensuring the accelerometers were level as shown in Figure 4.4. At Stations 16 and 23, the triaxial accelerometers were similarly protected in a steel box which was, in-turn, attached to a steel mount that also houses the laser reflection targets as shown in Figure 4.5. The steel mount was also fabricated to compensate for the slope of the ties. The lasers were attached to the wall of the tunnel and leveled to face the steel targets. The lasers were protected by steel sheathes to minimize dust accumulation and protect against projectiles. Strain gages were installed as shown in Figure 4.6 at all three locations by first cleaning and sanding the rails, adhering the strain gages, and applying a paint-on protective layer shown in Figure 4.7. All accelerometer and strain gage cables were run through flexible conduit to the walkway hand holes.
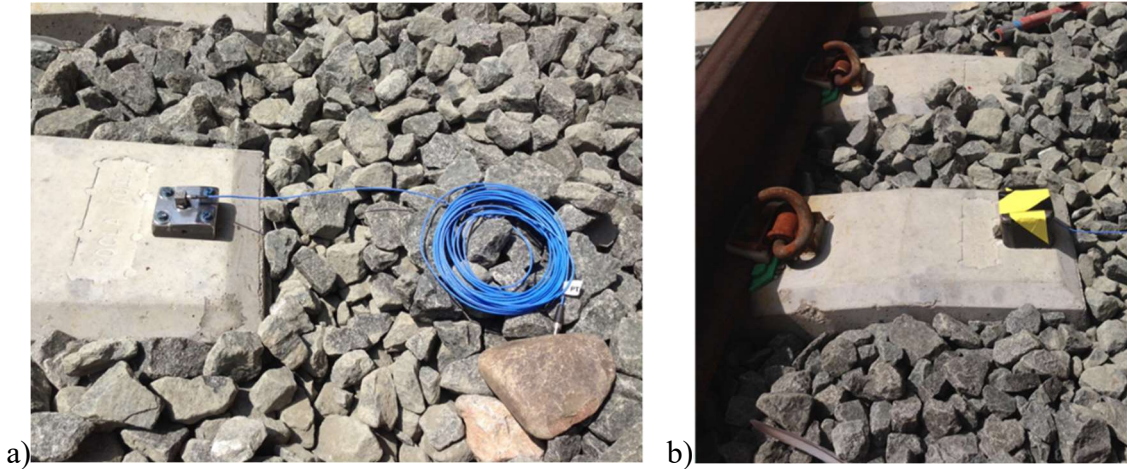
Figure 4.4. Portal triaxial accelerometer a) with levelling base, and b) fully enclosed
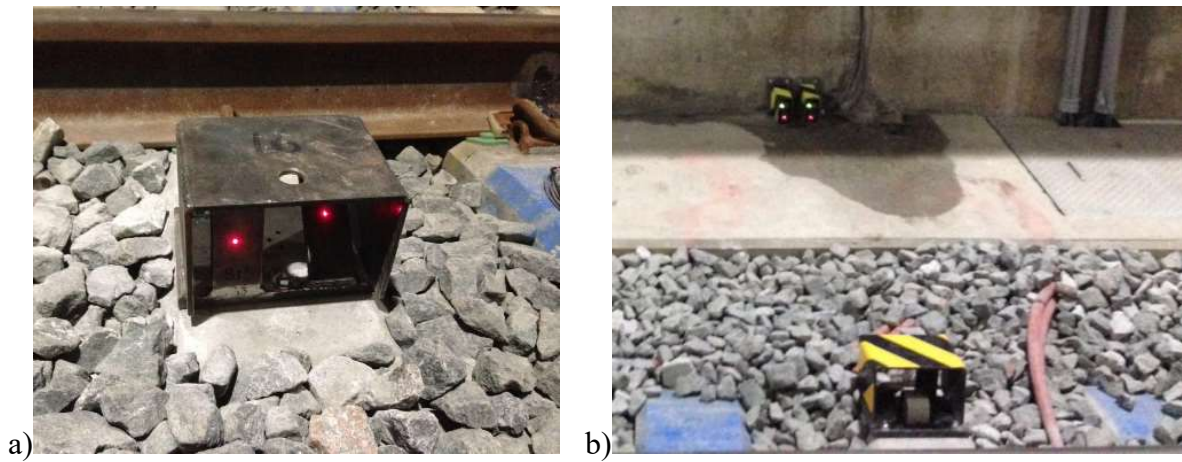
Figure 4.5. Displacement system a) laser target mounted on the tie, and b) lasers mounted on the tunnel wall directed at laser targets
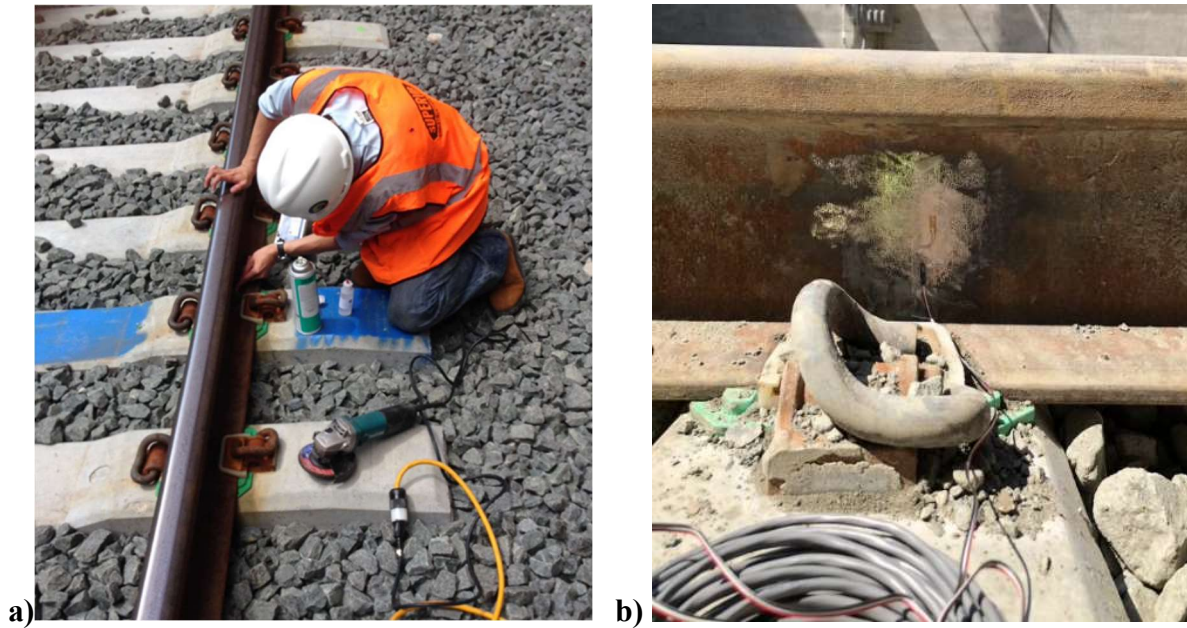
Figure 4.6. Strain gage a) during installation, and b) adhered in vertical orientation to prepared rail surface
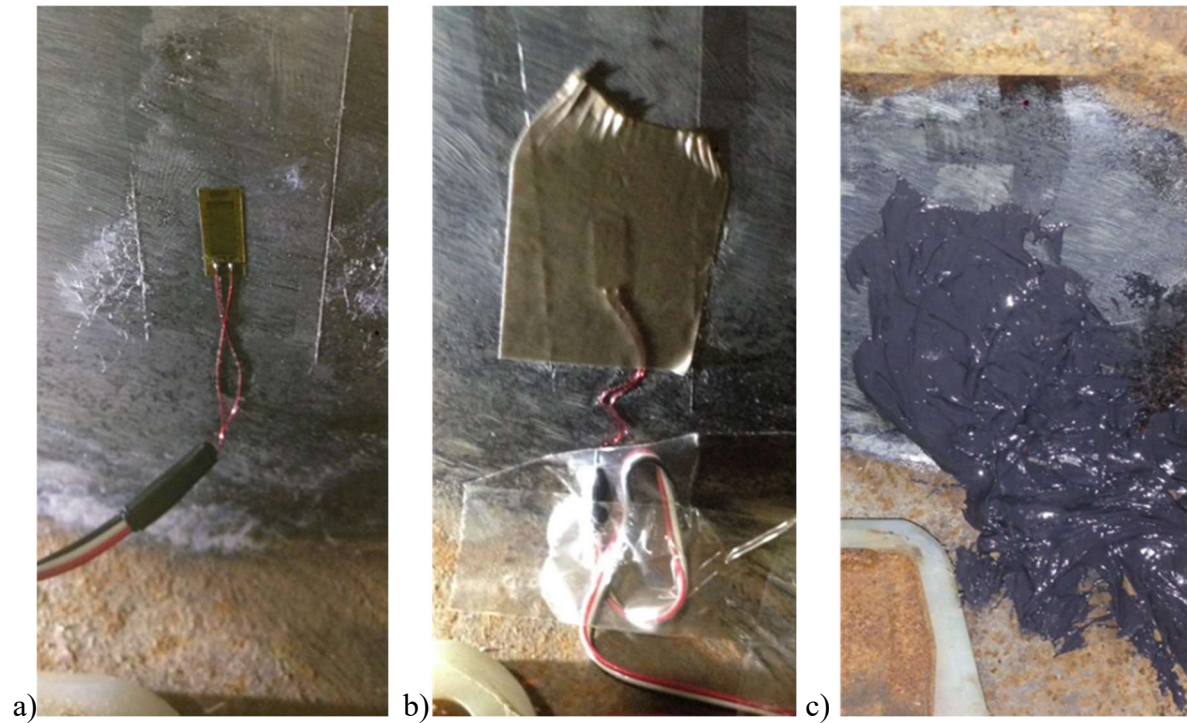
Figure 4.7. Strain gage installation process showing a) strain gage adhered to steel surface, b) strain gage covered with adhesive tape, and c) tape covered in waterproof painted-on protective layer

4.3 Data Acquisition Equipment Installation

Each monitoring location includes a data acquisition cabinet where all sensors cables were connected to the DAQ and the DAQ was connected to the network switch. Recesses were made in the tunnel wall at Stations 16 and 23 to accommodate the cabinets while ensuring they did not protrude excessively into the walkway shown in Figure 4.8. The cabinets were mounted inside the recesses with brackets. At the portal, the cabinet was mounted to the wall outside the tunnel to facilitate better cellular signal strength, as shown in Figure 4.9. The Portal cabinet was larger than the tunnel cabinets to accommodate the computer and the cellular modem. At each location, conduit was run from the walkway hand hole, and up the wall to the cabinet. Both sensor cables and communication fiber were run through the wall-mounted conduit. Power was provided to the cabinets via extension cords run to a nearby electrical outlet.

a)   b)
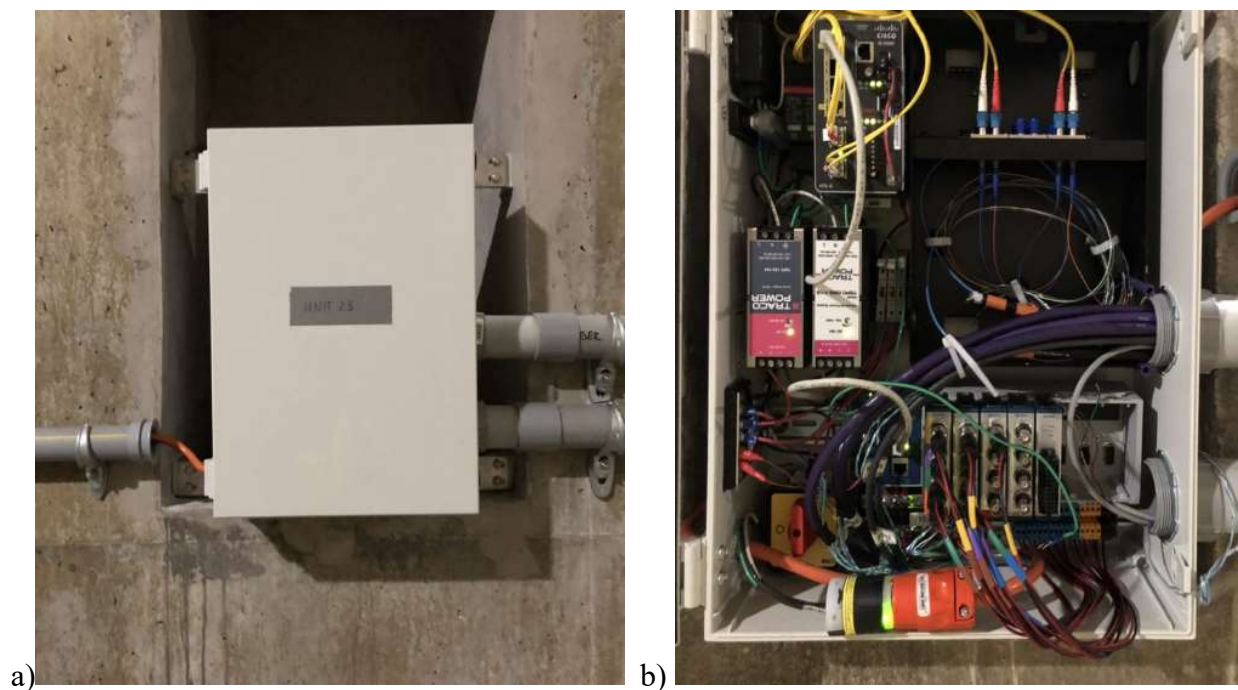
Figure 4.8. Station 23 DAQ cabinet a) mounted in recess, and b) opened showing DAQ, power, and communications components

Figure 4.9. Portal DAQ cabinet a) mounted outside of tunnel, and b) inside of Portal DAQ cabinet showing the cellular modem and computer in addition to DAQ components

4.4 Networking Equipment Installation

Fiber optic cable was used to provide networking between the three monitoring stations. The fiber was run through conduit in the walkway, up the conduit in the wall, and terminated at a LIU in each DAQ cabinet. The electrical/communications contractor for tunnel construction pulled the fiber prior to the installation of the cabinets and the research team made the connection in the cabinets and ensured they could communicate with one another. Once the fiber network was established between the stations, it was connected to the cellular modem at the Portal to enable remote access and communication. The operation of the modem was verified onsite to ensure it had reasonable cellular signal strength to support data collection and communication needs.

5. Data Processing and Filtering

Track condition data was collected between July 16th, 2018 (when the first train on the newly constructed track ran) and February 26th, 2020. Data collected between September 2nd and October 3rd, 2018 was incomplete and was not included in this analysis because of problems with triggering algorithms to collect train data. Figure 5.1 summarizes the data analysis process used in MATLAB to post-process and analyze data collected.
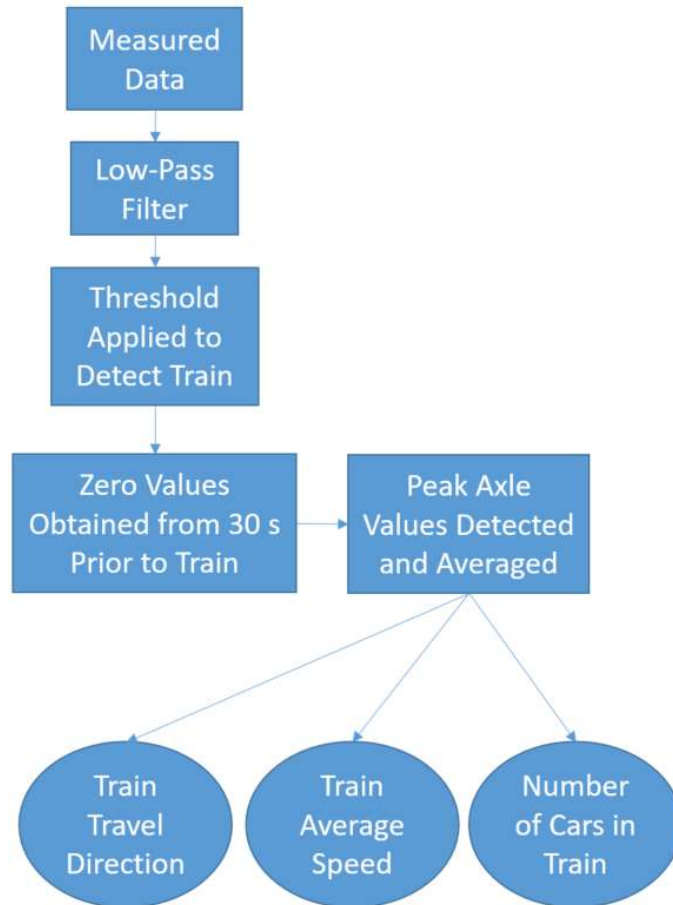
Figure 5.1. Flowchart showing the initial data analysis process

5.1 Representative Time History of Data

A representative pressure data plot has numerous pressure peaks during the passage of a train, as shown in Figure 5.2. These peaks correspond to the pressure spikes caused by the passage of the wheels of the train, and when investigated more closely, each peak has various sub-peaks. The typical locomotive has three axles on each end of the car, while the typical freight train car has two axles on each end of the car, as illustrated in Figure 5.3. The number of sub-peaks corresponds to the number of axles at the beginning and end of each train car (Figure 5.4). The typical train was shown to have two engine cars at the beginning of the train and freight cars for the remainder of the train.
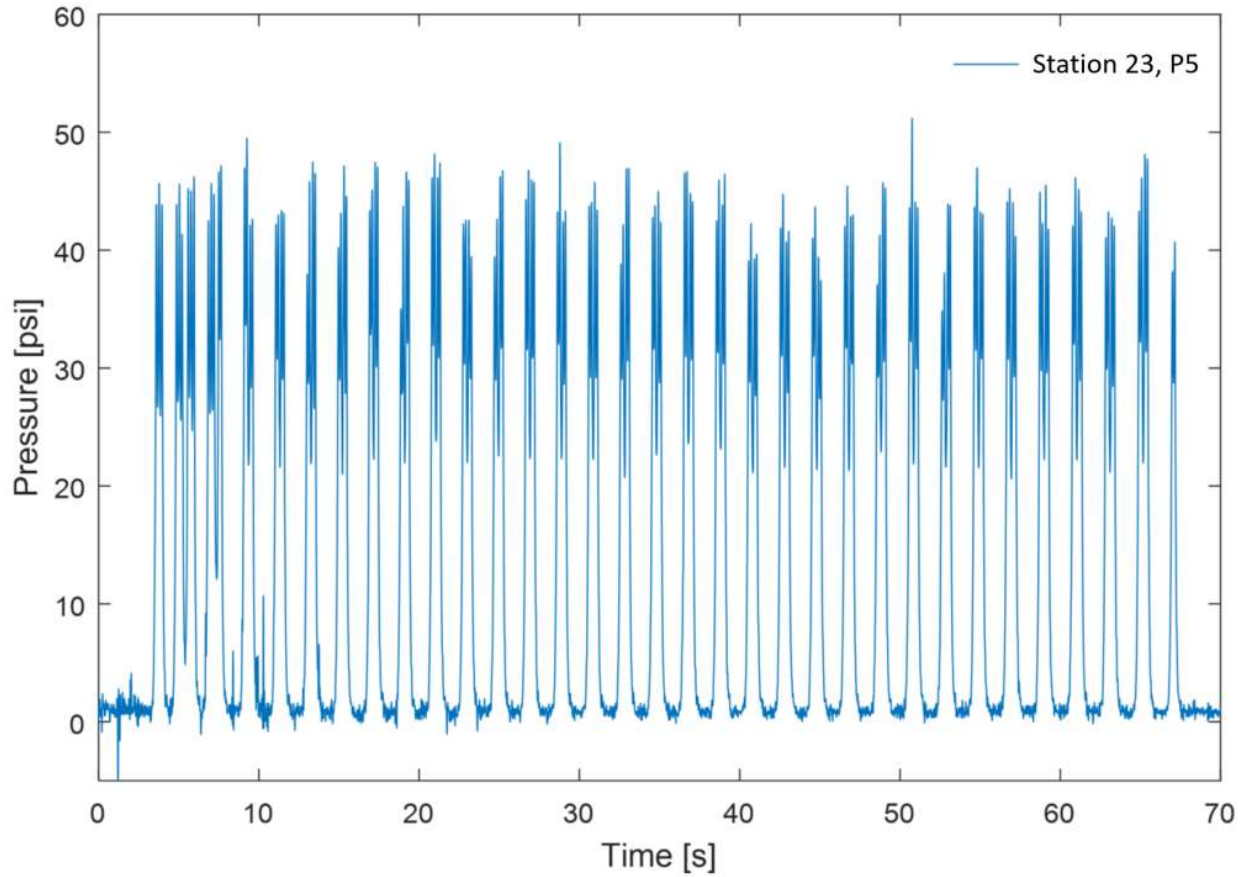
Figure 5.2. Representative sample of pressure data from pressure cell at Station 23, P5
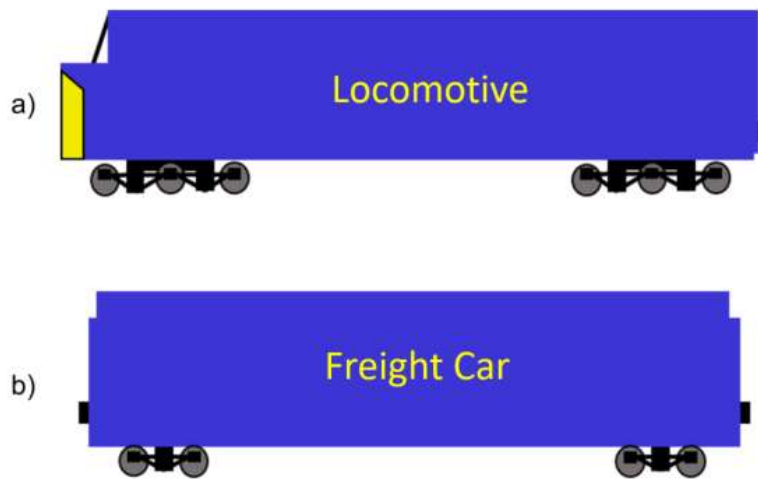
Figure 5.3. Profile view of representative train cars showing a) a train engine car and b) a typical freight train car.
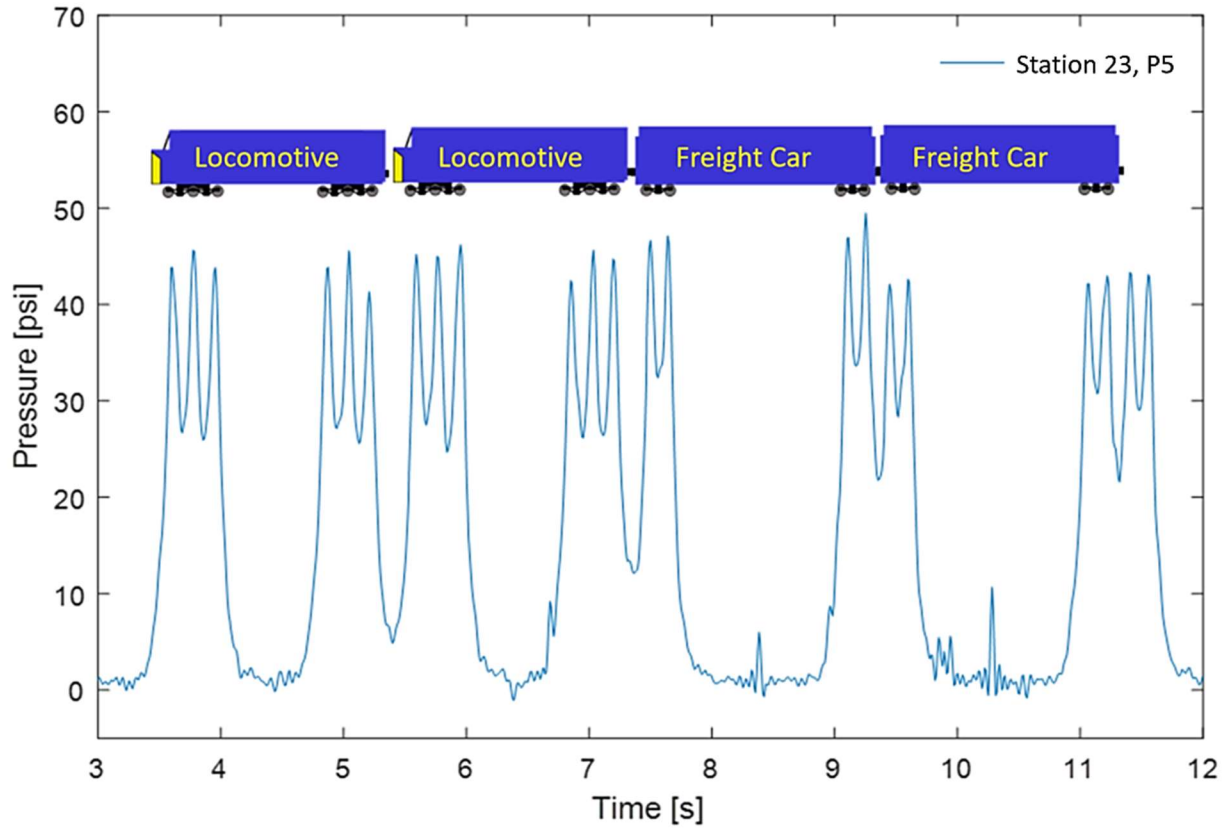
Figure 5.4. A closer look at the first 12-seconds of data from Figure 5.2 to illustrate the cause of each pressure sub-peak

A representative plot of acceleration in Figure 5.5 shows a repeating pattern of high acceleration during the passage of a train, followed by a decrease to nearly zero acceleration. Comparing the

acceleration data to the pressure data in

a)

b)
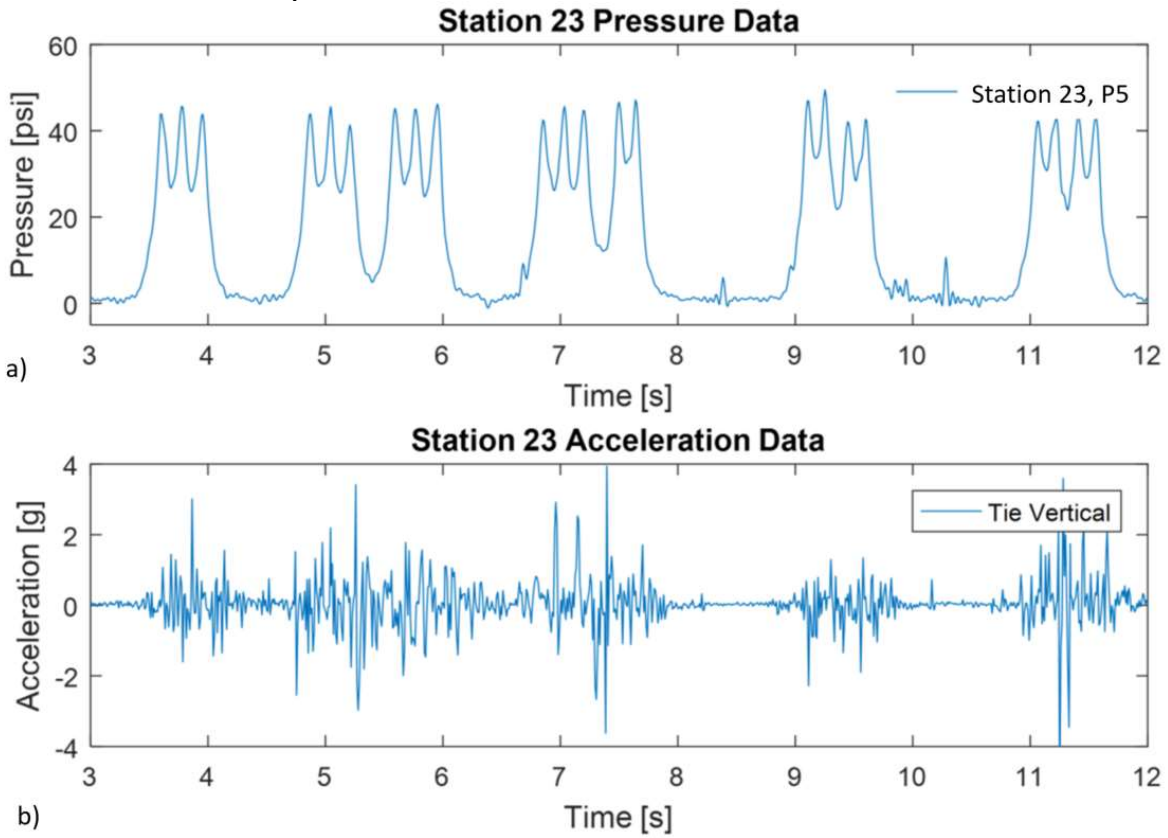
Figure 5.6, it can be shown that the highest accelerations at the ties occur while the axles of the train cars are passing over the instrumented tie.
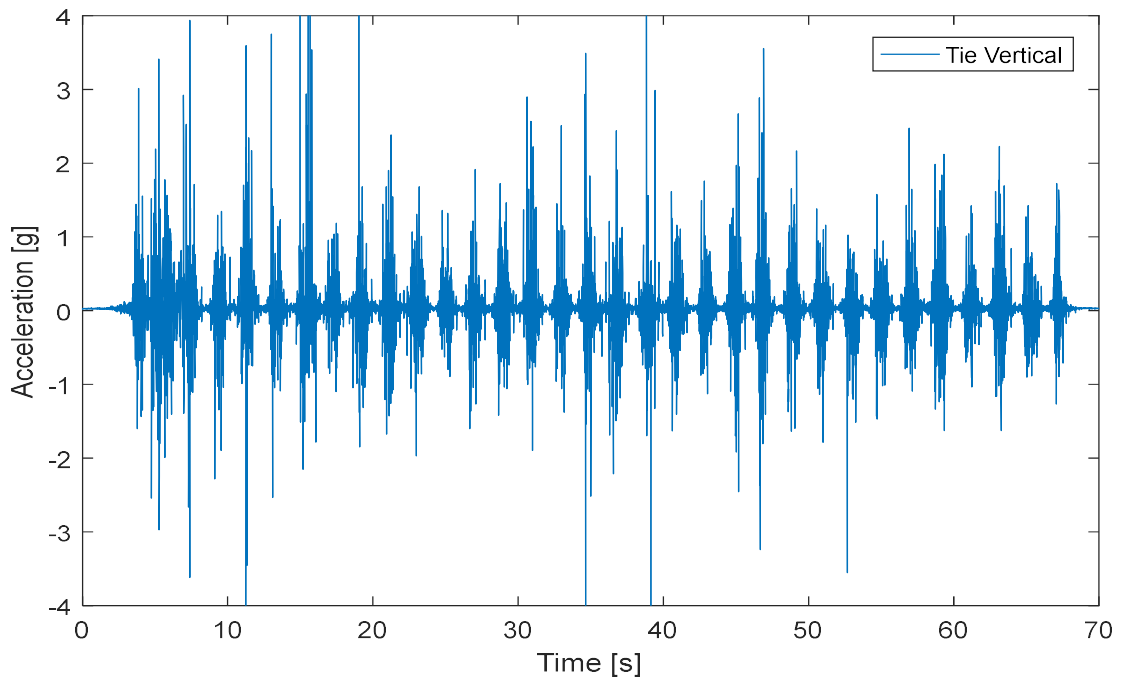
Figure 5.5. Representative sample of acceleration data at Station 23
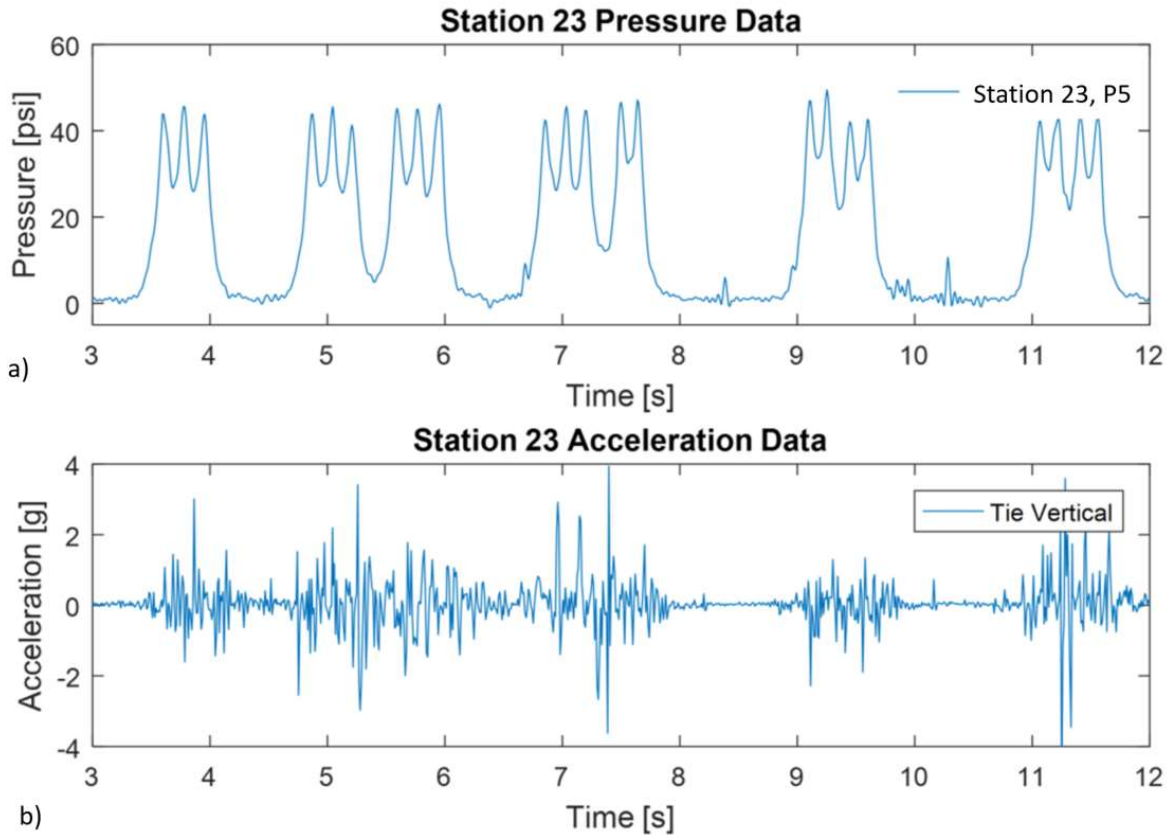
Figure 5.6. A closer look at the first 12-seconds of data from a) pressure sensor and b) accelerometer mounted on a tie

5.2 Isolating Train Data

While the sensors were sampled continuously, only five to ten trains passed through the tunnel per day. As a result, only small portions of the sensor data contained information on the effect of trains on the track system. To minimize limit the amount of data that needed to be analyzed, the data output by the sensors during the passage of individual trains was isolated using data parsing techniques before the data was analyzed.

5.2.1 Triggering

The goal of triggering was to only save the data being output by sensors when a train was passing through the tunnel. LabVIEW code was written that used the data being output by the strain gages at the Portal and Station 23 to identify the presence of a train in the tunnel. The data output by the strain gages was used because there was little-to-no strain in the track until the moment a train was passing overhead. In contrast to the accelerometers, the stain gages did not detect any strain when a train passed on the neighboring tunnel making train detection straight forward.

43

Once a train was detected, LabVIEW running on the field computer was triggered to open a new data file and start saving the data being output by all sensors. A two-minute buffer of data collected before the detection of a train was also saved to ensure that all the data from each train is collected. Once LabVIEW no longer detected a train for three-minutes, it closed the data file, and the system continued to monitor for more trains. Three minutes was selected to avoid false determination of a slow-moving train having left because of the presence of lightweight cars.

This triggering system was implemented between September 2nd and October 3rd; however, problems with the LabVIEW code led to incomplete data being collected during this period. The triggering approach was abandoned in favor of collecting all data and later parsing the data to extract only those parts when a train was passing.

5.2.2 Data Parsing

As mentioned previously, MATLAB code was written to locate train data within the larger data files and save it as an individual file to limit the amount of data that needed to be analyzed. The parsing code analyzed data output by pressure sensor PP5 at the Portal and pressure sensor 23P5 at Station 23 to determine when trains were passing through the tunnel. These sensors were selected because they measured consistently high pressure data during the passage of each train. Furthermore, using one sensor on each end of the tunnel ensured that the beginning of the train data was captured regardless of the direction of travel of the train.

To determine if a train was passing through the tunnel at a given point in the time history data, the algorithm looked at the data one minute at a time and calculated the difference between the maximum pressure value and the minimum pressure value for that one-minute of data. If the difference was over a threshold, which was set as four times the amplitude of the noise in the data of the sensor, the program determined a train was passing through the tunnel during that minute, as shown in Figure 5.7. This threshold was used to minimize false positive detection of trains caused by noise, which is low level variance in the output of a sensor that does not represent any real measurements, while still being sufficiently low that the pressures caused by a lightweight train car could surpass it, as shown in Figure 5.8. Because this method was able to detect the presence of a train accurately through the use of pressure sensors, the strain gauge readings became redundant and were not used any further in the data analysis.
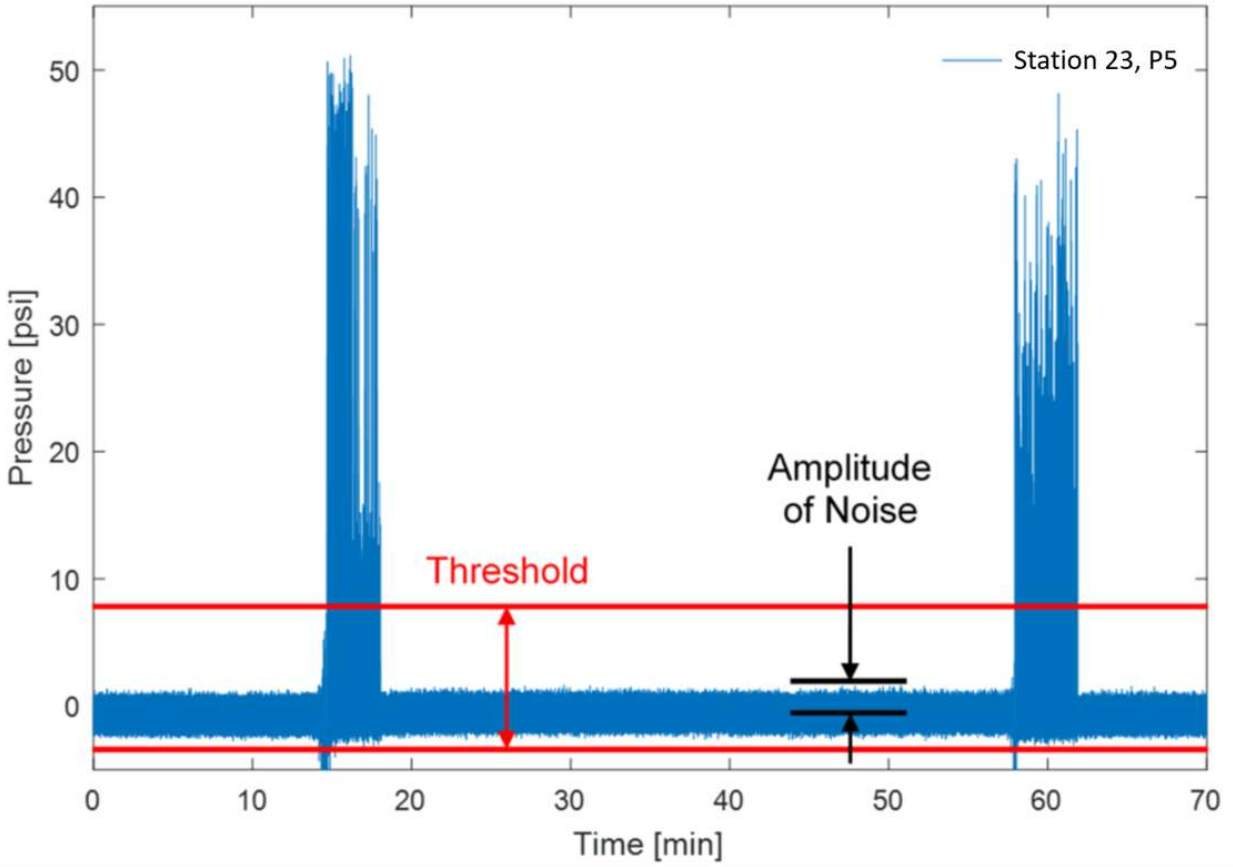
Figure 5.7. Plot of non-isolated pressure data obtained from sensor 23P5 showing the peaks in pressure caused by the passage of two trains
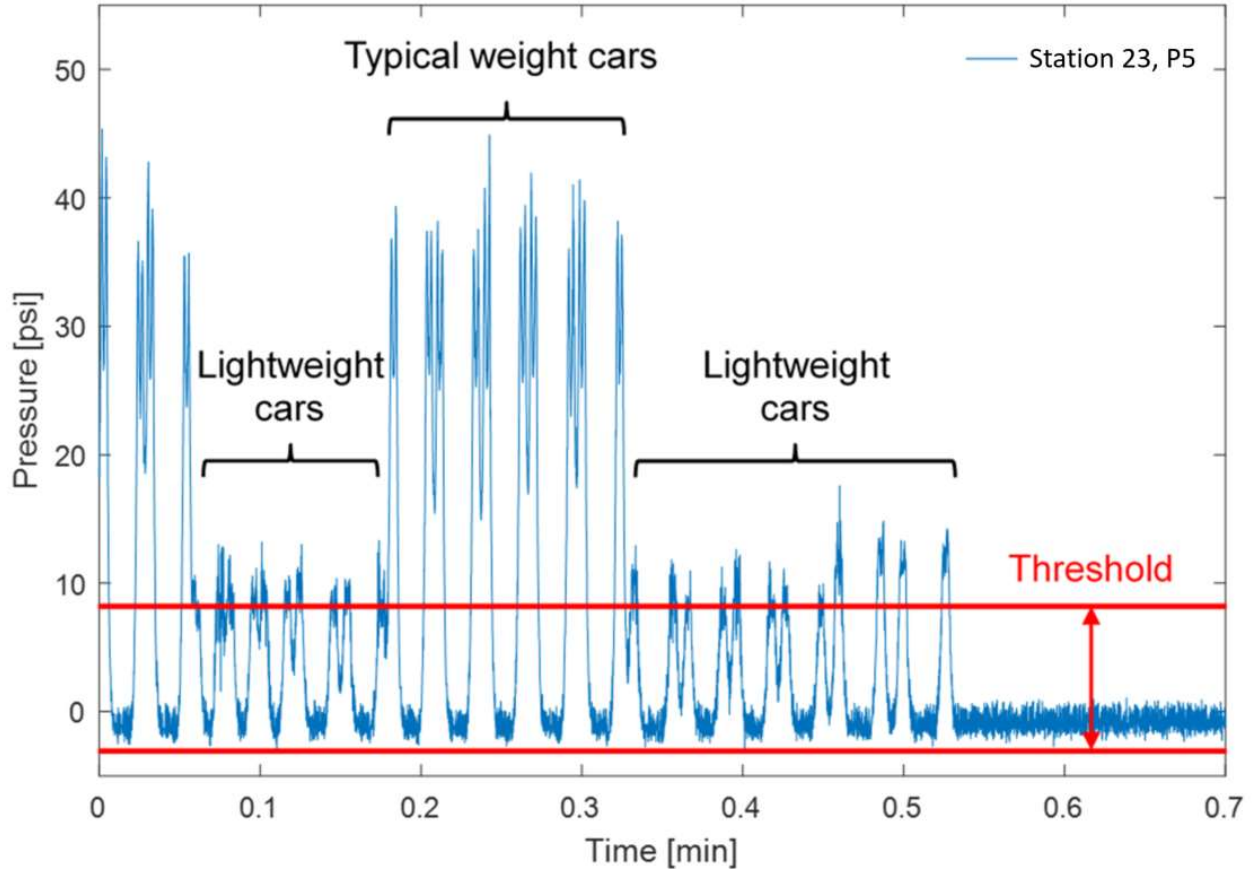
Figure 5.8. Closer look at the data from Figure 5.7 showing the data parsing threshold being surpassed by the pressure cause by lightweight cars

Once the algorithm detected that a train was present during a certain period, it saved that data as a separate file starting one minute before the beginning of the train data and ending three minutes after the train data ended. The additional data before and after each train was saved to decrease the likelihood of any train data being accidentally discarded. The file name format of each individual train included the date and time of train passage.

The data parsing algorithm detected 2,349 trains during the given time period, and reduced the amount of data requiring further analysis by an order of magnitude. During the process of developing the data parsing code, it was discovered that roughly five percent of trains that passed through the tunnel stopped in the tunnel. These trains were initially separated into two files by the algorithm, because during the time while the train was stopped, the difference between the maximum and minimum pressure values fell beneath the threshold. These split train files were recombined using another MATLAB code. There were no instances where the algorithm was unable to detect a train that was manually detected by researchers.

5.3 Sensor Data Analysis

Once the train data was separated into individual files by the data parsing code, the data was analyzed using MATLAB. This algorithm performed analysis on all the individual trains and used the information gathered to assess changes in the system over time.

5.3.1 Pressure Data

Before analyzing the pressure data, the average pressure recorded during the first 30 seconds (which does not include the train) was subtracted from the data to ensure that the pressure recorded while there was no train present was zero. The data was also filtered using a low-pass filter to remove any high frequency noise above 20 Hz in the data. A peak picking feature built into MATLAB was used to find the peak pressure value for each set of wheels of each train (Figure 5.9). A minimum peak threshold of four times the amplitude of the noise was used, similarly to the data parsing code, as well as a minimum peak spacing of one-second. The minimum peak spacing was used to ensure that only one peak was selected for each group of axles. The peak value, as well as the time at which the peaks occurred, allowed for determination of the direction of travel, average travel speed, and number of cars of each train. The average peak pressure value recorded by each sensor during each individual train, referred to as Pp_{avg}, was determined. The train shown in Figure 5.9, for example, had Pp_{avg} of 47 psi. The magnitudes of pressures recorded by some pressure cells showed unexpectedly high loads in some locations compared to the pressured obtained by other pressure cells at the same location.
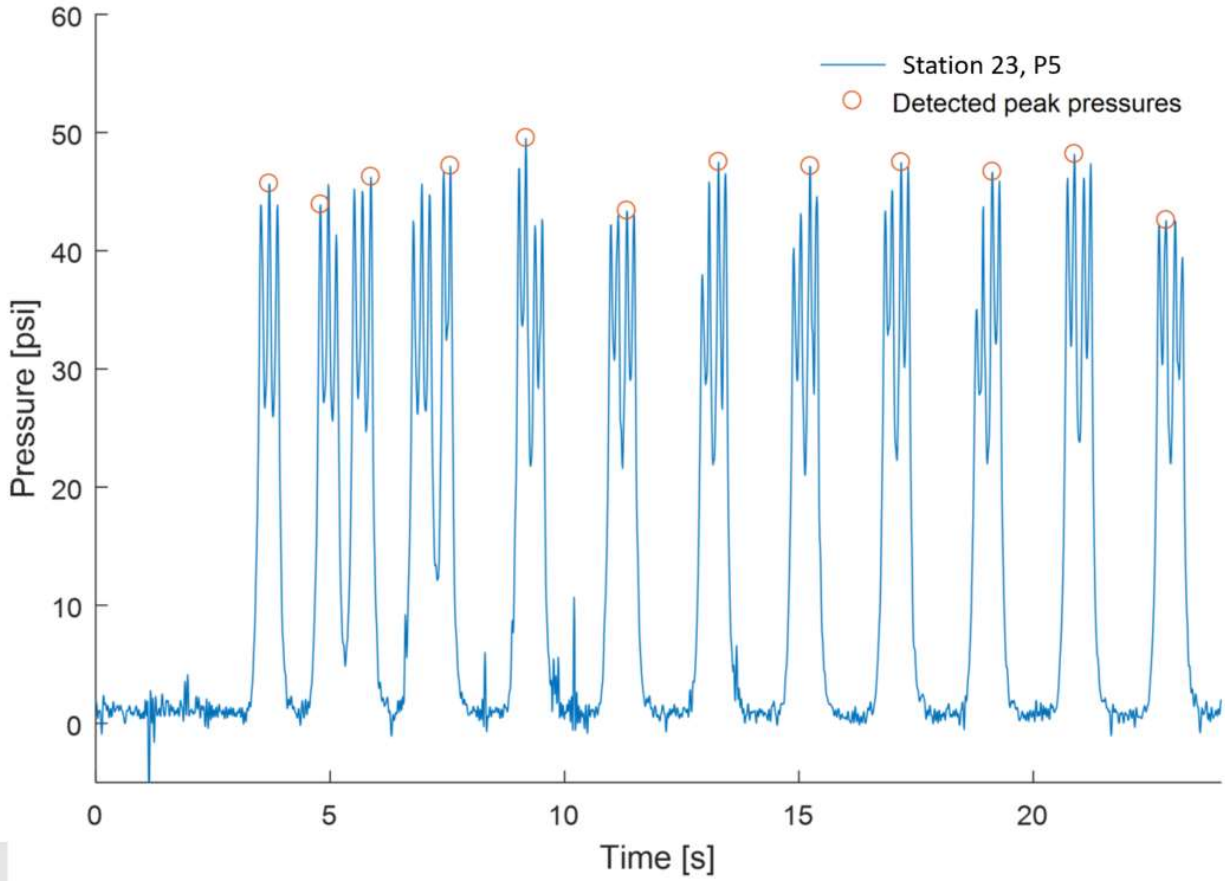
Figure 5.9. Closer look at the first part of pressure data from Figure 5.2 with peaks identified

6. Results

Track data was collected, filtered and examined as a case study in track performance when UTP and UBM are used to decrease the track modulus. Track force distribution across ties was calculated at the Portal, Station 16, and Station 23. Track settlement with time was measured at Station 16.

6.1 Train Characteristics

The direction of travel of each train was determined by comparing the times at which the first pressure peak was recorded at the Portal or Station 23. Trains detected at the Portal first were travelling east while trains detected at Station 23 first were travelling west. An example of how the train direction was determined from the pressure data is shown in Figure 6.1. The train shown in Figure 6.1 was detected first at Station 23, indicating that it was traveling west. The travelling direction of each of the trains was recorded, and it was determined that there was a near even split between trains traveling east and west. 1,174 trains of the 2,349 trains detected traveled west. The time of train passage through the tunnel is shown in Figure 6.2.
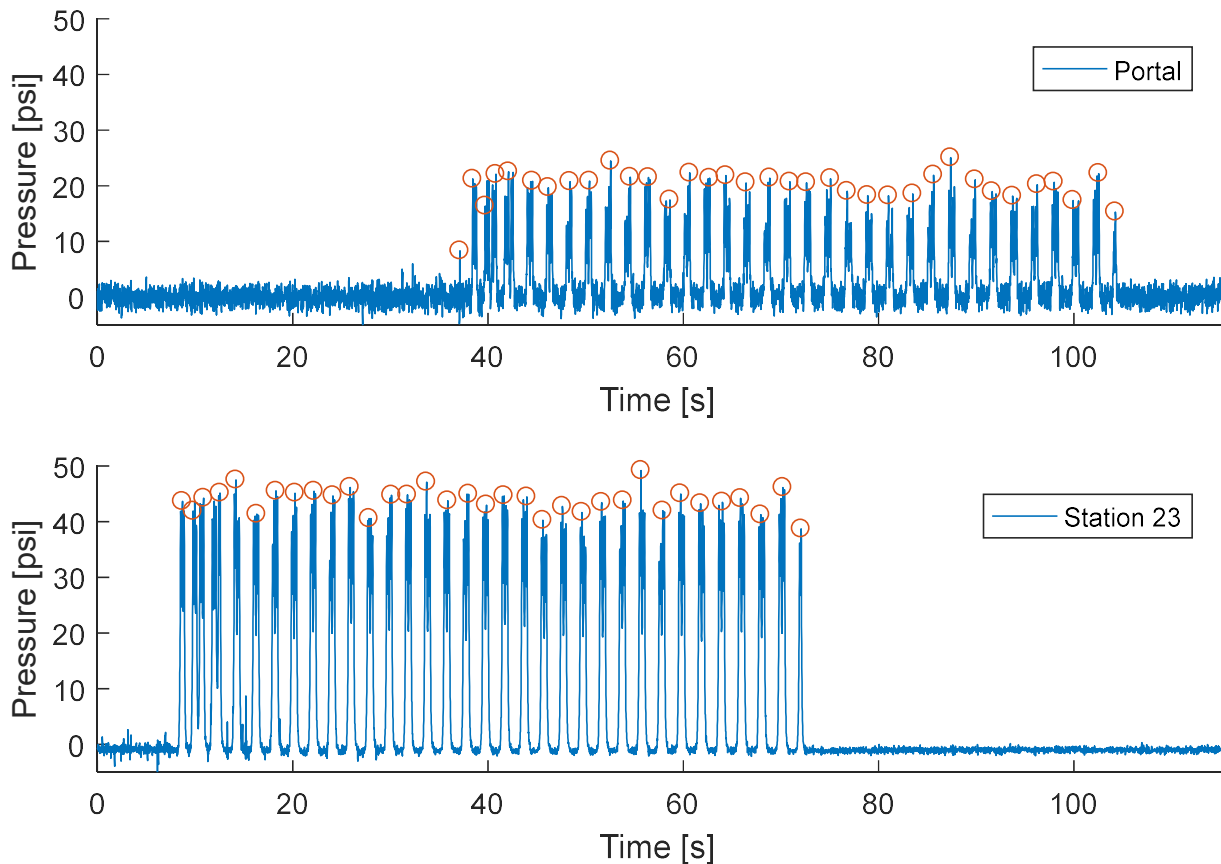

Figure 6.1. Pressure data obtained at A) the Portal and B) Station 23, showing the difference in time of arrival of the train to the two locations
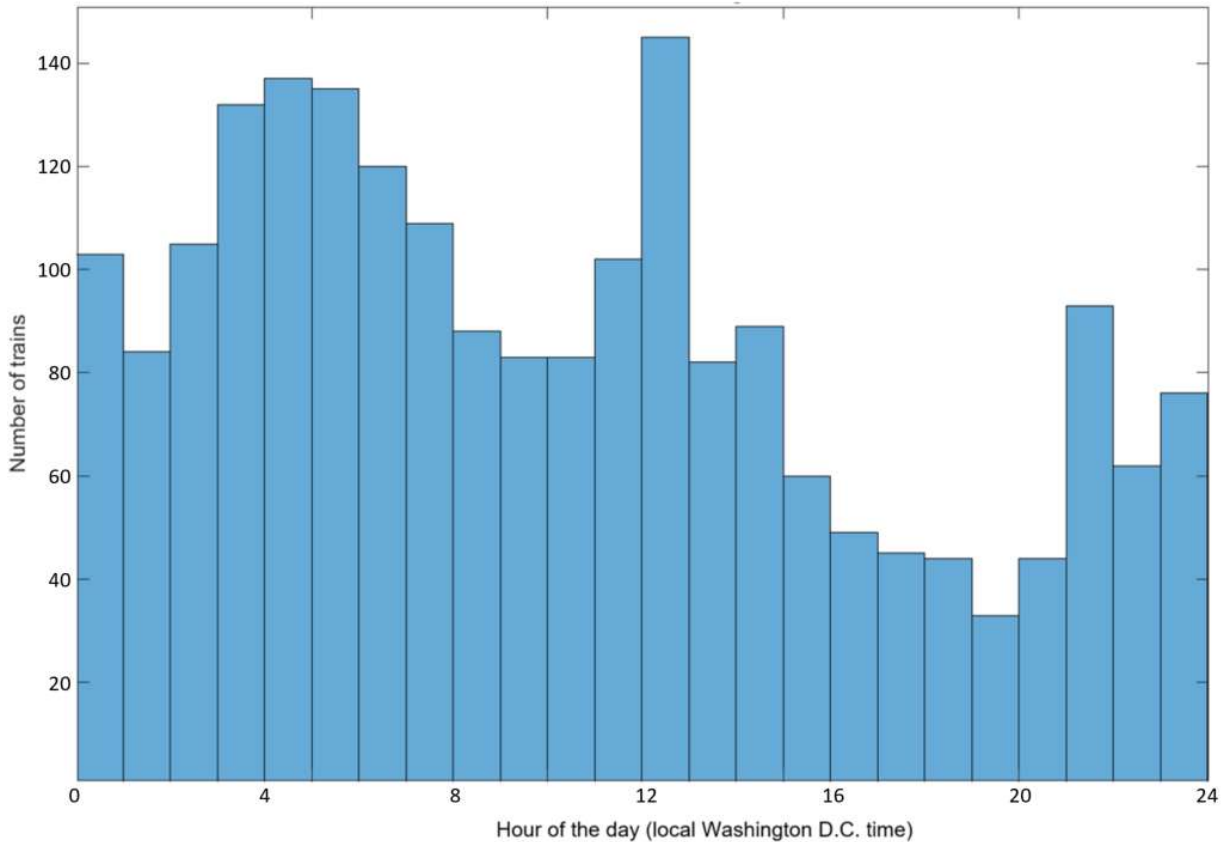
49

Figure 6.2. Number of trains by (military) time of day

Using the times at which the first pressure peaks occur at each location, as well as the known distances between the three locations instrumented in the tunnel, the train speed was calculated by dividing the distance traveled by elapsed time. To make the calculation less susceptible to error, the speed calculation was performed using the time of arrival of the first five peaks of every train, as well as the last five peaks of every train, at the Portal and Station 23. The average of the speed valued obtained using this technique was taken as the estimated average speed of the train in the tunnel. The estimated average speed of each train while in the tunnel was recorded, and these values were plotted as a histogram in Figure 6.3. The histogram has a left-skewed distribution, with a mode of 20 to 22 mph, and very few trains traveling faster than 26 mph.
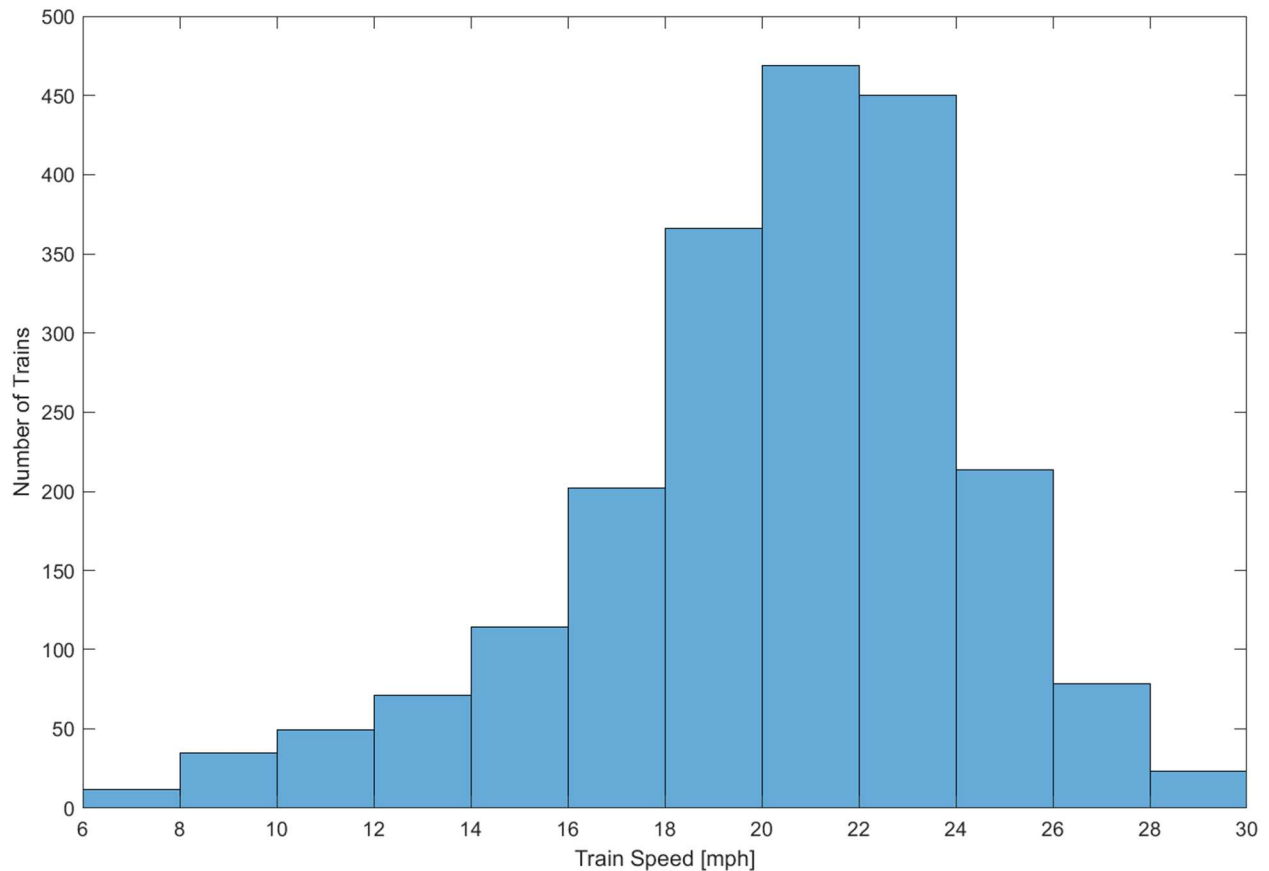
Figure 6.3. Histogram showing the estimated average speed of trains that passed through the tunnel

The number of train cars on each train was estimated by counting the number of pressure peaks found by the peak selecting feature. Only train cars that were sufficiently heavy to cause pressures that exceed the threshold were found by the peak selecting feature, therefore, relatively light cars did not register peak values. To accurately estimate the number of cars per train, large time gaps between pressure peaks were divided by the average time gap between peaks, to estimate the number of light cars passed during those extended gaps. The estimated number of train cars per train are plotted as a histogram (Figure 6.4). The majority of trains had between 100 and 150 train cars.

Figure 6.4. Histogram showing the number of train cars per train
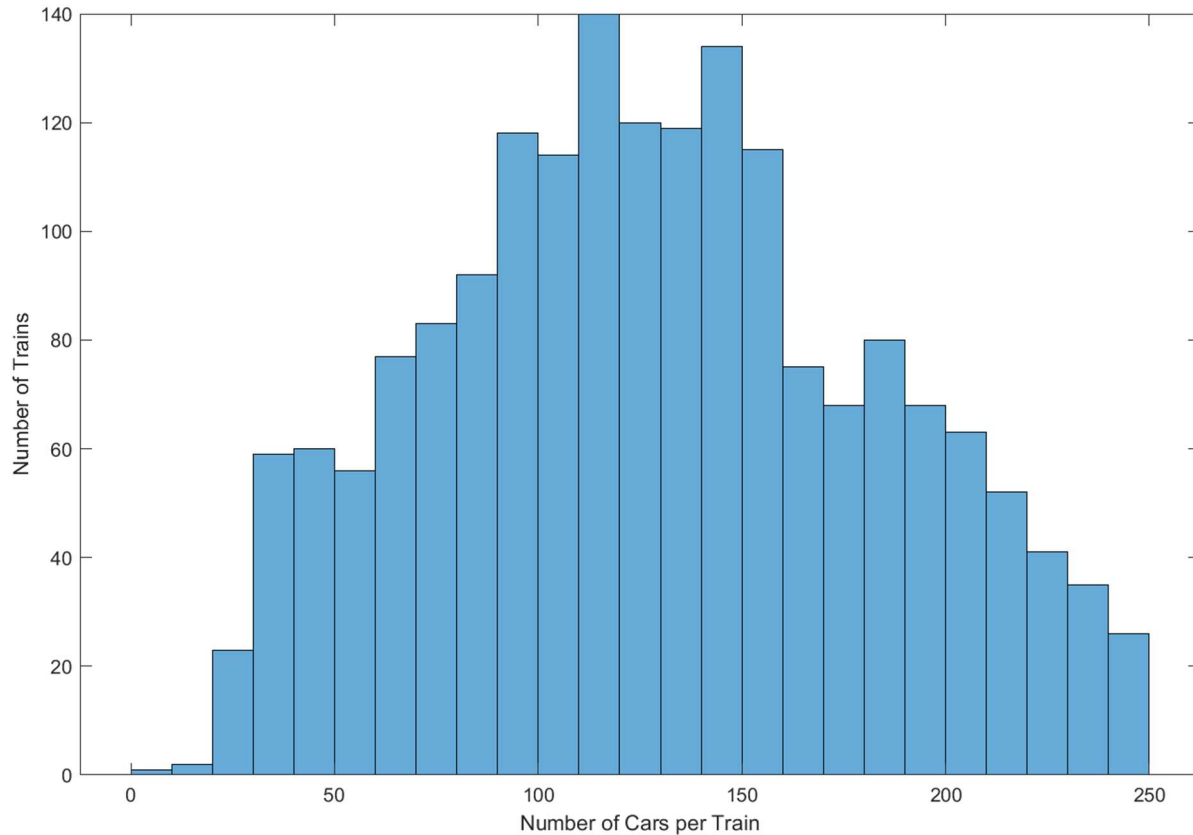
6.2 Change in force distribution over time

To quantify the change in the distribution of forces throughout the rail system over time at each monitoring location, Pp_{avg} recorded by each pressure sensors in the tunnel was found for each train. Appendix A shows the root mean squared peak pressure for each train measured with time for the pressure sensors in the tunnel. The data shown for sensor 23P6 is believed to be noise resulting from sensor malfunction.

The pressures measured by the sensors embedded in the concrete ties at the transition area were compared. Figure 6.5 shows the average peak pressured measure over time for sensors PP4 and PP5. The pressure seen in PP5 over concrete was on average 2.2 times higher than PP4 over asphalt. The difference increased slightly with time and was higher during the winter months. It is currently not known why the pressure measured decreased significantly during the winter. One possible explanation is that the rubber used in the UTP stiffens in cold weather, causing a load bridge around the sensors. The variation in pressure recorded coincided with the seasonal differences in temperature in Washington D.C., suggesting this could be a reason.
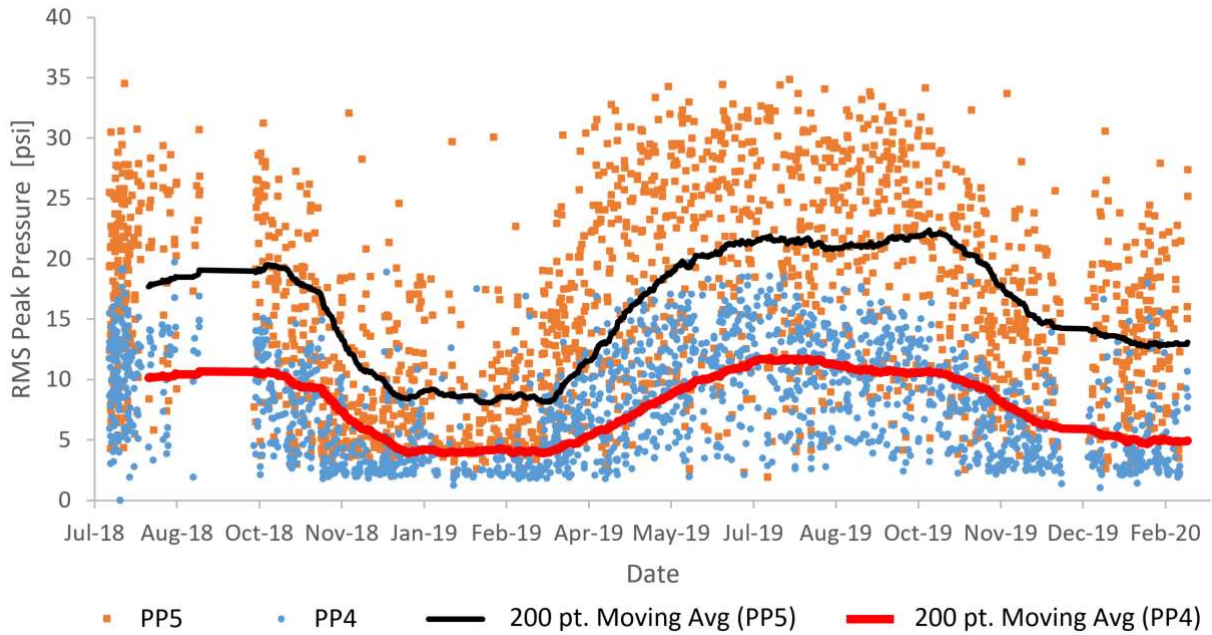
Figure 6.5. Average peak pressure measured over time for sensors embedded on the concrete tie bottom in the area of the railseat at the portal over asphalt (PP4) and over concrete (PP5)

A comparison of the pressures measured by the pressure sensors is shown in Figure 6.6. The pressure measured on the concrete was approximately 2.0 times that measured on the asphalt floor, while the pressure in the transition area floor was on average 2.7 times that measured on the asphalt floor. This illustrates the impact the floor stiffness has on the pressures measured. The transition area showed the highest pressures likely because of dynamic loading created by the change in stiffness.

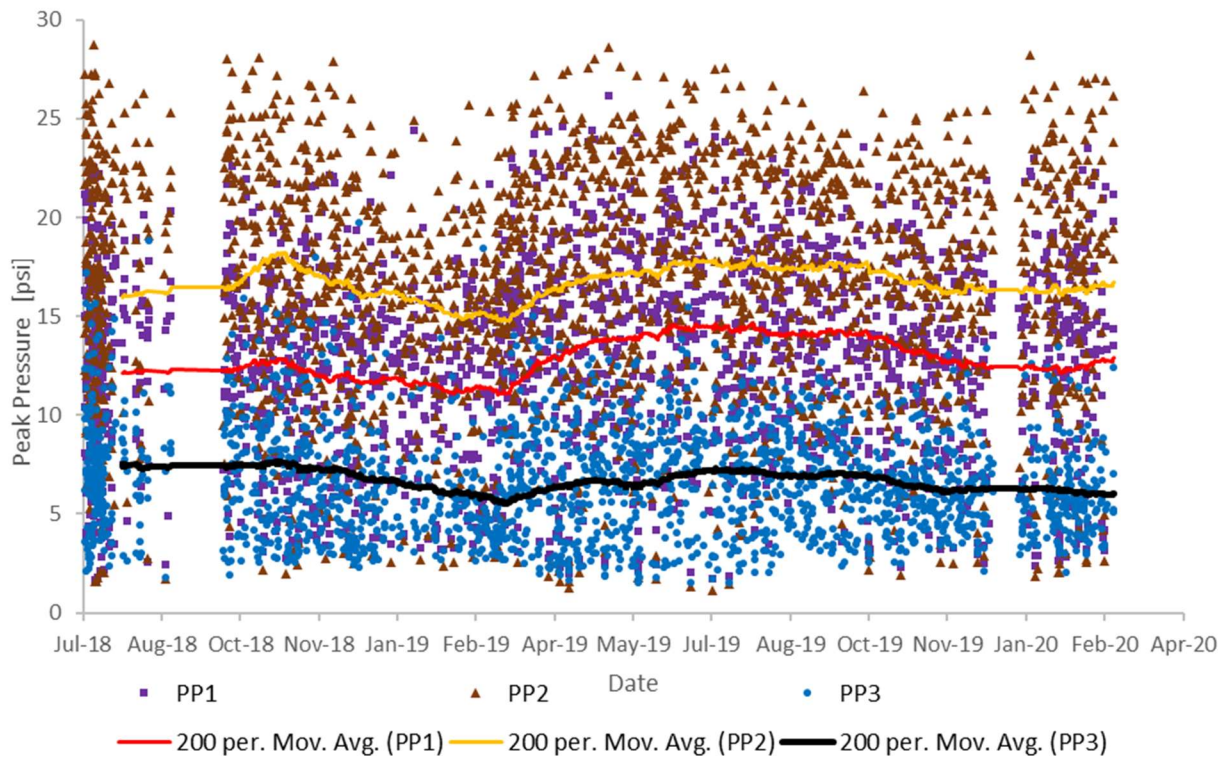**Figure 6.6. Average peak pressure measured over time in the portal transition area for sensors on top of the concrete floor (PP1), on top of the asphalt and concrete floor (PP2), and on top of the asphalt floor (PP3)**

Figure 6.7 shows a comparison of the pressure measured on top of the UBM and aligned with the railseat (23P3), embedded in the tie and aligned with the railseat but without a UTP (23P4), and embedded in the tie and aligned with the tie center with a UTP (23P5). The sensors measure the pressure on nearby but different ties, making it difficult to ascertain the cause of the change, in November 2019 when the pressure dropped to close to zero in the tie center and on top of the ballast mat, and the pressure in the railseat increased. There could have been some changes in the ballast particles at that point in time where one tie was slightly center-bound before that point, after which something shifted in the ballast and reduced the pressure in the center significantly. It is also possible that the sensor 23P5 stopped working, however that is not consistent with the more gradual decrease seen in sensor 23P3 that is not indicative of sensor malfunction. Until November 2019 the measured pressures in the sensor above the UBM and in the railseat area without the UTP were significantly higher in Station 23 than those measured at the portal and at the railseat in the tie with the UTP.
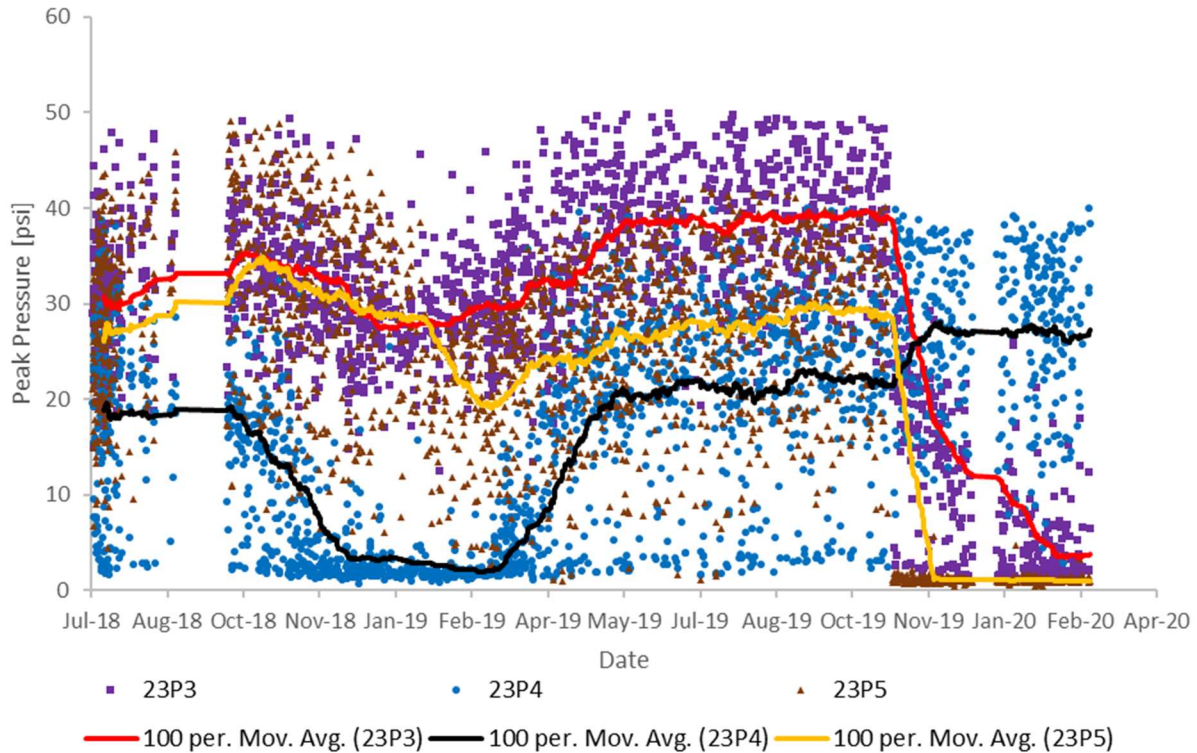
Figure 6.7. Average peak pressure measured over time at Station 23 for on top of the UBM and aligned with the rail (23P3), embedded in the tie aligned with the rail but without a UTP (23P4), and embedded in the tie and aligned with the center of the tie with a UTP (23P5)

The pressure during loading was examined to determine how well the ties distribute rail loading. A video taken of a specific train passage event on July 17, 2019 was manually analyzed to determine car types. This analysis was used to judge the reasonableness of the pressure data by comparing the locomotive type and its estimated load with the measured pressures. For this train, there were 153 cars, including five locomotives. The weight of most rail cars is difficult to estimate, however the empty and full of fuel locomotive weights were used to bound the axle loads to be between 71.3 and 76.9 kips. The peak pressure recorded for sensor PP5 (embedded in the concrete tie bottom under the railseat and above the concrete portion of the transition area outside the portal) for the six axles on each of the locomotives was recorded, giving an average of 27.6 psi and a standard deviation of 2.2 psi.

To quantify the distribution of axle loads between ties, the pressure distribution for the third axle on the first locomotive was examined for each train recorded during this study. The peak pressure at each sensor was considered the point in time that the axle was directly over the sensor. Using the measured train speed and tie spacing, the time when the axle was one tie over, two ties over, three ties over, and four ties over was calculated and used to determine the pressure at the sensor at those points in time, as shown in Figure 6.8. The total pressure P_T supporting the axle was then calculated using Equation 6.1:

55

$$P_T = P_0 + \sum_{i=1}^{5} 2P_i \qquad \textbf{Equation 6.1}$$

Where P_0 is the pressure at the sensor when the third axle is directly over the tie containing the sensor, P_i is the pressure at the sensor when the third axle is i ties over. The percentage of the total pressure for each tie in relation to the axle location was then calculated for each train. The average and standard deviation of the pressure distribution was calculated for different train speeds, seasons, and locations in the tunnel. For example, Figure 6.9 shows the pressure distribution with distance from the axle for sensor 23P5 (embedded in the concrete tie bottom center) for the 306 trains measured traveling between 24 and 26 miles per hour (mph). The error bars in Figure 6.9 show plus and minus one standard deviation of results. The pressure recorded at the tie-ballast interface is similar in magnitude to the pressures recorded by other studies [10] [11] [12]. One study by the University of Illinois Urbana-Champaign showed that the train wheel load is typically distributed amongst three to five concrete cross ties in tangent track, with the tie being loaded having a railseat loading varying from 16 to 67% of the wheel load, typically "about 50% of the total applied vertical load [13]."
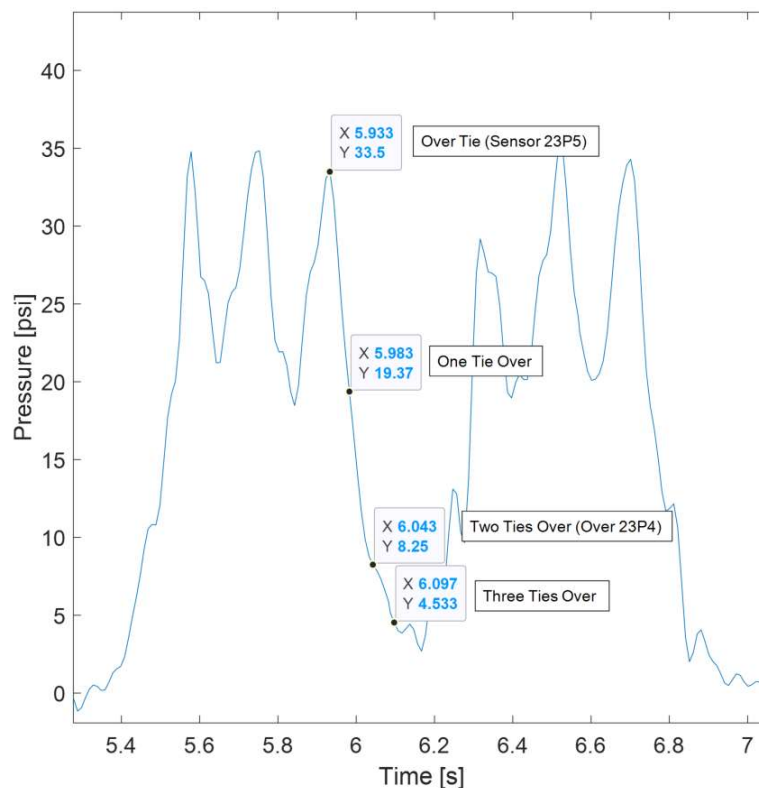

Figure 6.8. Example of pressure data recorded for sensor embedded in the concrete tie bottom under the railseat for the first locomotive of a train, with data points picked off when the axle was directly over the tie being measured, one tie over, two ties over, and three ties over
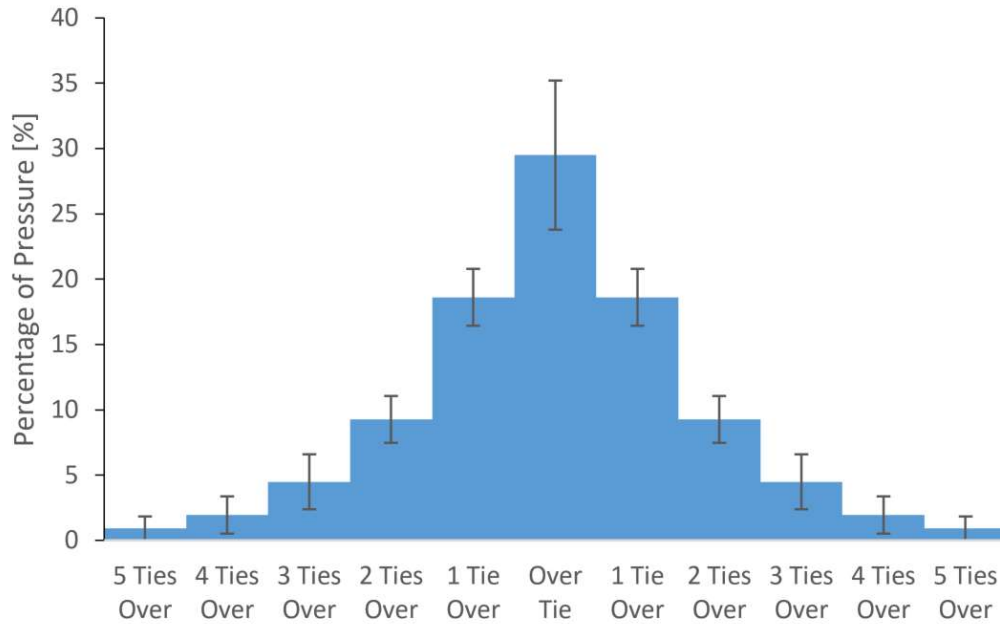
Figure 6.9. Pressure distribution for sensor 23P5 (embedded in the concrete tie bottom center and placed in Station 23 of the tunnel) for the 306 trains with speeds between 24 and 26 (mph)

The effect of speed on the pressure distribution was also investigated. Figure 6.10 shows the pressure distribution measured by the sensor embedded in the concrete tie bottom railseat area and placed in Station 16 (sensor 16P6) for different speed trains. Given the standard deviation seen in pressure distributions, the difference in pressure distribution was found to be minimal. The pressure distribution found for sensor 16P6 was compared in Figure 6.11 to the pressure distributions measured in the pressure sensors at the transition between the asphalt and concrete just outside of the tunnel portal. The pressure distribution was similar for the sensors above the concrete and asphalt. The sensor inside the tunnel at Station 16 showed the tie under the wheel taking less load as a percentage of the total load. The differences in distribution can be attributed to the better support conditions inside the tunnel. Although only 8 in. of ballast was provided under the ties inside the tunnel compared to the 14 in. of ballast provided just outside the tunnel at the transition area, the UBM reduced the overall track modulus, more than making up for the reduced ballast.
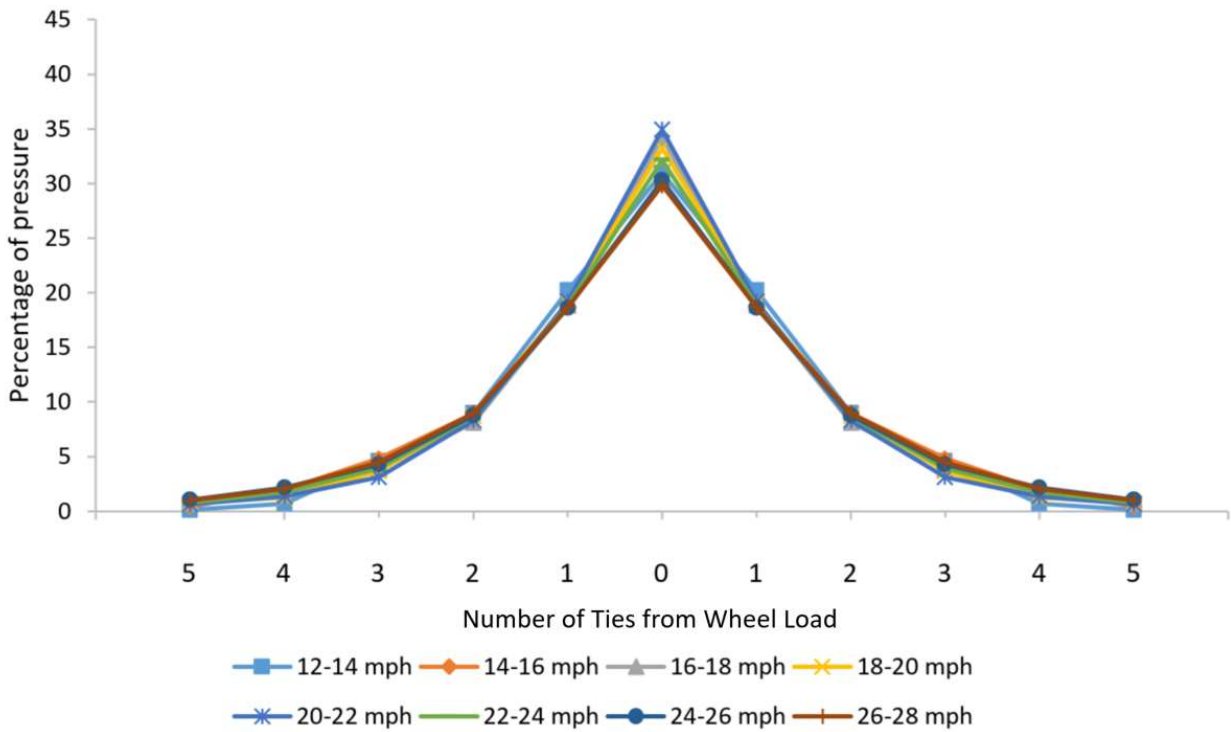
Figure 6.10. Pressure distribution by tie location in relation to the axle for Station 16 sensor P6 (embedded in the concrete tie bottom railseat area and placed in Station 16) based on train speed
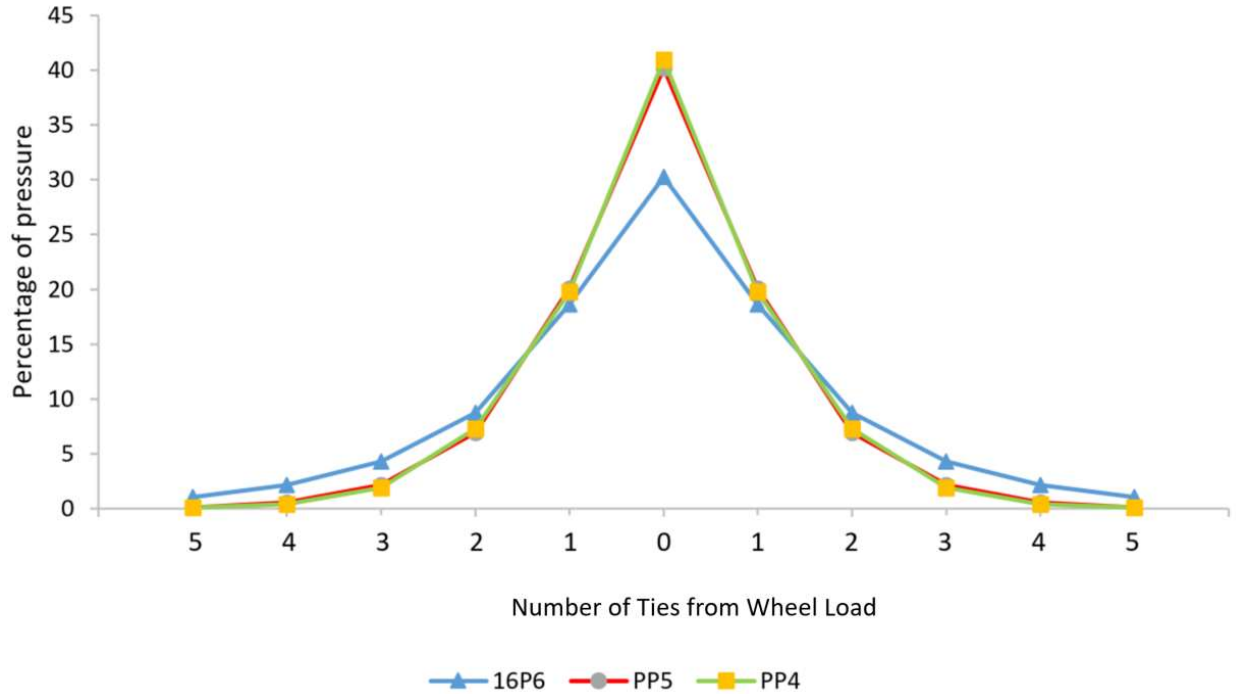
Figure 6.11. Pressure distribution by tie location in relation to the axle for sensor 16P6 (embedded in the concrete tie bottom railseat area and placed in Station 16) inside the tunnel, at the Portal sensor P5 (PP5) (embedded in the concrete tie bottom under the railseat) over concrete just outside the tunnel portal, and at the Portal sensor P4 (PP4) (embedded in the concrete tie bottom under the railseat) over asphalt just outside the tunnel portal

6.3 Track Displacement

Track deflection measurements at Station 16 during loading was calculated from the laser distance measurements against the plate perpendicular to the laser direction and 45° to the laser direction. The baseline distance to each plate before the train arrived was subtracted from each of the laser distance measurements with time. The change in the horizontal distance from the baseline value at each point in time was then subtracted from the change in distance from the 45° plate from the baseline value at each point in time to give the vertical displacement of the tie at each point in time. The vertical displacement for three trains in Oct. 2018 were examined to determine the peak displacement from the locomotive axles. The peak displacement for those three trains varied between 0.17 and 0.26 in. (4.4 and 6.6 mm). The maximum displacement for the locomotives for three of the trains was used to estimate the track modulus. A track modulus k was fit to the measured displacement values using the Kerr Method [14]:

$$w(0) = \frac{P\beta}{2k} + \frac{P\beta}{2k}e^{-\beta l_1}[\cos(\beta l_1) + \sin(\beta l_1)]$$

$$+ \frac{P\beta}{2k}e^{-\beta l_2}[\cos(\beta l_2) + \sin(\beta l_2)]$$

$$+ \frac{P\beta}{2k}e^{-\beta l_3}[\cos(\beta l_3) + \sin(\beta l_3)]$$

$$+ \frac{P\beta}{2k}e^{-\beta l_4}[\cos(\beta l_4) + \sin(\beta l_4)]$$

$$+ \frac{P\beta}{2k}e^{-\beta l_5}[\cos(\beta l_5) + \sin(\beta l_5)]$$

Equation 6.2

$$\beta = \sqrt[4]{\frac{k}{4EI}}$$

Equation 6.3

Where w is the rail deflection at the first wheel load, l_1 is the distance between the first wheel load and the second wheel load, l_2 is the distance between the first wheel load and the second wheel load, l_3 is the distance between the first wheel load and the second wheel load, l_4 is the distance between the first wheel load and the second wheel load, l_5 is the distance between the first wheel load and the second wheel load, E is the steel modulus, I is the rail moment of inertia, and k is the track modulus. For an assumed locomotive weight of 426,000 lb and steel modulus of 30,000 ksi, a track displacement between 0.17 and 0.26 in. (4.4 and 6.6 mm), the track modulus was calculated to be between 3500 and 2300 psi.

Analysis of the laser displacement data with time at Station 16 showed a total of 0.156 in. (4 mm) of sustained vertical displacement over the study period, as shown in Figure 6.12. The settlement principally occurred during the first six months of the track life and stabilized after that. Vertical displacement data showed the vertical position of the tie after a train was within ± 0.047 in. ($\pm$ 1.2 mm) of its position before the train 68% of the time. The small vertical change could be attributed to shifting ballast particles during loading. Figure 6.13 shows the change in horizontal distance from the laser sensor mounted on the wall to the tie vertical target, along with the average daily temperature recorded by the weather station at the nearby Reagan National Airport [15]. The horizontal movement of the tie coincided with the region seasonal temperature. The horizontal track movement was likely influenced by temperature-induced strains in the steel rail slightly altering the track location by the radius of nearby track curves.
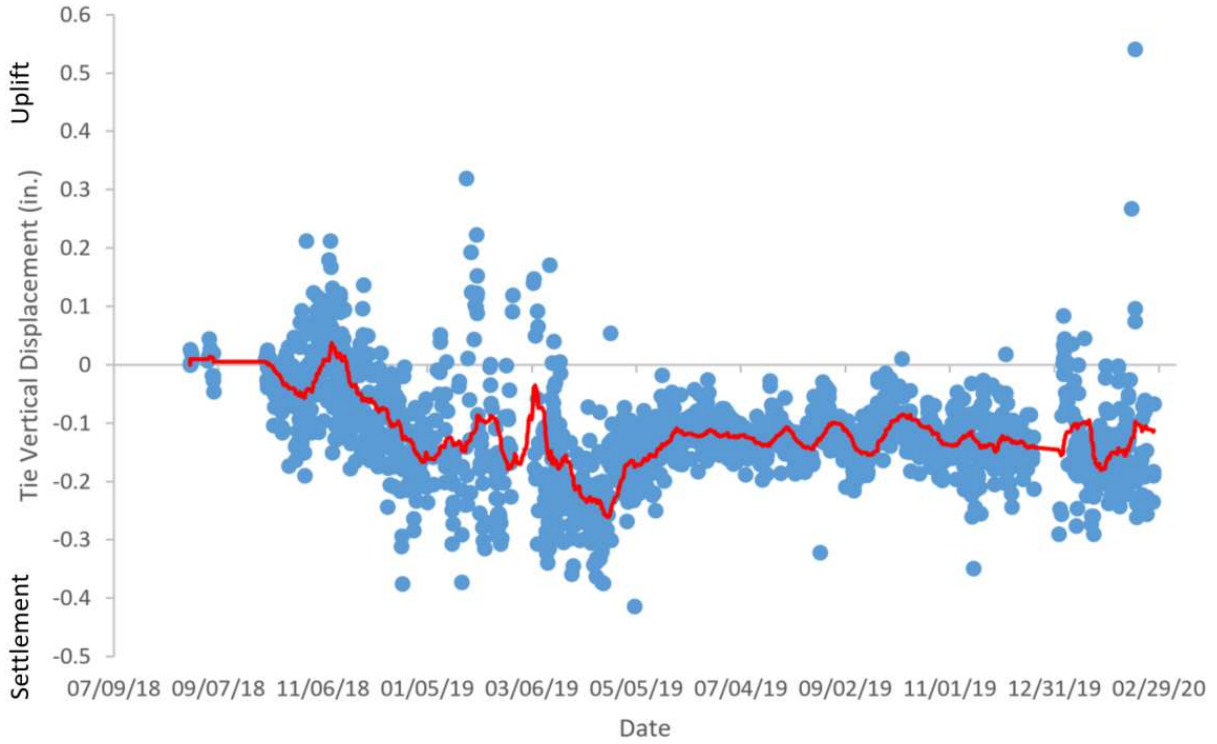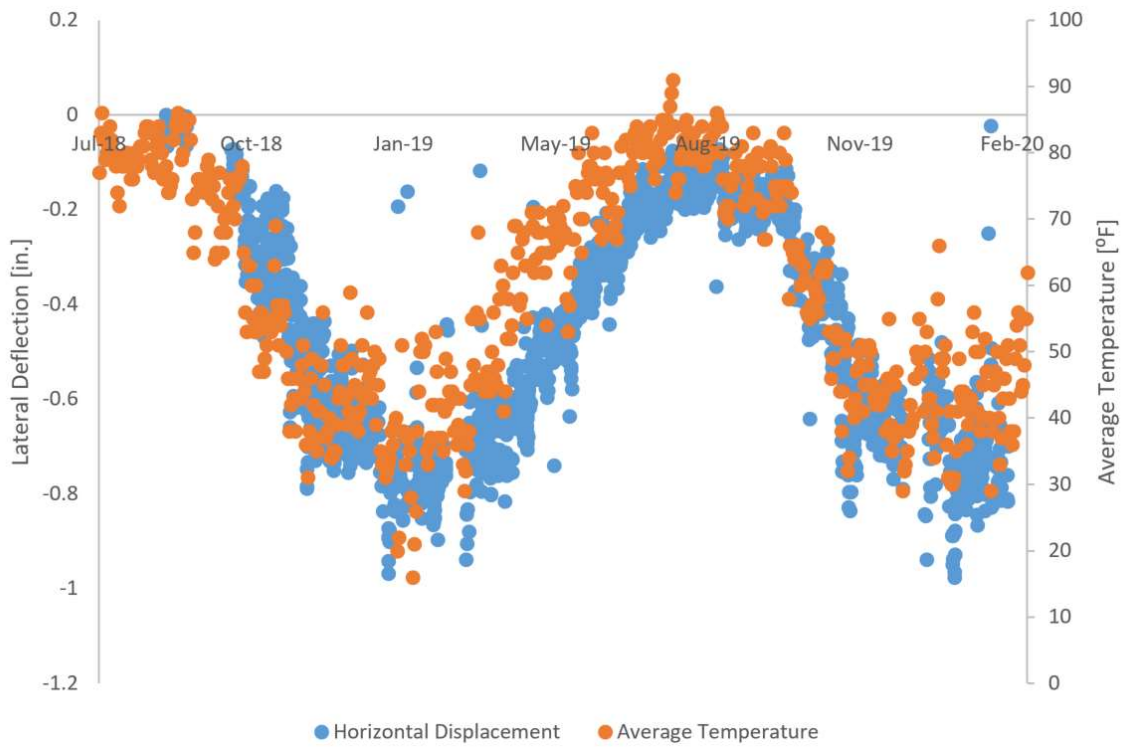
Figure 6.12. Track settlement at Station 16

Figure 6.13. Track horizontal movement at Station 16 inside the tunnel correlated with average recorded air temperatures

6.4 Track Acceleration

Before analyzing the acceleration data, it was de-trended to remove any offset or linear trends in the data. The magnitude of the acceleration data collected during the passage of each train was quantified by determining the root mean square (RMS) of the acceleration data obtained from each sensor, as shown in
Table 6.1. To quantify any changes in the propagation of accelerations throughout the system over time, the ratio of the RMS values for the different accelerometers at each location were analyzed. This ratio is referred to as R_A. The data points on these plots were fitted using a piecewise linear curve fit. One linear curve fit was used for the data points collected before the gap in data between September 2nd and October 3rd, and two linear curve fits of equal length for the remainder.

Table 6.1. Average RMS and standard deviation values of the acceleration data collected.

Location	Vertical Location	Direction	Average Acceleration RMS [g]
Portal	Tunnel floor	vertical	0.061
	Tie	perpendicular to rail	0.278
		parallel to rail	0.232
		vertical	0.416
Station 16	Tunnel floor	vertical	0.127
	Tie	perpendicular to rail	0.125
		parallel to rail	0.261
		vertical	0.350
Station 23	Tunnel floor	vertical	0.060
	Tie	perpendicular to rail	0.107
		parallel to rail	0.172
		vertical	0.389

A comparison of the vertical acceleration at the floor and tie shows that R_A (average RMS value) of vertical acceleration at the tunnel floor is much lower than the vertical acceleration at the tie. The same is true for R_A of the horizontal acceleration at the tie to the vertical acceleration at the tie; the ratio remained relatively constant, indicating that there was not a change in horizontal acceleration relative to vertical acceleration over the measurement period.

6.5 Moisture Condition

An analysis was performed on the moisture data obtained from the tunnel. The moisture sensor is designed to measure the volumetric water content (VWC) of soil in which it is embedded. The VWC is a percentage with 0% meaning there is no moisture present and 100% meaning the sensor is immersed in water. The average VWC was determined for the times at which a train passed through the tunnel. The moisture data from Station 16 is plotted in Figure 6.14. The

sensor at Station 16 stopped functioning properly in August 2019, whereas the moisture sensors at the other locations were damaged during construction and never gave accurate measurements. For the majority of the time period analyzed, the moisture is between 0 and 3%. At the end of January, the moisture readings increase rapidly to nearly 100%, which may signify that there was water in the tunnel at that time. Given that there was no extraordinary amount of rainfall at this time, the sump pump at Station 16 may have temporarily failed. The user manual for the moisture sensor advises against using it in soil with large air pockets, such as ballast, indicating that the harsh track environment was likely responsible for the sensor reading issues.
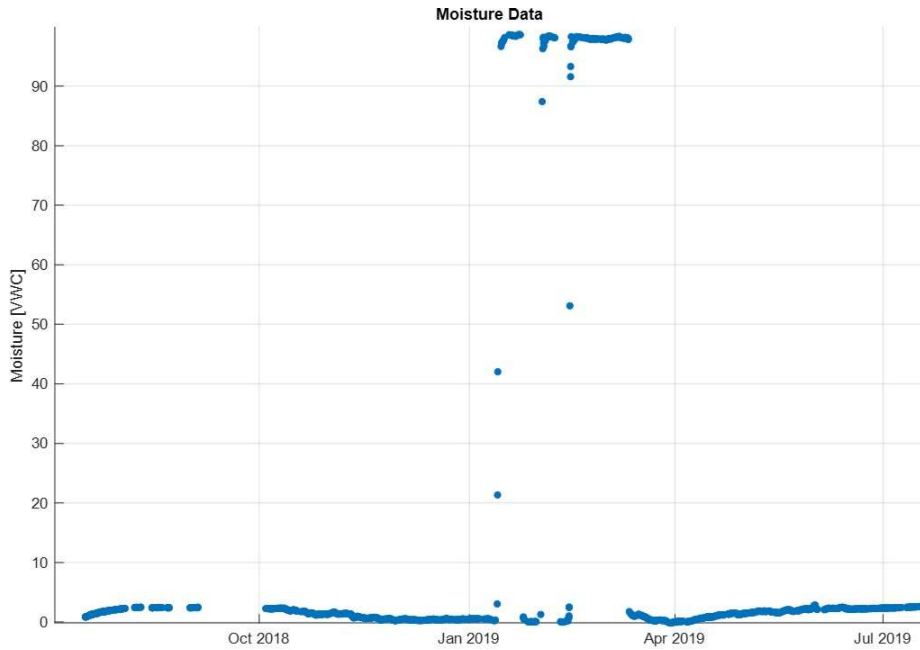
Figure 6.14. Moisture sensor readings at Station 16

6.6 ATIP Geometry Car Results

Geometry cars contain sensors that scan and document track conditions as part of routine track inspections. The research team obtained track data from the FRA Automated Track Inspection Program (ATIP) database. ATIP cars DOTX 220 collected data on Track Number 3 in the tunnel (the track adjacent to the one with the sensors installed, but with identical track structural design) twice over the instrumented period on July 10, 2018, and May 9, 2019, while ATIP car DOTX 219 also collected data twice on Track Number 2 on January 23, 2019 and April 26, 2019. The Virginia Avenue Tunnel is approximately located between mile markers 112.9 and 113.7. The data from Track Number 3 showed that the peaks in all data were consistently offset by 14 ft. After accounting for that shift in the readings, the difference between the two readings was calculated to determine any changes in the track conditions in the 10 months between measurements. Figure 6.15 and Figure 6.16 show the change in the left and right track profiles calculated, respectively. The left and right profiles showed similar and low changes throughout the tunnel, with less than 0.1 in. change in the 10 months between measurements. Track gage was shown to change less than 0.06 in. throughout the tunnel, as shown in Figure 6.17. Figure 6.18 shows the change in crosslevel between measurements, with an average change in crosslevel of 0.029 in. Little difference in curvature was seen between measurements, as shown in Figure 6.19. These measurements are indicative of little change in track conditions with time in track number 3. Measurements for track number 2 were examined, however the measurements did not show consistent locations of peak values, making analysis difficult.
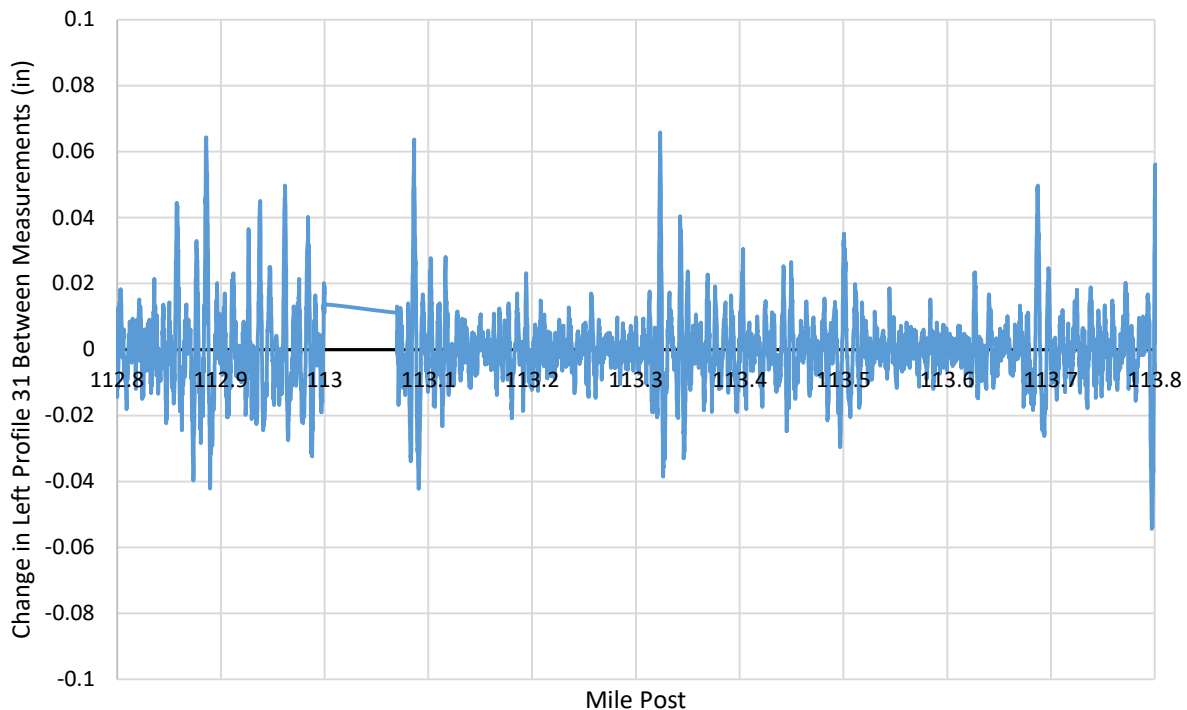

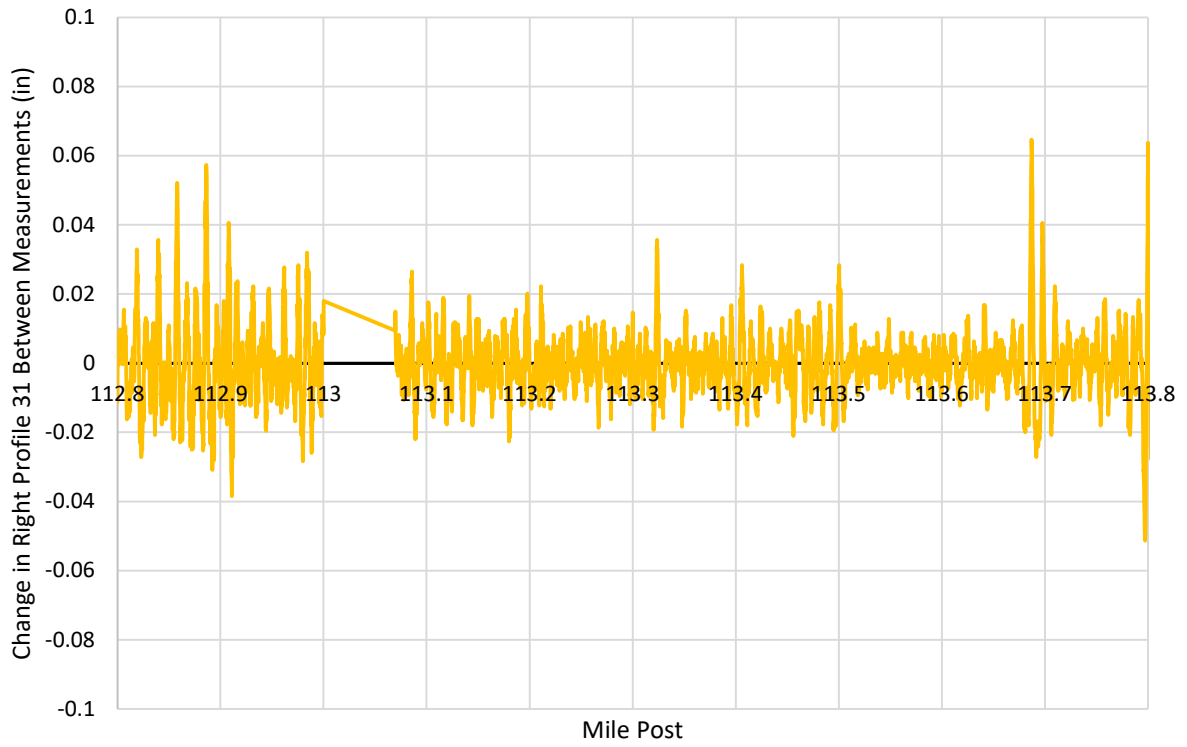**Figure 6.15. Change in left profile 31 between measurements for track number 3**

Figure 6.16. Change in right profile 31 between measurements for track number 3
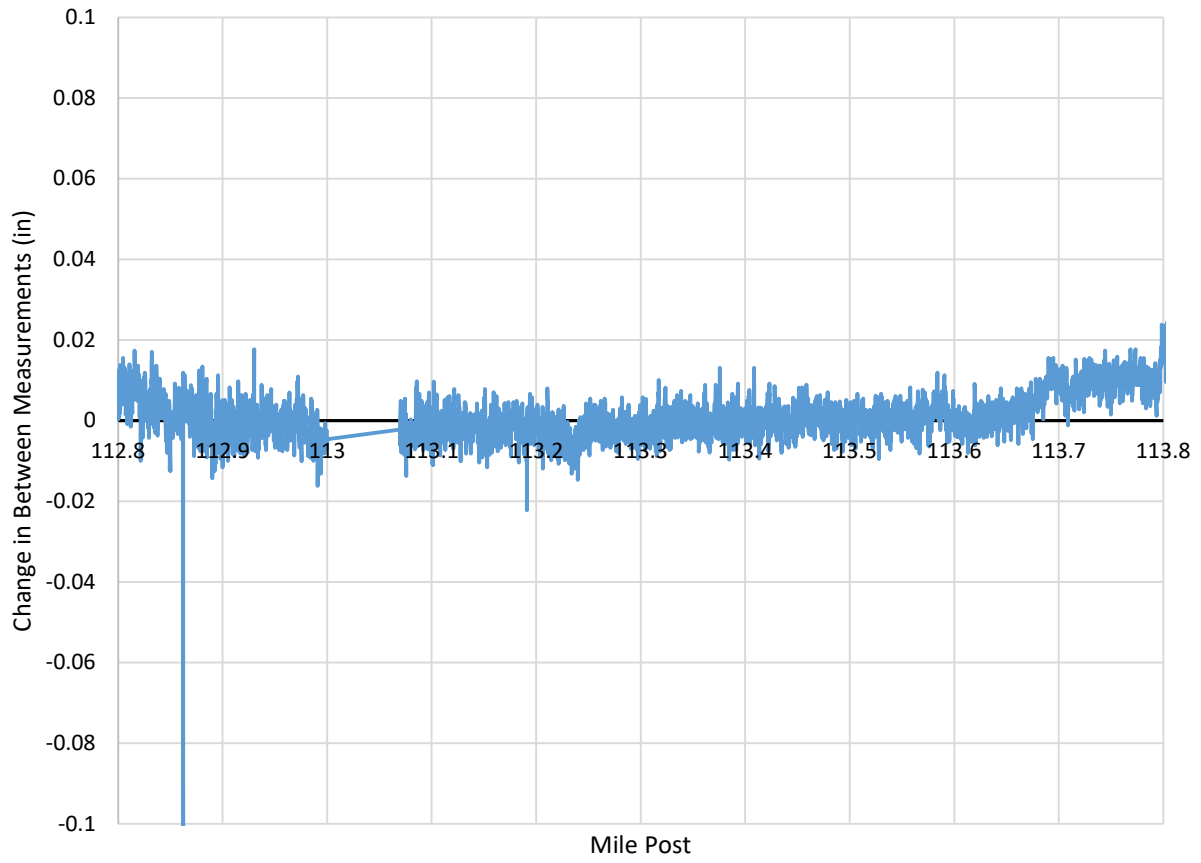
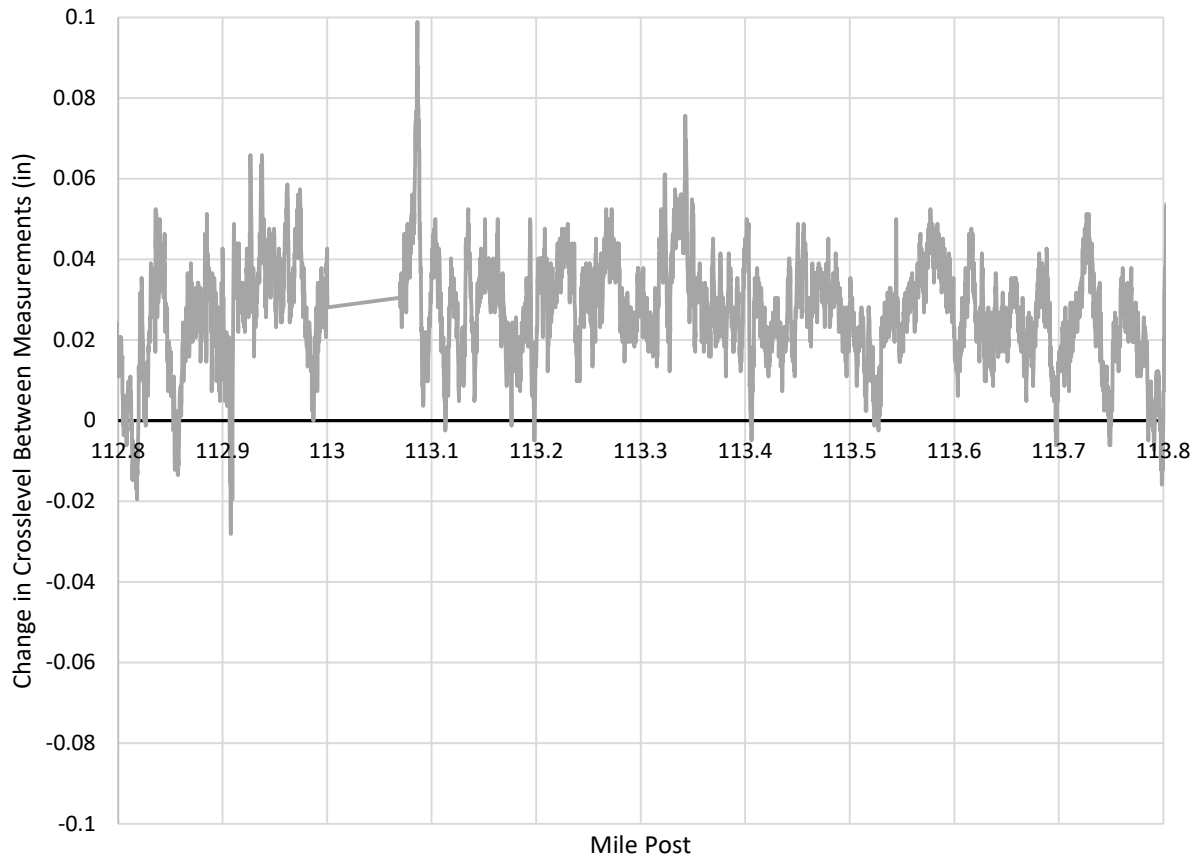**Figure 6.17. Change in track gage between measurements for track number 3**

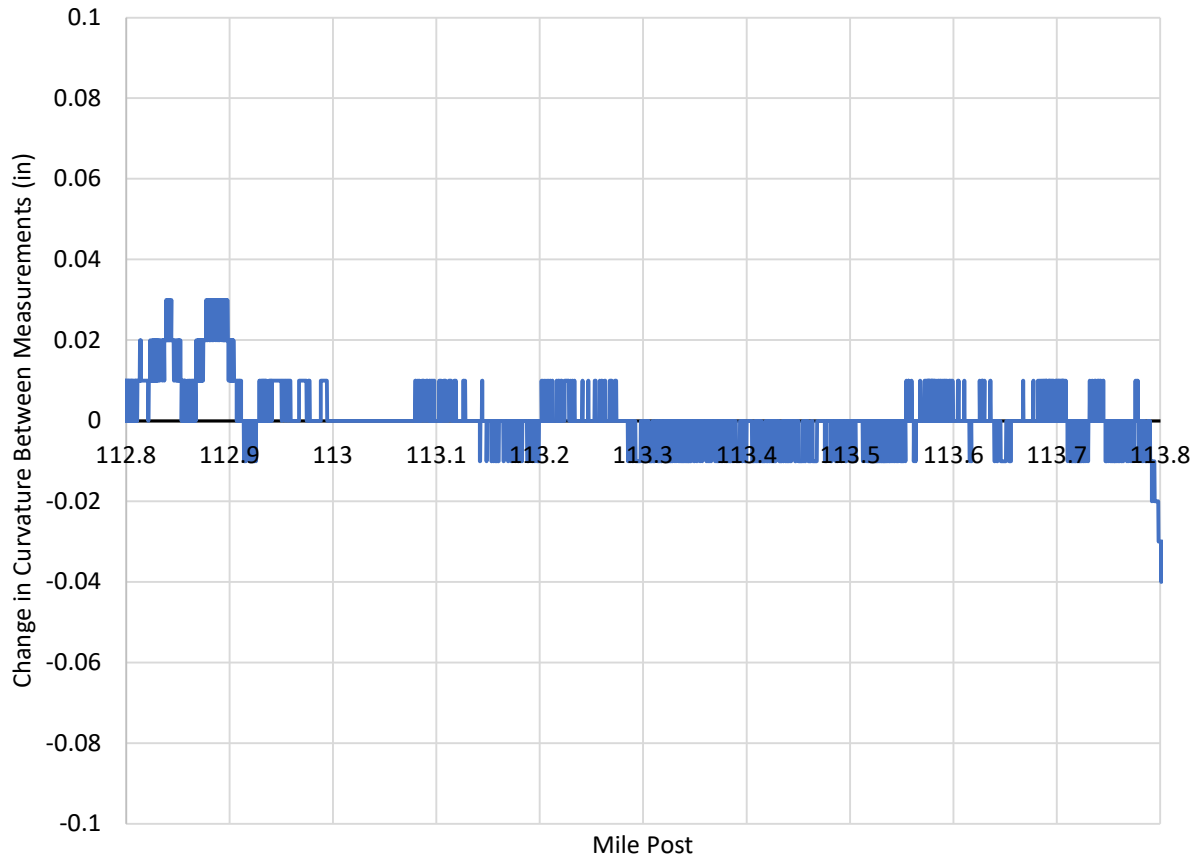**Figure 6.18. Change in track crosslevel between measurements for track number 3**

Figure 6.19. Change in track curvature between measurements for track number 3

7. Conclusions

Three sections of new track at the Virginia Avenue Tunnel were instrumented to measure track performance after being put into service when UTP and UBM are included in the track structure. Based on the data collected from sensors installed at three locations instrumented for the first 20 months of use at a new tunnel, the following conclusions can be drawn:

- Pressure distribution between ties was not shown to vary significantly based on train speed

- A track modulus k of between 2300 and 3500 psi was calculated from the tie vertical displacement

- UTP helped produce a stable track structure, with track settlement only lasting for approximately six months, after which the track stabilized to less than 0.157 in. (4 mm) of settlement. The stable track system should help reduce track tamping frequency and ballast breakdown.

- Track horizontal movement corresponded to the region's seasonal temperature variations

8. References

[1] C. F. Bonnett, Practical Guide to Railway Engineering, Imperial College Press, 2003.

[2] M. S. P. A. M. a. T. N. J. Taherinezhad, "A Review of Behaviour of Prestressed Concrete Sleepers," *Electronic Journal of Structural Engineering,* vol. 13, no. 1, pp. 1-13, 2013.

[3] E. T. Selig and J. M. Waters, Track Geotechnology and Substructure Mananagement, London: Thoman Telford, 1994.

[4] Pandrol CDM Track, *Technical Data Sheet CDM-UMB-H300-S,* Belgium.

[5] Pandrol CDM Track, *Technical Data Sheet CDM-USP-R-07e,* Belgium.

[6] Google, *[Google Maps Showing Location of Virginia Avenue Tunnel],* 2019.

[7] P. A. Costa, R. Calcada and A. S. Cardoso, "Ballast Mats for the Reduction of Railway Traffic Vibrations," *Soil Dynamics and Earthquake Engineering,* vol. 42, pp. 137-150, 2012.

[8] B. Indraratna, S. Nimbalkar and C. Rujikiatkamjorn, "Performance Evaluation of Shock Mats and Synthetic Grids in the Improvement of Rail Ballast," in *Advances in Transportation Geotechnics II*, Hokkaido, Japan, 2012.

[9] Geokon 3515, "Instruction Manual Model 3500 Series Earth Pressure Cells," 2017. [Online]. Available: http://www.geokon.com/content/manuals/3500_Earth_Pressure_Cells.pdf. [Accessed 4 October 2018].

[10] B. Indraratna, Advanced Rail Geotechnology - Ballasted Track, London: Taylor & Francis Group, 2011.

[11] H. Askarinejad, P. Barati, M. Dhanasekar and C. Gallage, "Field Studies on Sleeper Deflections and Ballast Pressure in Heavy Haul Track," *Australian Journal of Structural Engineering,* vol. 19, no. 2, pp. 96-104, 2018.

[12] T. J. Watts, "Direct Measurement of Crosstie-Ballast Interface Pressures Using Granular Material Pressure Cells," University of Kentucky, Lexington, KY, 2018.

[13] J. R. Edwards, M. S. Dersch and R. G. Kernes, "Improved Concrete Crosstie and Fastening Systems for US High Speed Passenger Rail and Joint Corridors: Volume 2," Federal Railroad Administration, Washington D.C., 2017.

[14] A. D. Kerr, Fundamentals of Railway Track Engineering, First Edition ed., Omaha, NE: Simmons-Boardman Books, Inc., 2003, pp. 137-141.

[15] National Oceanic and Atmospheric Administration, "National Centers for Environmental Information," 2020. [Online]. Available: https://www.ncdc.noaa.gov/cdo-web/datasets/GHCND/stations/GHCND:USW00013743/detail.

Appendix A.
Pressure Sensor Changes with Time

For all figures in Appendix A, blue dots represent the RMS peak pressure for one train, while the red line represents a 200 pt moving average.
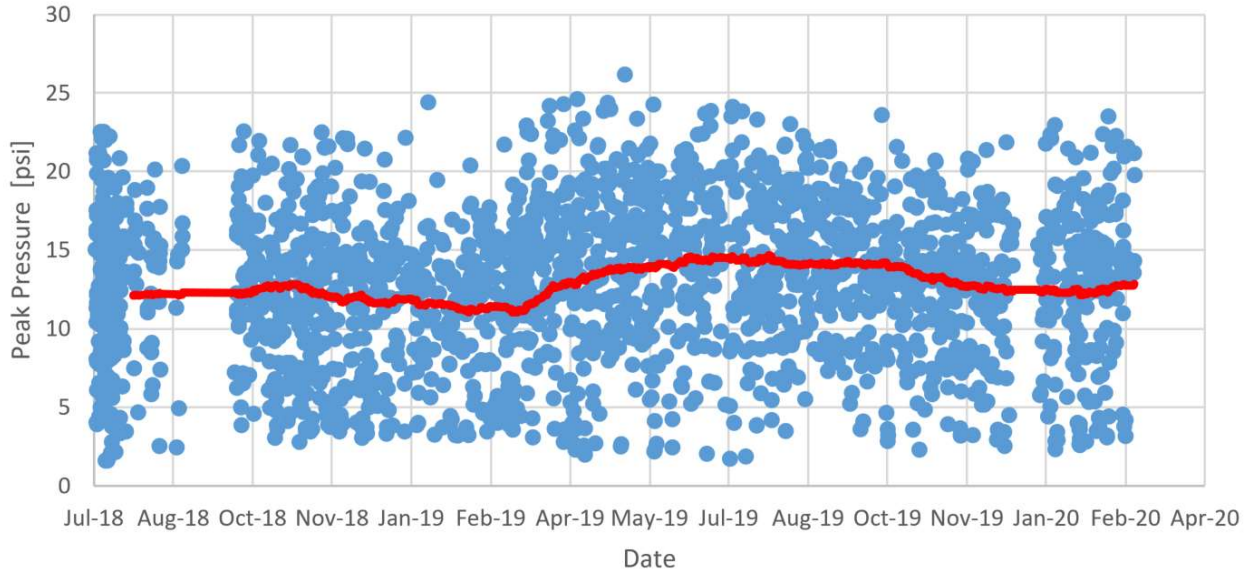

Figure A.1. Average peak pressure for each train vs date for portal sensor 1, along with a 200 point moving average
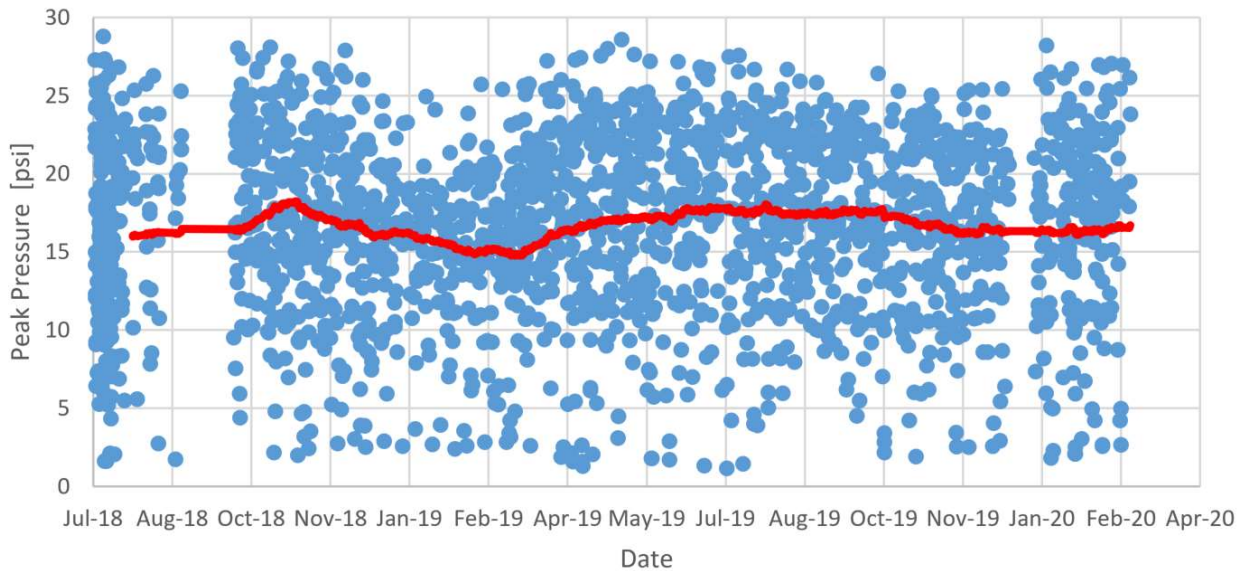

Figure A.2. Average peak pressure for each train vs date for portal sensor 2, along with a 200 point moving average
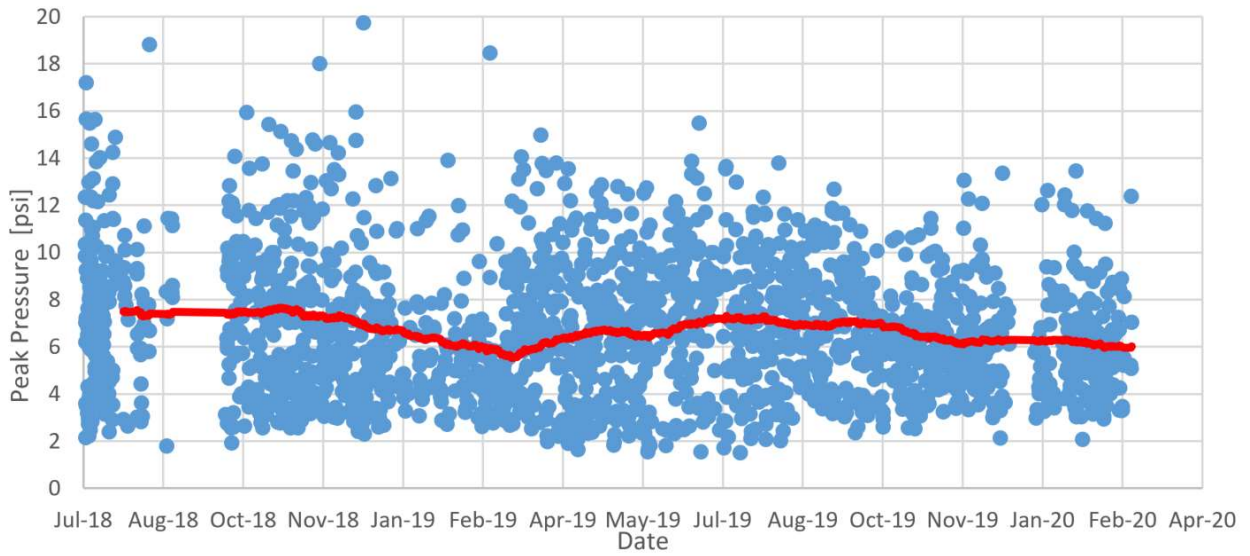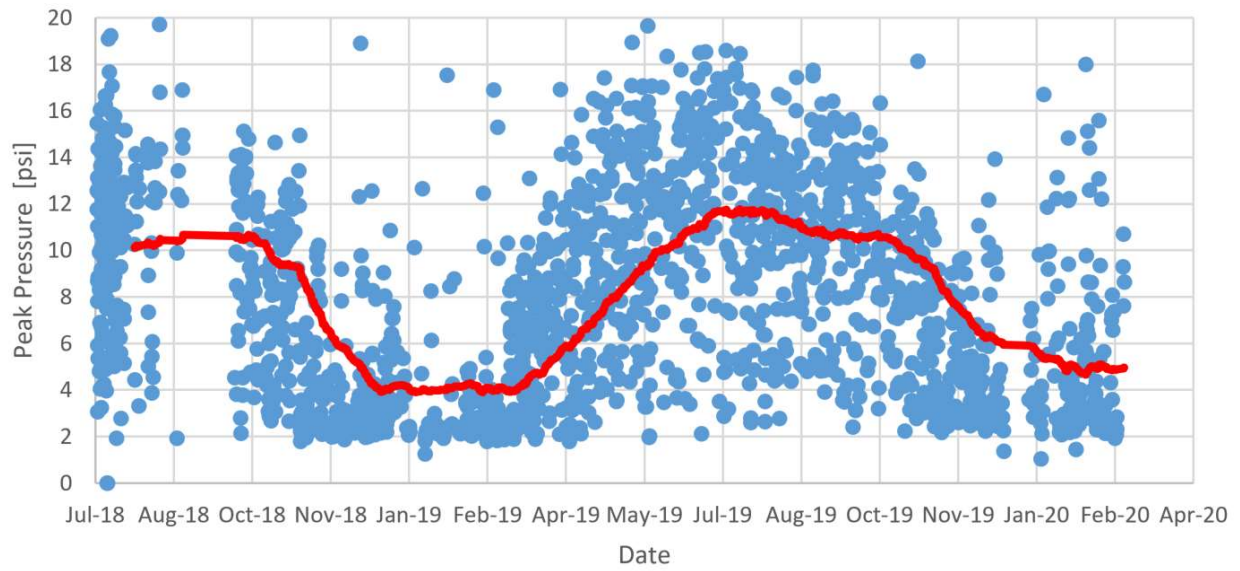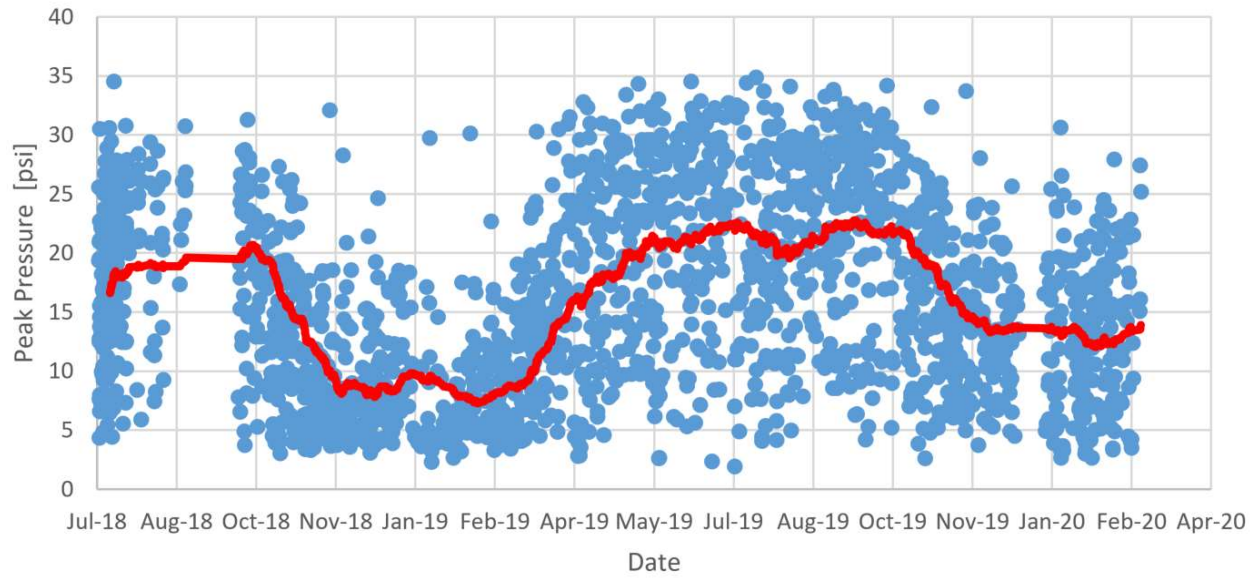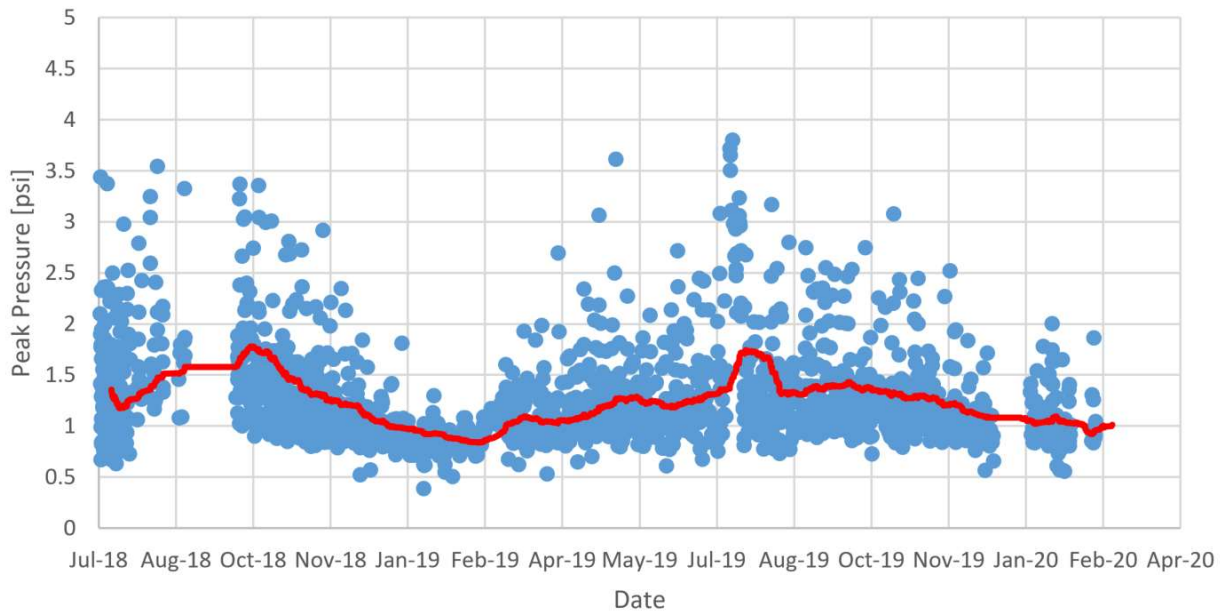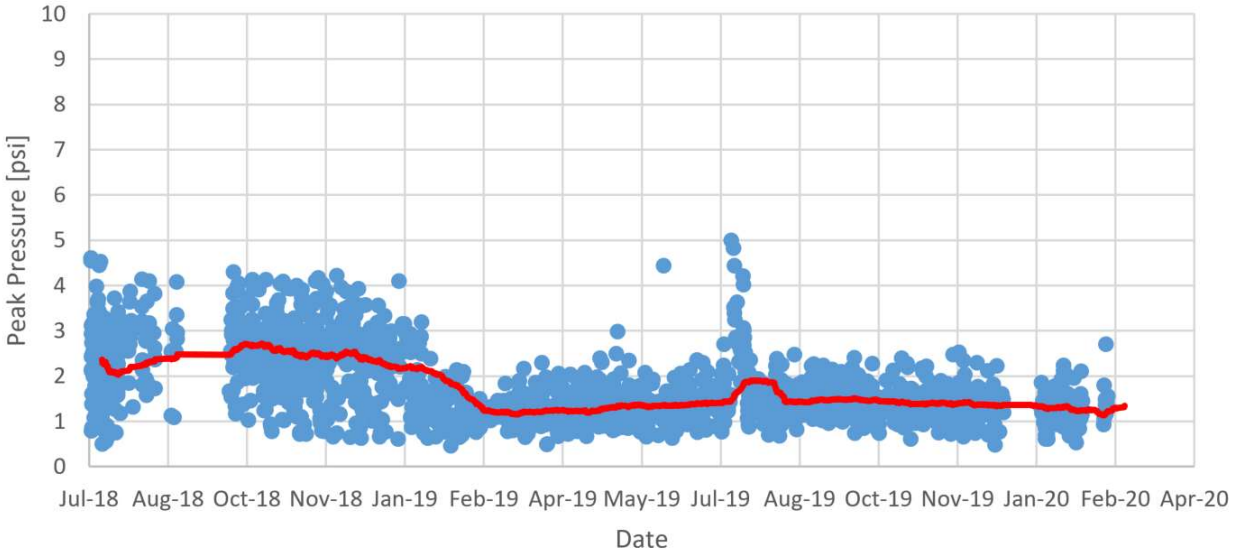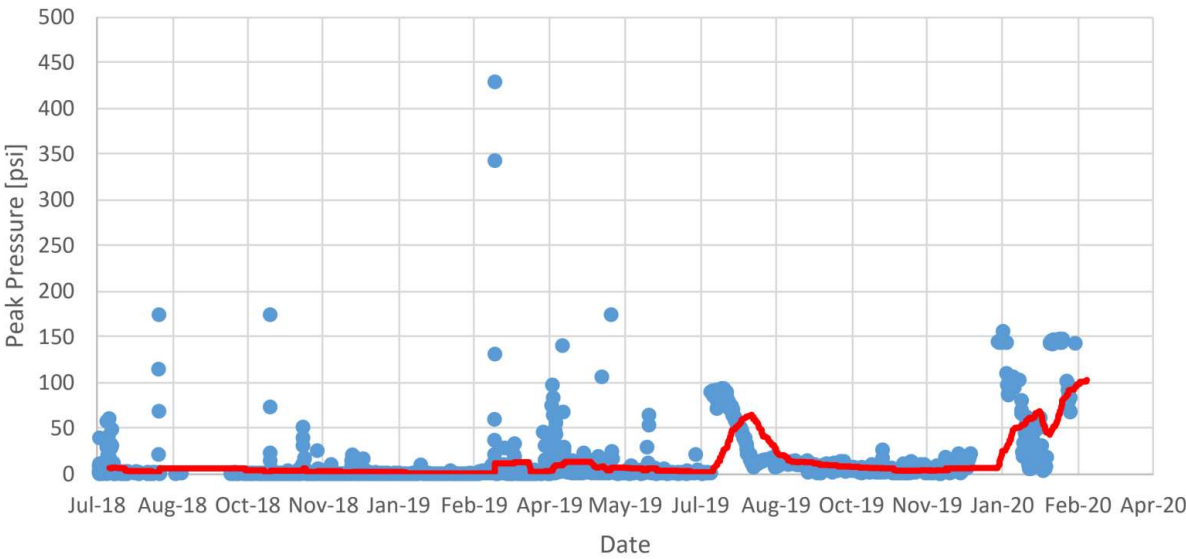
Figure A.3. Average peak pressure for each train vs date for portal sensor 3, along with a 200 point moving average
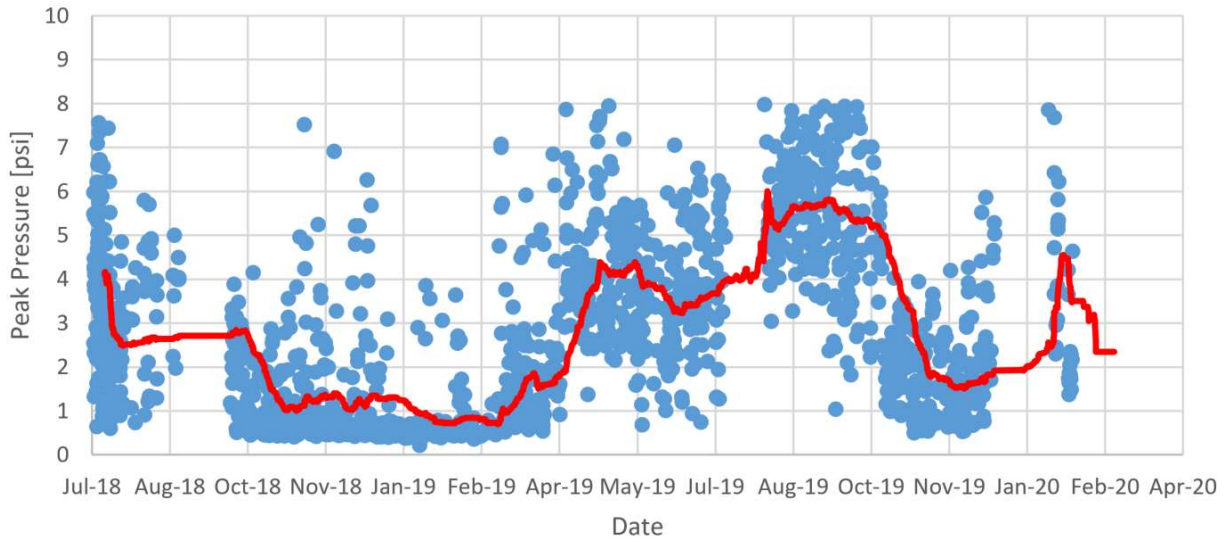

Figure A.4: Average peak pressure for each train vs date for portal sensor 4, along with a 200 point moving average

Figure A.5: Average peak pressure for each train vs date for portal sensor 5, along with a 200 point moving average

Figure A.6: Average peak pressure for each train vs date for Station 16 sensor 1, along with a 200 point moving average
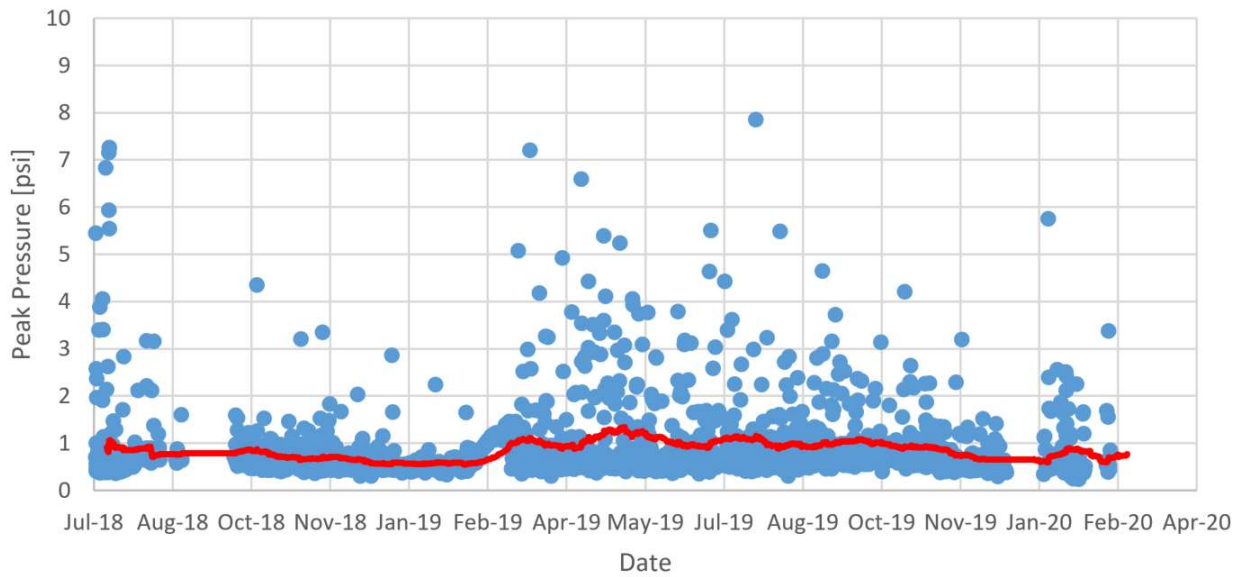
Figure A.7: Average peak pressure for each train vs date for Station 16 sensor 2, along with a 200 point moving average

Figure A.8: Average peak pressure for each train vs date for Station 16 sensor 3, along with a 200 point moving average
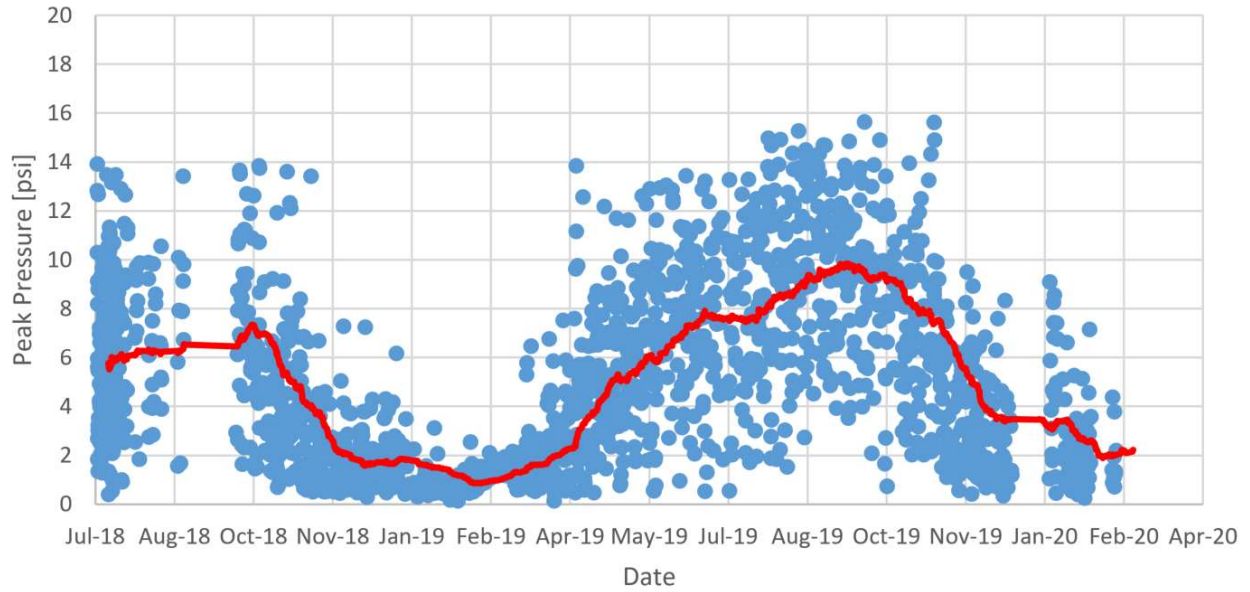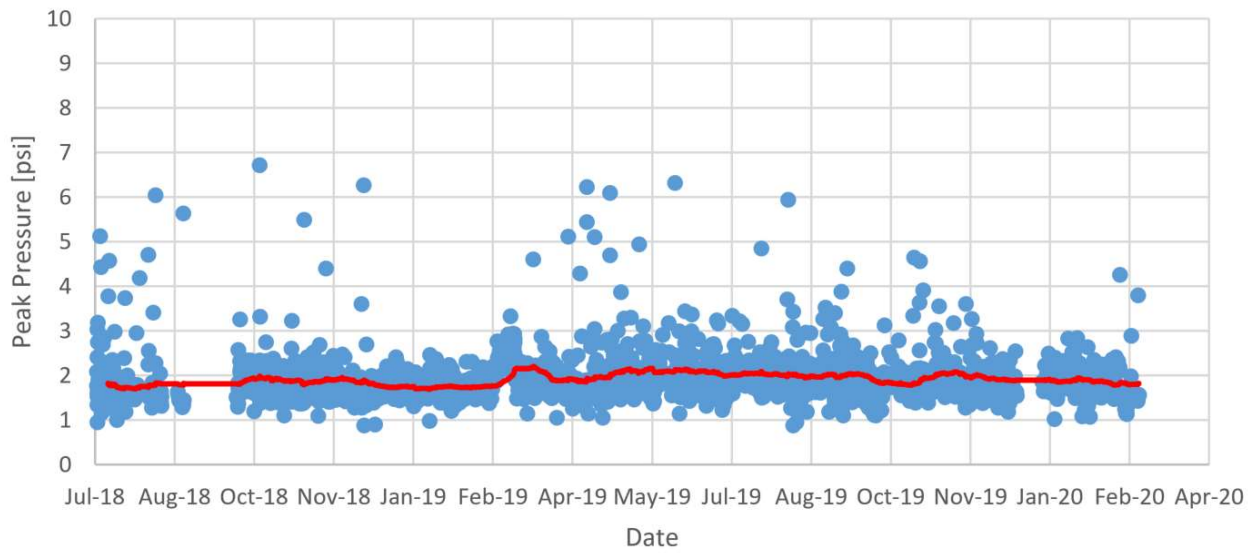
Figure A.9: Average peak pressure for each train vs date for Station 16 sensor 4, along with a 200 point moving average

Figure A.10: Average peak pressure for each train vs date for Station 16 sensor 5, along with a 200 point moving average

Figure A.11: Average peak pressure for each train vs date for Station 16 sensor 6, along with a 200 point moving average

Figure A.12: Average peak pressure for each train vs date for Station 23 sensor 1, along with a 200 point moving average
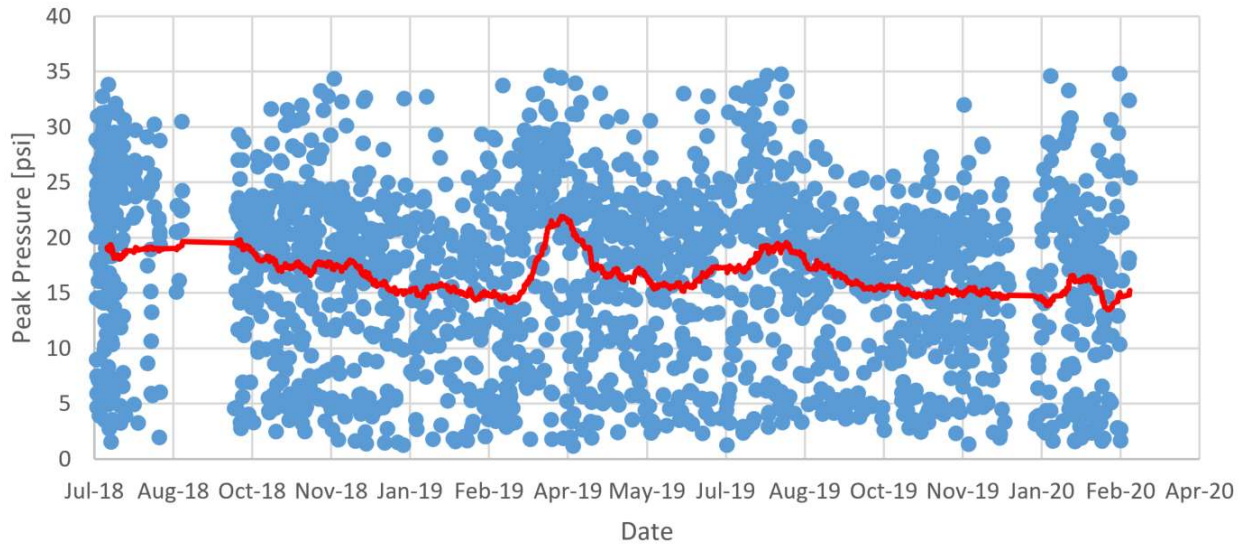
Figure A.13: Average peak pressure for each train vs date for Station 23 sensor 2, along with a 200 point moving average
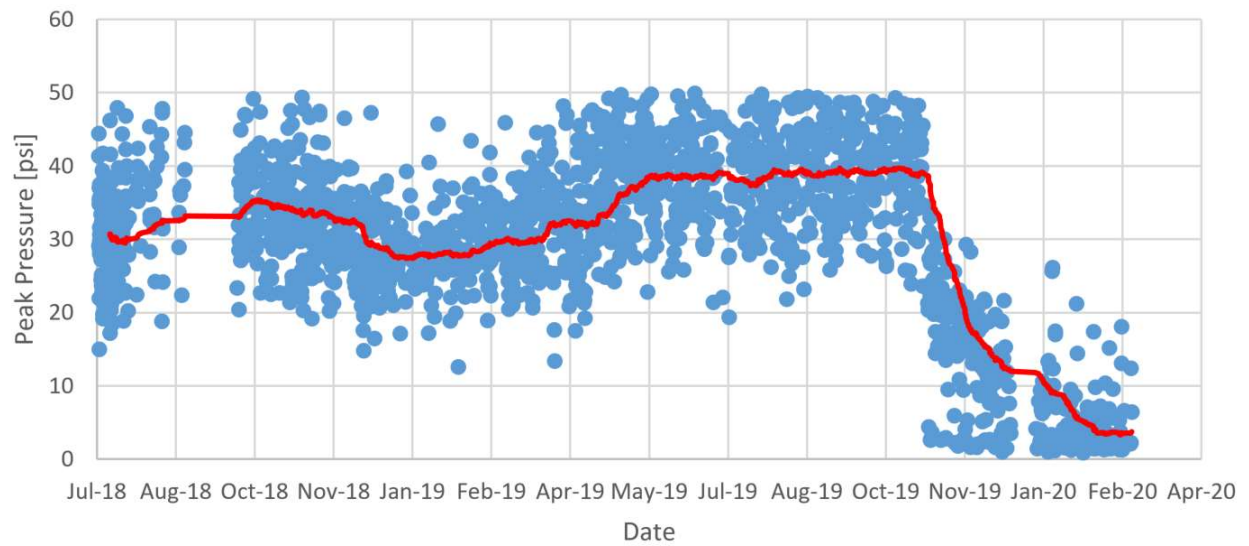

Figure A.14: Average peak pressure for each train vs date for Station 23 sensor 3, along with a 200 point moving average
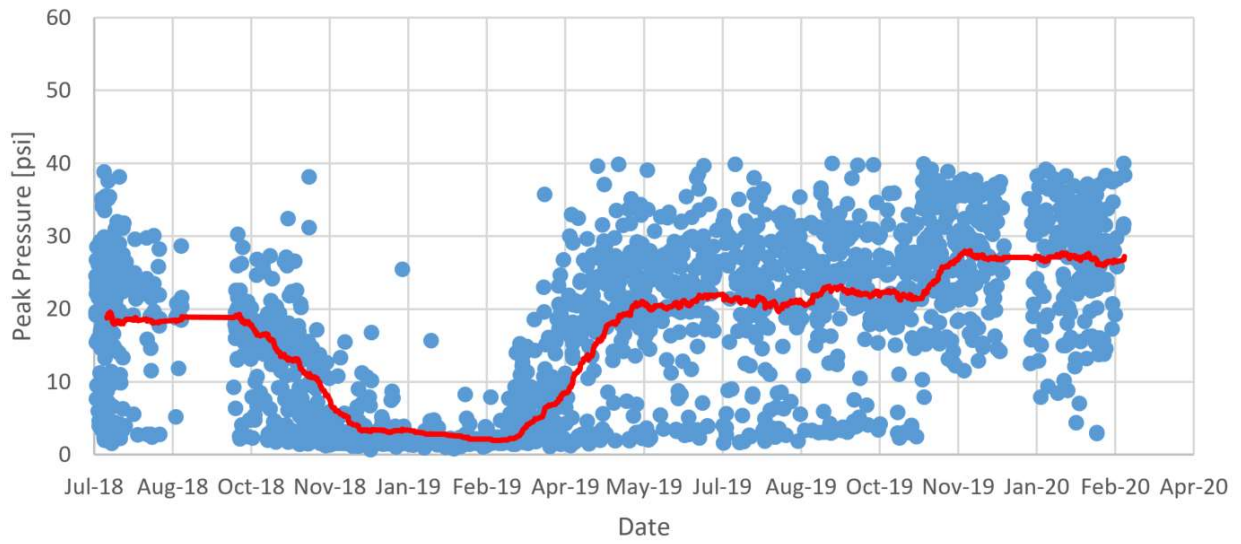
Figure A.15: Average peak pressure for each train vs date for Station 23 sensor 4, along with a 200 point moving average
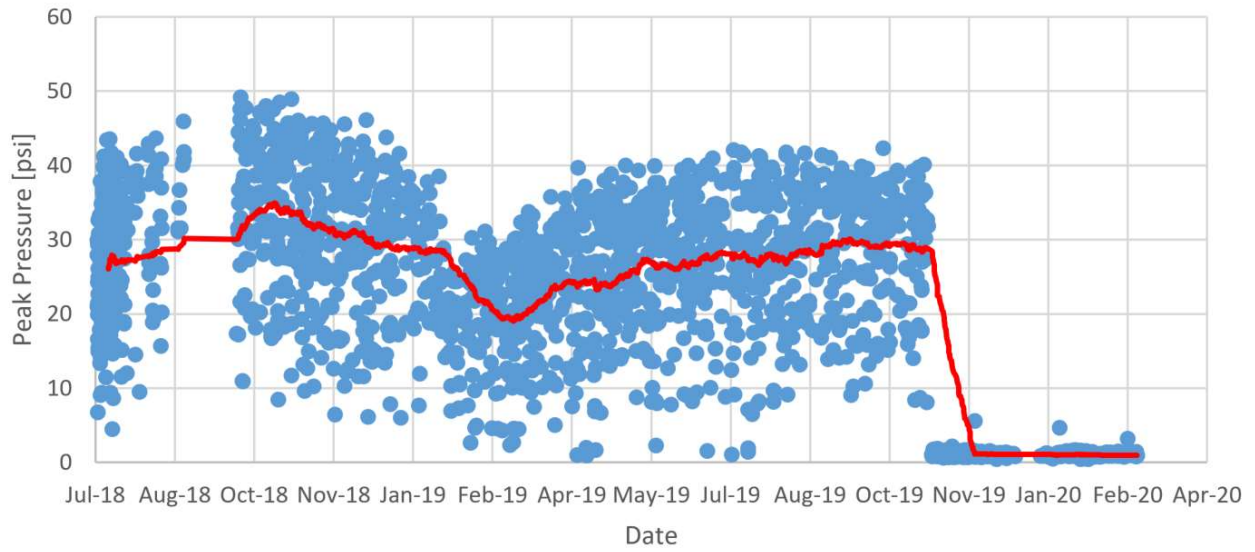

Figure A.16: Average peak pressure for each train vs date for Station 23 sensor 5, along with a 200 point moving average
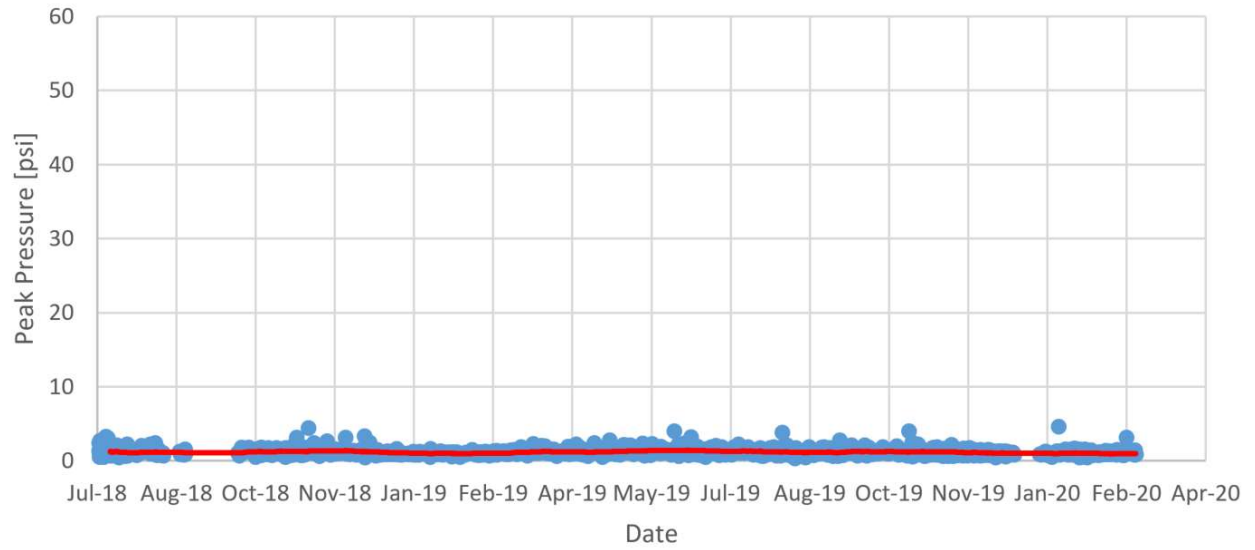
Figure A.17: Average peak pressure for each train vs date for Station 23 sensor 6, along with a 200 point moving average

Abbreviations and Acronyms

AC	Alternating Current
ATIP	Automated Track Inspection Program
DAQ	Data Acquisition
DC	Direct Current
DMVPN	Dynamic Multipoint Virtual Private Network
LIU	Light Interface Unit
MPH	Miles Per Hour
RMS	Root Mean Square
UBM	Under Ballast Mat
UF	University of Florida
UPS	Uninterruptable Power Supply
UTP	Under Tie Pad
VAC	Volts of AC Power
VAT	Virginia Avenue Tunnel
VI	Virtual Instrument
VWC	Volumetric Water Content
VPN	Virtual Private Network
AC	Alternating Current
ATIP	Automated Track Inspection Program
DAQ	Data Acquisition